JYVÄSKYLÄ STUDIES IN COMPUTING
210

Tuomo Räisänen

Efficient Numerical Methods for Simulating Continuous Casting Processes

JYVÄSKYLÄN YLIOPISTO

JYVÄSKYLÄ STUDIES IN COMPUTING 210

Tuomo Räisänen

Efficient Numerical Methods for Simulating Continuous Casting Processes

Esitetään Jyväskylän yliopiston informaatioteknologian tiedekunnan suostumuksella
julkisesti tarkastettavaksi yliopiston Agora-rakennuksen auditoriossa 2
joulukuun 18. päivänä 2014 kello 12.

Academic dissertation to be publicly discussed, by permission of
the Faculty of Information Technology of the University of Jyväskylä,
in building Agora, auditorium 2, on December 18, 2014 at 12 o'clock noon.

UNIVERSITY OF JYVÄSKYLÄ

JYVÄSKYLÄ 2014

Efficient Numerical Methods for Simulating Continuous Casting Processes

JYVÄSKYLÄ STUDIES IN COMPUTING 210

Tuomo Räisänen

Efficient Numerical Methods for Simulating Continuous Casting Processes

UNIVERSITY OF JYVÄSKYLÄ

JYVÄSKYLÄ 2014

Editors
Timo Männikkö
Department of Mathematical Information Technology, University of Jyväskylä
Pekka Olsbo, Ville Korkiakangas
Publishing Unit, University Library of Jyväskylä

URN:ISBN:978-951-39-6014-8
ISBN 978-951-39-6014-8 (PDF)

ISBN 978-951-39-6013-1 (nid.)
ISSN 1456-5390

Jyväskylä University Printing House, Jyväskylä 2014

ABSTRACT

Räisänen, Tuomo
Efficient numerical methods for simulating continuous casting processes
Jyväskylä: University of Jyväskylä, 2014, 106 p.
(Jyväskylä Studies in Computing
ISSN 1456-5390; 210)
ISBN 978-951-39-6013-1 (nid.)
ISBN 978-951-39-6014-8 (PDF)
Finnish summary
Diss.

This study considers modeling, approximating, and simulating of continuous casting processes. The focus is especially on the numerical efficiency of methods.

We approach the casting processes using enthalpy based modeling. This leads to a three-dimensional transient convection dominated two-phase Stefan problem with the nonlinear boundary condition. Under suitable assumptions the problem is mathematically well posed. We introduce a three-dimensional model and show qualitative properties.

Fully discrete Galerkin approximation of the model leads to a large-scale nonlinear discrete problem for which the convection dominance also causes stability issues. To overcome these, we apply the method of characteristics and the upwinding technique. Furthermore, we are able to apply so-called nonlinear Chernoff formula to these approximations and, as a result, the discrete approximated model can be solved using only linear algebraic equations at each time step.

All together, we consider four different approximations. We show their convergence and describe the implementation using matrix formulations. By solving a numerical example, we compare approximations in terms of the rate of convergence and solution time.

Finally, we study how the presented approximations perform on an industrial scale. For this purpose, we use an artificial machine producing stainless steel to get an example of a detailed model and realistic computational challenges. We discuss the changes in the solution algorithms compared to the model problem and introduce an efficient solution algorithm. We validate our software, compare our approximations, and make conclusions about the numerical efficiency.

Keywords: continuous casting, two-phase Stefan problem, nonlinear Chernoff formula, upwinding, method of characteristics

Author

Tuomo Räisänen
Department of Mathematical Information Technology
University of Jyväskylä
Finland

Supervisors

Professor Timo Tiihonen
Department of Mathematical Information Technology
University of Jyväskylä
Finland

Professor Jari Toivanen
Department of Mathematical Information Technology
University of Jyväskylä
Finland

Reviewers

Professor Alexander Lapin
Institute of Computational Mathematics and Information Technology
Kazan Federal University
Russia

Professor István Faragó
Department of Applied Analysis
Eötvös Loránd University
Hungary

Opponent

Dr. Erkki Laitinen
Deparment of Mathematical Sciences
University of Oulu
Finland

ACKNOWLEDGEMENTS

This thesis was made at the Department of Mathematical Information Technology of the University of Jyväskylä. The doctoral study was partly financially supported by Academy of Finland.

I am grateful to my supervisors Prof. Timo Tiihonen and Prof. Jari Toivanen for their help and useful advice. I would like to express my gratitude to the Seppo Louhenkilpi for giving me the opportunity to use Tempsimu software and especially Marko Petäjäjärvi at the Outokumpu, Tornio Steel Factory for his cooperation and the use of actual industrial data.

I would like to thank the reviewers, Prof. Alexander Lapin and Prof. István Faragó, for their valuable comments. I appreciate their reviews, which definitely improve my work.

I am thankful to Tattikuja Darts for providing spare time activities. My mother, sister, and brother are acknowledged for their continuous support.

Lastly, but most importantly, I am grateful to my wife Pirjo for all her love. This work is dedicated to my sons, Eetu and Veeti.

Varkaus, November 2014

Tuomo Räisänen

LIST OF FIGURES

LIST OF TABLES

CONTENTS

1 INTRODUCTION

1.1 Background

1.1.1 History

The idea of continuous casting was introduced by G.E. Sellars in mid 1880's but it took more than hundred years to apply it as an industrial technology in steel industry. Sellars applied the idea originally to the production of lead tubings. Continuous casting could not yet be applied to steel owing to too many technical problems associated with high temperatures and low thermal conductivity.

The first patent for the possibility of solidifying steel using water cooled mold open at the top and bottom was established by R.M. Daelen in 1887. During the 1900s the process was developed using numerous pilot plants for steel casting and little by little, it become an industrial standard. Since the 1970s, the continuous casting processes have been applied increasingly and nowadays 90 percent of steel is produced in continuous casting machines.

Before the continuous casting process was ready for full-scale industrial production, steel was cast in a full-length mold having a suitable shape. In the continuous casting, a continuous slab is formed when the steel is cast through an open-ended mold. After passing this mold area, steel should have a solid shell and process can be safely controlled.

During the development of the process, empirical relations like

$$\text{Shell thickness} = K\sqrt{\text{Distance}/\text{Casting speed}}$$

were found and used. Naturally the value of K had to be defined using costly plant trials, ending possibly in breakouts. A breakout means that, due to improper cooling of the process, the solidified shell cracks and liquid material flows to the plant's floor. On a plant level these trial tests are very costly, even without a breakout and if it happens, they are even more expensive.

In the 1970s when the continuous casting process was ready to the full-range industrial production, computers also became affordable and numerical simula-

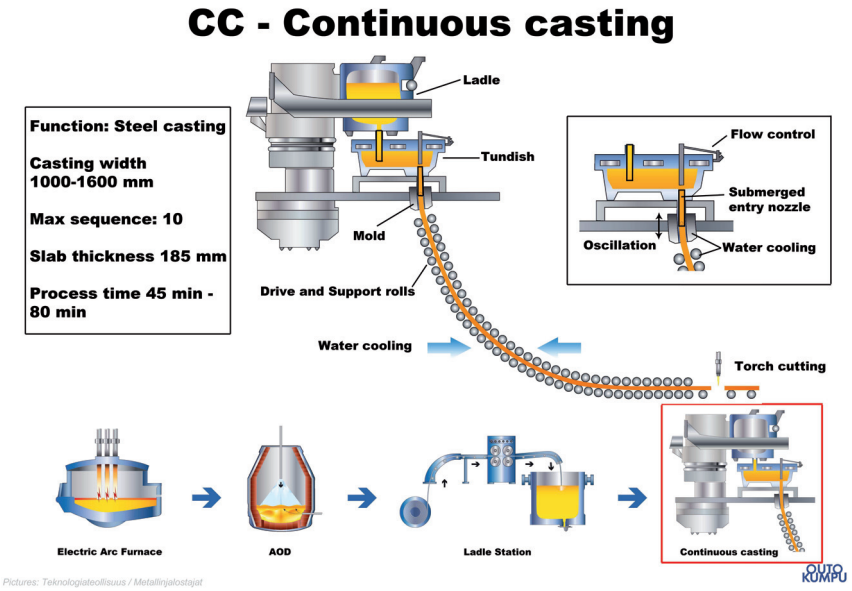

FIGURE 1 Curve type continuous casting machine. Image: Kind permission of Outokumpu Stainless Oy, Tornio, Finland

tion of the continuous casting process started [52]. At the present time, the process is no longer developed by experimental tests only. Several computer-aided tools are used to control and simulate the process to ensure the products' quality and productivity. Breakouts are very rare nowadays due to the proper control of the system.

1.1.2 Modeling goal

The continuous casting process involves several physical phenomena: turbulent fluid flow coupled with the heat transfer including phase changes under thermal stresses. One of the most important considerations during the continuous casting process is the capability of attaining defect free slabs. Typical defects are different types of caused by the mechanical tensile strains or improper cooling practices. Excessive spray cooling or insufficient spray length lead to the surface reheating, which induces tensile stresses beneath the surface, even up to the solidification front. On the other hand, too rapid cooling will cause thermal stresses leading to the cracks as well. Most of these cracks can be predicted if the evolution of the temperature distribution is known.

During the production, the slab quality depends on the proper combination of the casting speed and different cooling practices. In offline one can study different combinations of water cooling and casting speeds, in order to improve productivity and quality. If one can simulate the processes fast enough, it is possible to control the process by keeping the cooling rate and temperature of the slab

in a feasible region in terms of metallurgical criteria even for online purposes.

Typically several simplifications are made in the modeling. The effect of turbulent flow to the temperature distribution is typically modeled by using an effective heat transfer coefficient. This leads to an enthalpy based model in which the temperature can be solved without coupling it to the turbulent flow.

Even the simplified heat transfer model is computationally expensive when applied to the actual industrial geometries with sufficient accuracy. For this reason, early industrial applications required some simplifications. By neglecting the heat conductivity to the casting or width directions or both of them one formed different types of models, still used in simulation [25, 29, 24]. Even with these simplifications the heat transfer can be approximated with such accuracy that these models can predict some of the defects.

The development of the simulation tools made it possible to model and resolve more and more details of the process.

1.1.3 Challenges and questions in numerical simulation

Currently, commercial finite element-based software, e.g., Fluent or Comsol have their own packages for simulations fluid flow, thermal stresses, heat transfer etc. The use of these models is still limited to offline simulation and the transient simulation of the plain heat transfer in an industrial size machine is very time consuming in terms of CPU time.

The modeling of the continuous casting processes leads to a large number of unknowns to be solved. First of all, machine dimensions are big, the length of the simulation area can be up to 20 meters, the width about one meter, and the thickness about 20cm. Then with the mesh size of 1cm and assuming some symmetry one ends up to the order of 10^6 unknowns in a system of nonlinear equations, to be solved in a fraction of a second in a real-time simulations.

The description of the proper boundary conditions is essential in the modeling of the industrial continuous casting machines. In the continuous casting machine, there are tens of supporting rolls. If the heat transfer around a roll contact is modeled as is, each roll has a contact length of $0.5 - 1$cm, with a typical heat transfer coefficient of order $1\text{kw}/\text{m}^2\text{K}$. On both sides of the rolls there are radiation areas to which the water cooling cannot reach, or is not aimed to reach. Length of these are (to the casting direction) typically more than 2 cm. This means that next to the roll, there is only natural convection and radiation and the value of the natural convection is about $0.04\text{kw}/\text{m}^2\text{K}$. In the water cooling area, the heat transfer coefficient varies typically between $0.3 - 1.2\ \text{kw}/\text{m}^2\text{K}$.

By neglecting some details in the water cooling area, the cooling effect can be handled by approximating the total heat transfer coefficient as function of the amount of water in each cooling zone. Then it is possible to decrease the size of the problem in discrete level and the amount of solution variables depend then on the accuracy of the solution, but eventually this will lead to a large-scale system also.

Typical differences in the temperature distributions between detailed and

zone cooling models are illustrated in Figure 2.

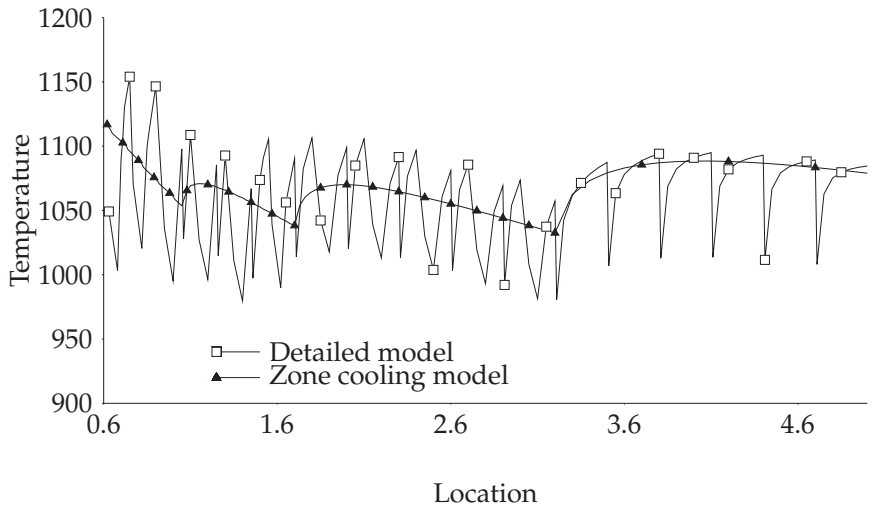

FIGURE 2 Surface temperature distributions on the midface

Most of the time, the continuous casting process is near a steady state, which is the typical starting point for the simulation modeling. In the transient simulations, the simplest approach is to use explicit approximations, i.e., obtain the solution from the previous time level by using simple matrix vector multiplication. However, in this type of approach there is a stability condition, where the time step τ is limited with the spatial discretization parameter h. In the case of steel with the linear heat equation, the condition is such that $\tau < Ch^2$, where $C \approx 10^{-4}$. Assuming the simulation scale $h \approx 0.01$ meter in the detailed model, this type of stability condition is obviously very restrictive.

From the point of view of scientific computing, the research questions are: how can the steady state be approximated efficiently, which are the less restrictive transient approximations in 3D, and how can they be solved efficiently in terms of CPU time and accuracy? From the computational science point of view, the main interest is naturally, how these methods can perform in real-life situations. Thus, we have to study and discuss at least the following:

1. Mathematical model
2. Qualitative properties of the model
3. Approximations of the model
4. Convergence and stability of the approximations
5. Numerical error estimates
6. Fast solution methods to the approximations
7. Implementation
8. Applications on the industrial scale

1.1.4 Approach

In the industrial applications, the casting products are typically alloys, which means in particular that the phase change takes place gradually over a temperature interval. Then one is tempted to restrict the studies to the efficient numerical methods for the regular nonlinear heat equation.

We approach the continuous casting processes by taking as a starting point the classical two-phase Stefan problem with sharp discontinuity on phase boundaries.

First, we consider theoretical results by using classical enthalpy formulation in the absence of convection. Then, we summarize some interesting numerical solution methods that have been developed by forming fully discrete approximations based on the techniques of showing the existence of a solution. We introduce a few of them and their basic properties.

After that, we state the problem in the continuous casting context by adding the casting speed in to the model. There are limited theoretical and numerical results. We introduce some of these results.

Our aim is to extend the theoretical results to free boundary models of continuous casting and to develop numerical approximations taking into account the numerical efficiency in industrial setup.

We introduce four fully discrete approximations to the model. We show the convergence of these approximations and perform some numerical tests.

As in the industrial applications, usually alloys are concerned, we discuss how this is related to the numerical efficiency of the given approximations. We apply all the approximations to alloys in industrial situations. Using efficient implementation of the approximations, we are able to solve continuous casting processes up to 10^6 unknowns in real time on a laptop. As a result we conclude that, starting from the free boundary formulation, very efficient numerical methods with the practical accuracy can be formed.

In what follows, we introduce the classical enthalpy formulation of the phase transition. We show how this can be formed from the classical two-phase Stefan problem. This will lead to the theory of free boundary problems which can be applied to modeling industrial processes. We discuss enthalpy based formulations and their numerical approximations first in the classical model problem and then in the continuous casting context in the degenerate and nondegenerate forms. After that, we give a detailed outline of the thesis.

1.2 Enthalpy based modeling of phase changes

Mathematical models for phase change phenomena originated in the 19th century. Starting from the works of Lamé, Clayperon, and Stefan, the energy conservation model for freezing of the water was developed and named after Stefan.

We start by describing the classical two-phase Stefan problem that consists

of the heat equation for the solid and liquid phases, which are combined with energy considerations on the phase boundary. The conservation of energy state that

$$\rho \frac{DE(\vartheta)}{Dt} = -\nabla \cdot \mathbf{q},$$

where E is total energy, $\frac{D}{Dt} = \partial_t + \mathbf{b} \cdot \nabla$ material derivative, $\mathbf{q}$ represents the heat flux, ϑ is the temperature, and $\mathbf{b} = (0, 0, b(t))$ describes the movement of the domain (i.e., casting speed in this work). Let ρ denote constant density and c specific heat capacity of the material. According the Fourier law, $\mathbf{q} = -k(\vartheta)\nabla\vartheta$, where k is thermal conductivity. Within a single phase, we can write the internal energy $E(\vartheta) = \rho c(\vartheta)$ and this leads to the heat equation

$$\rho c(\vartheta)(\partial_t + \mathbf{b} \cdot \nabla)\vartheta = \nabla \cdot (k(\vartheta)\nabla\vartheta).$$

Consider now the situation when the domain contains both liquid and solid material. We normalize the temperature so that the phase change happens at constant temperature $\vartheta = 0$. In space-time domain, we denote $Q = \Omega \times [0, T] = Q_s \cup S \cup Q_l$, where S is the liquid solid interface. The material properties change in a discontinuous manner on the surface S, let $[e]_-^+$ denote the discontinuity of the quantity e across S, i.e.,

$$[e]_-^+ = \lim_{x^+ \to \phi} e(x) - \lim_{x^- \to \phi} e(x).$$

From the conservation of the energy, it follows that on the interface

$$[E]_-^+(\mathbf{w} - \mathbf{b}) \cdot \mathbf{n} = [\nabla k(\vartheta)]_-^+ \cdot \mathbf{n} \text{ on } S,$$

where $\mathbf{w}$ denotes the velocity of the interface S. The amount of energy released in the phase change $[E]_-^+ = \rho L$, where L is called the latent heat. So

$$\rho L(\mathbf{w} - \mathbf{b}) \cdot \mathbf{n} = [\nabla k(\vartheta)]_-^+ \cdot \mathbf{n}. \tag{1}$$

The resulting equation is

$$\begin{cases} \rho c(\vartheta)(\partial_t + \mathbf{b} \cdot \nabla)\vartheta & = \nabla \cdot (k(\vartheta)\nabla\vartheta) \text{ in } Q_s \cup Q_l, \\ \rho L(\mathbf{w} - \mathbf{b}) \cdot \mathbf{n} & = [\nabla k(\vartheta)]_-^+ \cdot \mathbf{n} \text{ on } S, \end{cases} \tag{2}$$

which is the classical formulation of the two-phase Stefan problem.

In the theoretical studies, (2) is typically simplified by using Kirchhoff transformation, which is

$$\theta := K(\vartheta) = \int_0^\vartheta k(s)ds,$$

and defining

$$\eta(\theta) = \rho \int_0^\theta \frac{c(K^{-1}(s))}{k(K^{-1}(s))} ds, \ \forall \theta \in R,$$

then (2) becomes

$$\begin{cases} (\partial_t + \mathbf{b}\cdot\nabla)\eta(\theta) & = \Delta\theta \text{ in } Q_s \cup Q_l, \\ \rho L(\mathbf{w}-\mathbf{b})\cdot\mathbf{n} & = [\nabla\theta]^+_-\cdot\mathbf{n} \text{ on } S, \end{cases} \tag{3}$$

such that $\theta = 0$ on S.

The existence of the solution for (3) is in general an open problem. It is not known if the level surfaces S always remain surfaces or may degenerate in regions (called as mushy regions) where the classical formulation looses its sense.

The development of mathematics in the 20th century made it possible the classical models for the phase change to be handled with more general assumptions and the so-called weak formulation of the two-phase Stefan problem was developed. We introduce now the distributional formulation of (3). We multiply (2) by $\psi \in \mathcal{D}(Q) = C_0^\infty(Q)$ (space of smooth functions with compact support), integrating over Q and using partial integration we have

$$\int_{Q_s\cup Q_l} \Delta\theta\psi = -\int_Q \nabla\theta\cdot\nabla\psi + \int_S [\nabla\theta]^+_-\cdot\mathbf{n}\psi, \tag{4}$$

and since $\eta(\theta)$ is continuous across S we get

$$\int_{Q_s\cup Q_l} (\partial_t + \mathbf{b}\cdot\nabla)\eta\psi = -\int_Q \eta(\partial_t + \mathbf{b}\cdot\nabla)\psi.$$

Introducing the characteristic function to liquid phase, i.e., $\chi_l = 1$ in Q_l and $\chi_l = 0$ in $Q\backslash Q_l$, we get by using the divergence theorem

$$\int_Q \rho L(\partial_t + \mathbf{b}\cdot\nabla)\chi_l\psi = -\rho L\int_{Q_l}\chi_l(\partial_t\psi + \mathbf{b}\cdot\nabla\psi) =$$
$$\rho L\int_S \psi(\mathbf{w}-\mathbf{b})\cdot\mathbf{n} = \int_S [\nabla\theta]^+_-\cdot\mathbf{n}\psi.$$

By defining

$$e(\theta) = \eta(\vartheta) + \rho L\chi_l(\theta),$$

and combining this with (1) and (4) we arrive at the single equation

$$\int_Q (-e(\theta)(\partial_t + \mathbf{b}\cdot\nabla)\psi + \nabla\theta\cdot\nabla\psi) = 0, \tag{5}$$

valid for all $\psi \in \mathcal{D}(Q)$. Thus (5) defines a linear functional acting on $\mathcal{D}(Q)$, so called distribution and we can write this formally as

$$(\partial_t + \mathbf{b}\cdot\nabla)e(\theta) - \Delta\theta = 0 \text{ in } \mathcal{D}'(Q). \tag{6}$$

Now all the references to the interface ϕ_0 have disappeared. Thus (5) is more general than the corresponding pointwise equation (2). In particular, it includes

the possibility of the degeneration of the level set $\theta = 0$ into a region without any requirement of smoothness except measurability.

In the distributional formulation, one can not add initial or boundary conditions to (6). This can be done by introducing the enthalpy formulation. Consider the maximal monotone graph H associated with the Heavyside function

$$H(\theta) = \begin{cases} 0 & \theta < 0, \\ [0,1] & \theta = 0, \\ 1 & \theta > 0. \end{cases}$$

For a given temperature θ, we define enthalpy u by the pointwise inclusion

$$u \in \Upsilon(\theta) = \eta(\theta) + \rho L H(\theta). \tag{7}$$

Denote by $\Sigma = \partial\Omega \times]0, T[$ the boundary of Q and assume, for simplicity, the Dirichlet boundary condition for the temperature

$$\theta = d(x,t) \text{ on }, \Sigma, \tag{8}$$

and an initial condition for the enthalpy

$$u = u(0) \text{ on } \Omega \text{ at } t = 0. \tag{9}$$

If ψ denotes a smooth test function such that $\psi(T) = 0$ and $\psi = 0$ on Σ, we obtain from (6) and integration by parts the variational condition

$$\int_Q (-u(\partial_t + \mathbf{b} \cdot \nabla)\psi + \nabla\theta \cdot \nabla\psi) = \int_\Omega u(0)\psi(0), \tag{10}$$

which is valid under suitable regularity conditions on $u(0)$, d, and Ω.

The problem of finding a weak solution to (10) consists of finding a pair $\{u, \theta\}$, such that conditions (7), (8), and (9) hold.

Remark. The equation (10) can also be presented in terms of the enthalpy by defining $\beta = \Upsilon^{-1}$. Then in the weak sense

$$(\partial_t + \mathbf{b} \cdot \nabla)\, u = \Delta\beta(u). \tag{11}$$

As $\frac{\partial\beta}{\partial u} = 0$, for $u \in [0, L]$, this is a degenerate nonlinear heat equation.

1.3 Well posedness of the enthalpy formulations

Theoretical studies of the enthalpy formulation use a wide range of different techniques (see, e.g., [48, 58, 44, 54]). Our approach is practical; we just describe the techniques that are needed in this work. We state the enthalpy formulation first

without convection (**b**=0), as this has been the starting point for the theoretical studies.

Assume that boundary of Ω is split as $\partial\Omega = \Gamma_d \cup \Gamma_n$ and

$$\theta = d(x,t) \text{ on } \Gamma_d \times]0,T[=: \Sigma_d,$$
$$-\frac{\partial\theta}{\partial n} = g(\theta), \text{ on } \Gamma_n \times]0,T[=: \Sigma_n.$$

Let $V(d) \in \{\psi \in H^1(\Omega) |\, \psi_{\Gamma_d} = d\}$. The basic problem in the weak form can be stated as follows:

PROBLEM (P^g): Find $\{u,\theta\}$, $u \in \mathrm{Y}(\theta)$ such that

$$u \in L^2(0,T;L^2(\Omega)), \theta \in L^2(0,T;V(d)),$$

and for all $\psi \in V := L^2(0,T;V(0)) \cap H^1(0,T;L^2(\Omega)) \cap L^\infty(Q)$, with $\psi(T) = 0$ the following equation holds

$$\int_Q (-u\partial_t\psi + \nabla\theta \cdot \nabla\psi) + \int_{\Sigma_n} g(\theta)\psi = \int_\Omega u(0)\psi(0).$$

In the optimal case the theoretical studies will lead to the existence of unique solutions that depends continuously on the data.

Starting from the works of Kamenomostskaya [19] and Oleinik [41], the theory of the gualitative properties of problem (P^g) has been developed by several authors, e.g., Ladyzenskaya [20], Friedman [17], Lions, [23], Damlamian, [9] , resulting to that when g is linear, the mixed boundary value problem is well posed. Generalizations to nonlinear boundary conditions have been treated by Pawlow and Niezgodka, [33], Visintin [56], Cannon and DiBenetto [4], and as a result of these studies (P^g) was found completely well posed under suitable regularity assumptions of the domain, data and, g.

1.3.1 Existence

The general strategy for proving the existence of a solution to (P^g) is to construct a family of approximating problems (P_a) with a unique solution. Then it is shown that these approximations have a limit and that the limit solves the original problem (P^g).

If the approximations are numerically implementable fully discrete problems, the convergence of the numerical method can be shown simultaneously with the existence proof.

Let x_a denote a solution to the approximation (P_a) of (P^g) and a some parameter(s). The basic procedure is the following:

- Approximate problem (P^g) with (P_a) to which exists a unique solution x_a
- Estimate solution x_a a priori in a suitable norm $\|x_a\| \leq C$, independent of a
- Show that the limit x_a, $a \to 0$, say x^* exists
- Show that x^* solves (P^g)

We state few approximations from which we can construct various fully discrete approximations to be discussed in this work. We discuss a priori estimates and the limit process when we introduce our fully discrete approximations.

There are numerous ways to construct (P_a), for example

- Approximate problem (P^g) by smoothing i.e. (P_ε)
- Approximate (P^g) by relaxation $(P_{\delta,\mu})$
- Approximate (P^g) by time discretisation (P_τ)
- Approximate (P^g) with $(P_{\varepsilon,\tau})$
- Approximate (P^g) by spatial discretisation of smoothed problem $(P_{\varepsilon,h})$
- Form fully discrete approximation for (P^g) in space time $(P_{h,\tau})$
- Form fully discrete approximation for (P^g) of the form $(P_{\varepsilon,h,\tau})$
- Approximate (P^g) by $(P_{\delta,\tau})$
- Form fully discrete approximation for (P^g) of the form $(P_{\delta,\tau,h})$

Approximations (P_a) are by no means unique, for example one can form time discrete approximation in various ways. Typically in the literature (see, e.g., [58]), approximations are not distinguished from each others. In the nondegenerate case, a standard approach is to define so-called Galerkin approximation, which is of type (P_h), but this will not work directly and this is why one typically starts from the smoothing approach.

A smoothing approximation P_ε. The regularization of the enthalpy by defining continuous enthalpy as Y_ε (or temperature as $\beta_\varepsilon(u)$) is a typical approach when working all the time on a continuous level. This can be done, for example, as

$$\beta_\varepsilon(s) := \begin{cases} \beta(s), & \text{if } s < 0 \text{ or } s > s_\varepsilon, \\ \varepsilon s & \text{if } 0 \le s \le s_\varepsilon, \end{cases}$$

where $s_\varepsilon = 1 + C\varepsilon$ is such that $\beta(s_\varepsilon) = \varepsilon s_\varepsilon$.

Then from the theory of mildly nonlinear partial differential equations the existence of a unique the solution is typically obtained [44], [58].

A relaxation approximation $P_{\delta,\mu}$. Another approach that leads to the solution of a linear equation heat equation is the phase relaxation technique [57]. The basic idea is to add a delay to the phase change with the so-called phase variable. In this method, Y is split as follows:

$$\mathrm{Y} = \mu I + \tilde{H},$$

where I is the identity, $\tilde{H}$ is still a maximal monotone graph, and $0 < \mu \le \frac{1}{L_\beta}$($L_\beta$ is the Lipschitz constant of β). Denoting $\chi := u - \delta\theta$ as phase variable, the classical constitutive relation reads

$$\chi \in \tilde{H}(\theta) \text{ or } \theta \in \Lambda(\chi) := \tilde{H}^{-1}(\chi).$$

As a substitute for the stationary relation Visintin introduced

$$\delta\chi_t^\delta + \Lambda(\chi^\delta) \ni \theta^\delta, \tag{12}$$

where $\delta > 0$ is a small relaxation parameter. Therefore, (74) incorporates a time delay in the constitutive relation. The original partial differential equation is now replaced by

$$\begin{cases} \mu\theta_t^\delta + \chi_t^\delta - \Delta\theta^\delta = 0, \\ \delta\chi_t^\delta + \Lambda(\chi^\delta) \ni \theta^\delta \end{cases}$$

Visintin [57], showed that this equation converges to the solution of $(P^g), \Gamma_n = \emptyset$ as $\delta \to 0$.

A time discretisation approximation P_τ. This type of approximations comes from the theory of nonlinear semigroups of contractions [3]. This theory leads also to existence, uniqueness, and global regularity results but also suggests some time-discrete algorithms that will be useful when the numerical approximations are discussed. The following approximation is known as the Crandall-Liggett formula [8].

$$\begin{cases} u^0 & = u_0, \\ u^n & -\tau\Delta\beta(u^n) = u^{n-1}. \end{cases}$$

This scheme corresponds to simple backward differences in time, when u is continuous.

An interesting alternatives for simulation purposes comes from the nonlinear Chernoff formula [2], which in simplest form can be presented as

$$\begin{cases} u^0 & = u_0, \\ \theta^n & -\frac{\tau}{\mu}\Delta\theta^n = \beta(u^{n-1}), \\ u^n & = u^{n-1} - \mu[\theta^n - \beta(u^{n-1})], \end{cases} \tag{13}$$

where $\mu \leq \frac{1}{L_\beta}$. In [2] it was shown that this approximation converges to the solution of the problem form $(P^g), \Gamma_n = \emptyset$ as $\tau \to 0$. The reason why the Chernoff formula is interesting for numerical purposes is that (13) is linear.

Method of approximations of type $P_{\varepsilon,h}$. The most popular way to construct this type of approximation is the semi-discrete Galerkin method. The semi-discrete Galerkin finite formulation consists of subdividing the domain Ω into elements and constructing a finite-dimensional subspace $V_h^p \subset V$. Here V_h^p consists of piecewise p-degree polynomial functions spanned by a set of basis functions ψ_i, i=1,..., M_h. For instance, p = 1, for piecewise linear finite elements. As the regularity of the problem is low, we will use piecewise linear approximation in the discrete space denoted by V_h. The Galerkin method consists of finding

$$u_h^\varepsilon(x,t) = \sum_{i=1}^{M_h} u_i^\varepsilon(t)\psi_i(x),$$

and

$$\theta_h^\varepsilon(x,t) = \sum_{i=1}^{M_h} \beta_\varepsilon(u_i^\varepsilon(t))\psi_i(x).$$

Then choosing piecewise linear test functions in $V_h(0)$ one arrives at the following approximation to the weak form of (P^g).

$$\begin{cases} \sum_{i=1}^{M_h} u_i^\varepsilon(0) \int_\Omega \psi_i \psi_j = \int_\Omega u^\varepsilon(0)\psi_j, j = 1, \ldots, M_h, \\ \sum_{i=1}^{M_h} \dfrac{\partial u_i^\varepsilon(t)}{\partial t} \int_\Omega \psi_i \psi_j + \theta_i^\varepsilon(t) \int_\Omega \nabla\psi_i \cdot \nabla\psi_j = 0,\ j = 1, \ldots, M_h. \end{cases}$$

By defining suitable projection $P_h u^\varepsilon(0) = u_h^\varepsilon(0)$ for the initial value and identifying the piecewise linear functions of V_h with the vectors of $\mathbb{R}^{M_h}$ containing their nodal values $U(t) = (u_1^\varepsilon(t), \ldots, u_{M_h}^\varepsilon(t))^T \in \mathbb{R}^{M_h}$ and $\Theta(t) := \beta_\varepsilon(u_1^\varepsilon(t), \ldots, u_{M_h}^\varepsilon) \in \mathbb{R}^{M_h}$ we get

$$\begin{cases} \mathbf{M}U(0) = \mathbf{M}u_h(0) \text{ at } t = 0, \\ \mathbf{M}\dfrac{\partial U(t)}{\partial t} + \mathbf{A}\Theta(t) = 0. \end{cases}$$

Components of the stiffness matrix $\mathbf{A} \in \mathbb{R}^{M_h \times M_h}$ are computed as

$$\int_\Omega \nabla u_i \nabla \psi_j = a_{ij},$$

and the for the mass matrix $\mathbf{M} \in \mathbb{R}^{M_h \times M_h}$

$$\int_\Omega \psi_i \psi_j = m_{ij}.$$

1.3.2 Uniqueness and continuous dependence

The proof of uniqueness is typically indirect and consists of showing that with the same data the integral of the difference of two possible different solutions is then zero.

Let $u, \hat{u}$ be two different solutions to the P^g and assume that $\Gamma_n = \emptyset$. After integrating, it holds that

$$\int_Q (u - \hat{u})\left(\frac{\partial \psi}{\partial t} + \alpha\Delta\psi\right) = 0, \psi \in V, \tag{14}$$

where $\psi \in V$ is such that $\Delta\psi \in L^2(Q)$ and $\frac{\partial\psi}{\partial n} \in L(\Sigma)$. Then we denote

$$\alpha = \begin{cases} \dfrac{\theta - \hat{\theta}}{u - \hat{u}} & u \neq \hat{u}, \\ 0 & u = \hat{u}, \end{cases}$$

for $u \in \Upsilon(\theta)$. Approximating α by a sequence of smooth functions α_n, we define ψ_n to be the solution

$$\int_Q (\frac{\partial \psi_n}{\partial t} + \alpha_n \Delta \psi_n) = f. \tag{15}$$

where $f \in \mathcal{D}(Q)$. Replacing ψ with ψ_n in (14) then

$$I = \int_Q (u - \hat{u}) f = \int_Q (u - \hat{u})(\alpha_n - \alpha) \Delta \psi_n. \tag{16}$$

Estimates on the solution of (15) will then imply that $|I| \to 0$ as $n \to \infty$, [15].

The continuous dependence in this type of technique is shown by developing previous ideas. By taking two different sets of data, (16) can be bounded by this difference under some suitable assumptions of the data and the boundary conditions. For a problem $(P^g), \Gamma_n = \emptyset$ this means

$$\int_Q |u - \hat{u}| \leq C \left\{ \int_\Omega |u(0) - \hat{u}(0)| + \int_Q |d - \hat{d}| \right\},$$

where constant C is independent of T.

Another way of the showing the uniqueness and continuous dependence of L^1 type is to use following technique [58]. One first shows the qualitative properties for the smoothed problem, i.e,

$$\langle \partial_t u^\varepsilon, \psi \rangle + \langle \nabla \theta^\varepsilon, \nabla \psi \rangle = 0, \forall \psi \in V(0),$$

and then using the regularity of the solution and passing to the limit,

$$\int_\Omega |u(t) - \hat{u}(t)| \leq \int_\Omega |u(0) - \hat{u}(0)|.$$

1.4 Numerical approximations of the enthalpy based models

By numerical approximation, we mean in this section a fully discrete problem. Numerical approximations to the free boundary problems were introduced the in 1950s [13]. The enthalpy formulation was first used by Rose [46] using explicit approximation and assuming that the problem is well posed.

The techniques of showing the convergence of the numerical approximations are essentially based on the existence procedure of section 1.3.1. Solomon [51] and D. R. Atthey [1] applied explicit approximations. Smoothed implicit approximations were introduced by Meyer [30]. The finite element method for a approximation of a problem type $(P_{\varepsilon,\tau,h})$ for (P^g) , when $\Gamma_n = \emptyset$ was introduced by Ciavaldini [7]. Then without regularization, approximations of type $(P_{\tau,h})$ were introduced by White [60] and Elliot [14].

The numerical approximations based on the theory on nonlinear semigroups of contractions were introduced by Rogers, Brezis, and Berger [2] and, e.g., [53, 55, 40].

In the 1990s, the development of the enthalpy based numerical approximations lead also to the adaptive methods. These methods have been studied in, e.g., [38, 34]. We restrict our studies to the fixed grid settings.

We describe some of these approximations assuming that $\Gamma_n = \emptyset$. Let U^n, Θ^n be piecewise linear approximations of $u_{h,t}(x,t)$, $\theta_{h,t}(x,t)$ respectively at $t = n\tau, n = 1, \dots N$.

Numerical approximations of type $P_{\varepsilon,h,\tau}$. These result in the mildly nonlinear equations of type

$$\mathbf{M}U^n + \tau\mathbf{A}\beta_\varepsilon(U^n) = \mathbf{M}U^{n-1}$$

or

$$\mathbf{M}\mathrm{Y}_\varepsilon(\Theta^n) + \tau\mathbf{A}\Theta^n = \mathbf{M}\mathrm{Y}_\varepsilon(\Theta^{n-1}).$$

Both of these equations can be solved using the theory of M-functions, resulting in the nonlinear Gauss Seidel method [42].

Numerical approximations of type $P_{h,\tau}$. The following approximation was introduced by White [61],

$$\mathbf{M}U^n + \tau\mathbf{A}\beta(U^n) = U^{n-1},$$

and the convergence of the Gauss Seidel method follows by using the properties of the matrices $\mathbf{A}$ and $\mathbf{M}$. The formulation

$$\mathbf{M}\mathrm{Y}(\Theta^n) + \tau\mathbf{A}\Theta^n = \mathbf{M}\mathrm{Y}(\Theta^{n-1}),$$

is not possible, as Y is now a graph. It can be replaced as

$$\mathbf{M}U^n + \mathbf{A}\Theta^n = \mathbf{M}U^{n-1},$$

but as U^n is not continuous, the theory of M-functions fails. Elliot [14] has introduced a converging algorithm for this type of formulation.

It is straightforward to form a fully discrete approximation for the Chernoff formula

$$\begin{cases} \mathbf{M}\Theta^n & +\frac{\tau}{\mu}\mathbf{A}\Theta^n = \mathbf{M}\beta(U^{n-1}), \\ U^n & = U^{n-1} + \mu[\Theta^n - \beta(U^{n-1})]. \end{cases}$$

The existence of a unique solution is then obtained from the theory of linear algebraic equations.

Similarly to the phase relaxation, the algebraic problem is of the form

$$\begin{cases} \mu\mathbf{M}\Theta^n + \mathbf{M}\chi^n + \tau\mathbf{A}\Theta^n = \mathbf{M}\Theta^{n-1} + \mathbf{M}\chi^{n-1}, \\ \delta\chi^n + \tau\Lambda(\chi^n) = \delta\chi^{n-1} + \tau\Theta^{n-1}. \end{cases}$$

We have not considered the boundary conditions in the approximations, but at least linear boundary conditions can be applied straightforwardly to the approximations. We discuss in detail how the boundary conditions can be added to the approximations later.

Numerical error estimates. In the case of linear boundary conditions, the error estimates depend on the shape and dimension of the domain, the regularity of the initial data, and the numerical integration method used. Error estimates were studied in [18, 36, 35], when the problem is of the type $P_{\varepsilon,\tau,h}$. Roughly speaking the basic rate of convergence in $L^2(Q)$ norm is $O(h^{\frac{1}{2}})$ when relation $\tau \sim h \sim \varepsilon$ is used. If the approximation is of type $P_{\tau,h}$ the same rate of convergence to the temperature has been shown. As u is discontinuous, error estimates to the enthalpy are limited to the $H^1(0,T;H^{-1}(\Omega))$ norm. Error estimates are discussed in e.g. [55, 31, 7, 28, 16, 36].

In the case of nonlinear boundary conditions, Nochetto [37] obtained error estimates in L^2 norm, when the solution is in the class of nondecreasing in time, which is not the case in the continuous casting processes. Thus we are limited to the methods to which we can show the convergence and the wide literature of the numerical analysis of the error estimates to the two-phase Stefan problem is not applicable to (P^g) in general level.

1.5 Numerical efficiency of the enthalpy formulations

Numerical efficiency depends on the proper combination of the available solution algorithm to the algebraic problem and accuracy of the approximation.

Within a given approximation, one may also consider different formulations, then one may prefer the method that is computationally more efficient. For example, which formulation is computationally more efficient

$$\mathbf{M}U^n + \tau\mathbf{A}\beta_\varepsilon(U^n) = \mathbf{M}U^{n-1},$$

or

$$\mathbf{M}\mathrm{Y}_\varepsilon(\Theta^n) + \tau\mathbf{A}\Theta^n = \mathbf{M}U^{n-1}\,?$$

Clearly, taking Θ^n as solution variable is more efficient, as the diffusion part is linear. In every iteration, one has to compute the value of the nonlinear function. If this evaluation is made to the diffusion part in 3D using the finite difference method, it has to be evaluated seven times in each iteration. If the nonlinearity is on the diagonal, it has to be computed only once in Gauss Seidel iterations.

As far as the iterative methods are concerned, however, the most efficient solution method to the approximations of type $(P_{h,\tau})$ is one defined by Elliot [14], as it allows to use over relaxation to accelerate the convergence. An Important feature in the iterative methods is the use of incomplete iteration [11]. This means that the stability of the solution can be preserved using some practical stopping criteria, and this is used especially in industrial applications. The

choice of stopping criteria is then made by comparing the results with different stopping criteria [26].

In the case of linear algebraic equations, there are two main approaches, iterative and direct solvers. The choice of the method depends radically on the number of the iterations needed in the iterative process, and this depends on the nature of the problem. In the diagonally dominant transient case, the iterative solvers can be very efficient. Thus, finding the most efficient solution method is a case-by-case study.

1.6 Applications to the continuous casting processes

The applicability of the model (P^g) to the continuous casting processes is rather limited. An important application for the problem (P^g) is to approximate the situation when the process is in a steady state. As the convection highly dominates the system, one can form a model approximating a steady state situation by neglecting the heat conductivity to the casting direction. This kind of simplification was used in the first simulations.

Simulation of the transient continuous casting processes consists of solving the following problem

PROBLEM (P^b): Find $\{u, \theta\}$, $u \in \mathrm{Y}(\theta)$ such that

$$u \in L^2(0,T;L^2(\Omega)), \theta \in L^2(0,T;V(d)),$$

and for all $\psi \in V$ following equation holds

$$-\int_Q u(\partial_t \psi + \mathbf{b}\cdot\nabla\psi) + \int_{\Sigma_n} u\psi\mathbf{b}\cdot\mathbf{n} + \int_Q \nabla\theta\cdot\nabla\psi + \int_{\Sigma_n} g(\theta)\psi = \int_\Omega u(0)\psi(0).$$

Qualitative properties. In the continuous casting processes where $(b \neq 0)$, the Stefan problem is a nontrivial variant of the model problem. Compared to the huge amount of available results in the case in which $b = 0$, only a few studies can be traced.

Theoretical studies of the model coming from the (P^b) were studied by Rogriques and Yi [45], where the existence and uniqueness were proven. They considered a general monotone nonlinear nondecreasing boundary condition to take into account the cooling using the Dirichlet boundary condition both on inflow and outflow boundaries. Stefan problem with enthalpy dependent convection was studied in [62], where the existence of the solution was shown with the following boundary condition

$$\mathbf{b}\cdot\mathbf{n}u - \frac{\partial\theta}{\partial n} = g(\theta).$$

By assuming the Dirichlet boundary condition they showed also uniqueness and error estimates between regularized and continuous problems.

Another type of approach introduced by Rulla [49] considered prescribed convection with the nonlinear boundary condition, however under various impractical limitations concerning boundary conditions [44].

Numerical approximations. Numerical approximations to the (P^b) are given by Chen *et al.* [6], where the following semi-implicit approximation was considered with the regularized enthalpy

$$\begin{cases} u^0 & = u_0, \\ u^n & -\tau\Delta\theta^n = u^{n-1} - \tau\mathbf{b^{n-1}}\cdot\nabla u^{n-1}, \quad 1 \le n \le N. \end{cases}$$

The fully discrete problem also includes the implicit nonlinear boundary condition and the solution was obtained with the nonlinear Gauss Seidel method.

Let us discuss the stability condition of this type of approximation. For simplicity, assume the linear case. Then, an FE-approximation looks like

$$(\mathbf{I} + \tau\mathbf{K})\Theta^n = (\tau c\mathbf{C} + \mathbf{I})\Theta^{n-1},$$

with material parameter c, which also includes the velocity constant b. Here $\mathbf{K}$ stands for the square matrix $\mathbf{M^{-1}A}$, $\mathbf{C} = \mathbf{M^{-1}\hat{C}}$ denotes the approximation of the convection term, and $\mathbf{I}$ is the identity matrix. In order to calculate the stability condition (the condition number of the iteration matrix must be less than one), we have the following estimates for the eigenvalues, with the discretization parameter h

$$\mathbf{K} = o(\frac{1}{h^2}), \mathbf{C} = o(\frac{1}{h}).$$

The stability condition of the numerical solution is now

$$1 + \frac{c\tau}{h} < 1 + \frac{\tau}{h^2},$$

which is true if

$$h < \frac{1}{c}.$$

The casting speed b is typically of order 10^{-1}. The volumetric specific heat is typically of order 10^4. Thus the discretization with respect to the space variable is restricted in the class of $h < 10^{-3}$. This would lead to order of 10^9 degrees of freedom in practical approximations.

Another type of approximation was introduced in [5], where the characteristic method and the phase relaxation formula were combined. In the phase relaxation with the prescribed convection, the approximation is

$$\begin{cases} \mu\theta_t^\delta + \chi_t^\delta + \mathbf{b}\cdot\nabla(\mu\theta_t^\delta + \chi_t^\delta) - \Delta\theta^\delta = 0, \\ \delta\chi_t^\delta + \Lambda(\chi^\delta) \ni \theta^\delta. \end{cases}$$

Now by using the method of characteristics one arrives at the coupled system with the linear diffusion part, namely

$$\begin{cases} \mu\bar{\partial}\theta^n + \bar{\partial}\chi^n - \Delta\theta^n & = 0 \\ \delta\bar{\partial}\chi^n + \Lambda(\chi^n) & = \theta^n \end{cases}',$$

where $\bar{\partial}$ denotes the characteristics approximation. Compared to the case in which $b = 0$, this algorithm requires a Picard type of iteration, as in the update formula the temperature is implicit. The reported number of the iterations were $3 - 5$ in a one-dimensional case with the Dirichlet boundary condition when the iteration was stopped when the L^∞ difference between iterations was less that 0.001, with the time step 0.05.

The characteristic Galerkin method with adaptive error control in 2D was introduced by Chen, Nochetto, and Schmidt [34], and it can be presented as

$$\begin{cases} u^0 & = \bar{u}(0), \\ u^n & -\tau\Delta\theta^n = \bar{u}^{n-1}, \quad 1 \leq n \leq N, \end{cases}$$

where $\bar{u}^n$ denotes the characteristic approximation. They used the linearized boundary condition in order to get posteriori error estimates.

Domain decomposition methods for continuous casting problems using both the characteristic method and upwinding approximation for the convection term in 2D were studied in [21].

1.7 Industrial applications

The basic model problem assumes that the solidification is isothermal and the free boundary is expected to have a smooth shape, which is typical for pure materials. The major difference between the continuous model problem and in the industrial applications is that most of the time we are dealing with the alloys. In the alloys there are several chemical elements in the material, each having different melting points. As a result, in the phase change, the latent heat is released in a certain temperature range rather than at a single temperature. The phase change region has a crystalline structure consisting of equi-axed grains and the solid/liquid interface has a complex shape that is not necessarily smooth or continuous. The enthalpy formulation is still the most useful approach, since it can be presented as

$$u = \Upsilon(\theta) = \eta(\theta) + \rho L H_r(\theta),$$

where H_r represents the phase fraction. Thus in various applications one might use the theory of mildly nonlinear partial differential equations.

In the case of copper casting, sometimes it is preferred to have as pure copper as possible leading to 99.95% content of the pure copper, which can be viewed as Stefan problem.

If the enthalpy is continuous in the alloys, it makes it possible to apply the theory of more regular problems to the continuous casting processes. This non degeneracy property combines with the weak formulation. This explains the popularity of the enthalpy based formulations as the simple weak formulation of

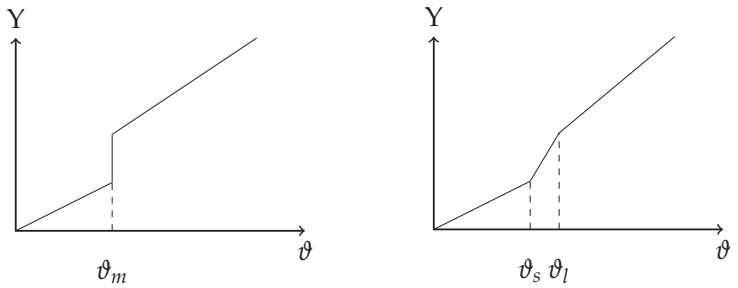

(a) Isothermal phase change

(b) Non isothermal phase change

FIGURE 3 Enthalpy in pure materials (a) and in alloys (b)

nondegnerate problems allows to track the solid liquid interfaces as level sets of the temperature.

It is possible to use upwinding or characteristic approximation [12] to the convection term. When the convection is not needed in the model, one may use standard approaches based on the finite element or finite difference approximations.

The fully discrete approximations we have presented can now be considered with fixed ε. The usage of Kirchhoff transformation θ or enthalpy u as a solution variable in the algebraic system is not a common practice. Typically in the industrial applications, the approximations are stated as a function of temperature ϑ, which is not most efficient way computationally.

One would naturally hope that numerical analysis would be widely available in this case. However, this is not true for what comes to the error estimates at a general level. When both the convection term and the nonlinear boundary conditions are present in the equation, there are no error estimates. In the case of $\mathbf{b} = \mathbf{0}$, Zlamal [63] showed linear rate of convergence for the temperature in L^∞ norm, for monotone nonlinear boundary condition. For a non degenerate problem, semi-discrete Chernoff approximation was shown to have linear rate of convergence in the case of $\Gamma_n = \emptyset, \mathbf{b} = \mathbf{0}$ in [27].

As discussed, typically in industrial applications some simplifications are made. By assuming a sufficiently fast casting speed, in the steady state situation the model equation

$$\frac{\partial u}{\partial t} + b\frac{\partial u}{\partial z} = \frac{\partial^2 \theta}{\partial x^2} + \frac{\partial^2 \theta}{\partial y^2} + \frac{\partial^2 \theta}{\partial z^2} \tag{17}$$

can be simplified. Since (17) is highly convection dominated, one can neglect the heat conduction to the casting direction by setting $\frac{\partial^2 \theta}{\partial z^2} = 0$ and develop a $2D$ simulation model for the steady state situation, $\frac{\partial u}{\partial t} = 0$. The review of these kinds of methods can be found in [59]. Other way is to set $\frac{\partial^2 \theta}{\partial y^2} = 0$ in (17), and in this case transient simulations can also be performed [25].

Applications in 3D have also been considered in [10], where method of characteristic method were applied and the temperature ϑ was used as the solution

variable in the nonlinear algebraic system.

The solution techniques are essentially based on the use of the nonlinear Gauss Seidel method in the algebraic system, and results of applying the Chernoff type of formula to the industrial applications have not been reported. The reason for this is probably that, in the case of continuous enthalpy the problem can be stated as a regular problem and the theory and algorithms coming from the of nonlinear semigroups of contractions are not needed. The treatment of the implicit boundary condition typically uses Newton Raphson iteration on the boundary or linearization.

1.8 Outline

First we introduce the basic continuous casting process and how the boundary conditions are formulated for the continuous model. Then, we discuss the qualitative properties of the model both nondegenerate and degenerate cases. We define four different types of fully discrete approximations to the continuous model with the variable casting speed. In order to avoid stability issues related to the convection dominated problem, we have two basic strategies: Characteristic method and use of upwinding approximations. We are also able to combine Chernoff type formulas with these approximations. We present here the ideas on time level n, $n = 1, \ldots, N$.

First approximation. This approximation is based on the method of characteristics, which is standard for the smoothed problem (alloys). At the semidiscrete level, this can be expressed as

$$\begin{cases} u^0 = u(0), \\ \bar{u}^{n-1} = u^{n-1}(x - \tau \mathbf{b}^{n-1}, t^{n-1}), \\ u^n - \tau \Delta \theta^n = \bar{u}^{n-1}. \end{cases}$$

We are able to prove the convergence without regularization (in free boundary form). Our technique, however, requires assumption $b\tau \leq h$ in the free boundary form. The boundary condition will be taken into account in an implicit manner.

Second approximation. The second approximation uses upwinding approximation for the convection term and can be expressed as

$$\begin{cases} u^0 = u(0), \\ u^n + \tau \mathbf{b} \cdot \nabla u^n - \tau \Delta \beta(u^n) = u^{n-1}. \end{cases}$$

We are able to show the convergence without any stability restrictions.

Third approximation. This can be viewed as a combination of the nonlinear Chernoff formula with the method of characteristics. Discrete in time approximation reads as follows, taking into account the algebraic correction formula with the method of characteristic

$$u^n = \bar{u}^{n-1} + \mu[\theta^n - \beta(\bar{u}^{n-1})],$$

we get the following approximation

$$\begin{cases} u^0 = u(0), \\ \bar{u}^{n-1} = u^{n-1}(x - \tau \mathbf{b}^{n-1}, t^{n-1}), \\ \theta^n - \frac{\tau}{\mu}\Delta\theta^n = \beta(\bar{u}^{n-1}), \\ u^n = \bar{u}^{n-1} + \mu[\theta^n - \beta(\bar{u}^{n-1})]. \end{cases}$$

We assume that the boundary condition is taken into account in an explicit manner. In this way we have a wider range of available efficient numerical solution methods. The assumption $b\tau \leq h$ is required for the convergence in the free boundary form.

Fourth approximation. We are also able to combine upwinding approximation and the Chernoff formula. Taking into account the algebraic correction formula

$$u^n = u^{n-1} + \mu[\theta^n - \beta(U^{n-1})],$$

we have also that in the weak sense

$$\mathbf{b} \cdot \nabla u^n = \mathbf{b} \cdot \nabla(u^{n-1} + \mu[\theta^n - \beta(u^{n-1})]).$$

This suggests the following approximation

$$\begin{cases} u^0 & = u(0), \\ \theta^n & + \tau \mathbf{b} \cdot \nabla\theta^n - \frac{\tau}{\mu}\Delta\theta^n = \beta(u^{n-1}) + \tau \mathbf{b} \cdot \nabla[\beta(u^{n-1}) - \frac{1}{\mu}u^{n-1}], \\ u^n & = u^{n-1} + \mu[\theta^n - \beta(u^{n-1})]. \end{cases}$$

Using stability assumption $b\tau < Ch$, we show the convergence of the method.

Implementation. Compared to the commercial software we are able to use some obvious benefits. As we have a simple parallelepiped domain, the use of finite difference method, leading to low memory storage, is the natural approach. Taking the benefit of this shape we can use various kinds of efficient numerical solution methods and we discuss some of these.

We describe the implementation using matrix formulations. We give numerical examples using the linear boundary condition and compare the numerical efficiency of the approximations in an academic test case.

Industrial applications. We use actual material data [32], and show how they can be applied to the given approximations. We determined that in the case of alloys, the iterative method of the form

$$\begin{cases} \theta^0 = \beta(u(0)), \\ \Upsilon(\theta^n) + \tau \mathbf{b} \cdot \nabla\Upsilon(\theta^n) - \tau\Delta\Theta^n = \Upsilon(\theta^{n-1}), \end{cases}$$

is computationally more efficient compared to the defined free boundary solution algorithm with the upwinding approximation.

We validate the implementations against existing industrial 2D software that can compute the steady state.

After that we are in a position to start comparing given approximations in transient situations. We start with a simple zone cooling model and then move to the detailed model.

Finally, we make some conclusions about the numerical efficiency of the given approximations in the industrial-scale problems.

2 MATHEMATICAL MODEL

In this chapter, we first describe a typical continuous casting machine and discuss how it can be linked to its environment through the boundary conditions. Various types of boundary conditions are used in industrial applications, and we discuss some of them. As a result we describe a general nonlinear boundary condition that it is locally monotone and Lipschitz continuous with respect to temperature. Then we introduce the corresponding model and study its qualitative properties. We use the isothermal formulation for the phase change (i.e., discontinuous temperature enthalpy relation), in order to work on as general level as possible.

2.1 Continuous casting machine

Continuous casting is a process where molten steel is solidified into a slab to be subsequently rolled in the finishing mills. Liquid steel flows out of the ladle into the tundish and then into a water-cooled copper mold. Solidification begins in the mold and continues due to the water cooling on the surface until the slab is fully solidified and can be cut. The slab is bent during the solidification to reduce the height of the machine and the hydraulic pressure to the molten steel.

To start a cast, the mold bottom is sealed by a steel dummy bar, which is held in place hydraulically by the Straightener Withdrawal Units. This bar prevents liquid material from flowing out of the mold. The steel poured into the mold is partially solidified, producing a metal strand with a solid outer shell and a liquid core. In this primary cooling area, once the steel shell has a sufficient thickness, about 10 to 20 mm, the Straightener Withdrawal Units are started, and proceed to withdraw the partially solidified strand out of the mold along with the dummy bar. Liquid metal continues to pour into the mold to replenish the withdrawn steel at an equal rate. The withdrawal rate depends on the cross-section, grade and quality of steel being produced, and may vary typically between 0.3 and 2 meters per minute. The casting time is typically $1.0 - 1.5$ hours per heat to avoid excessive ladle heat losses. The new heat is then started by changing the ladle.

Upon exiting the mold, the strand enters a roller containment section and secondary cooling chamber, in which the solidifying strand is sprayed with water or a combination of water and air (referred to as Air-Mist) to promote solidification. This area preserves the integrity of the cast shape and product quality. Larger cross-sections require extended roller containment. Once the strand is fully solidified and has passed through the Straightener Withdrawal Units, the dummy bar is disconnected, removed, and stored. Following the straightener, the strand is cut into individual pieces of cast products: slabs, blooms, billets, rounds, or beam blanks, depending on the machine design.

Billets have cast section sizes up to about 20 square centimeters. Bloom sections sizes typically range from approximately 20 centimeters square to about 50 centimeters. Round castings include diameters of approximately 10 to 50 centimeters. Slab castings range in thickness from 5 to 40 centimeters, and up to 200 centimeters wide. The width-to-thickness ratio, referred to as the, "aspect ratio", is used to determine the dividing line between blooms and slabs. An aspect ratio of 2.5:1 or greater constitutes an as-cast product referred to as a slab. We will use the general term slab hereafter, to denote the cast product.

To summarize, the casting process is compromised of the following sections:

1. A tundish, located above the mold to feed liquid steel to the mold at a regulated rate.
2. A primary cooling zone or water-cooled copper mold through which the steel is fed from the tundish, to generate a solidified outer shell sufficiently strong enough to maintain the strand shape as it passes into the secondary cooling zone.
3. A secondary cooling zone in association with a containment section positioned below the mold, through which the still mostly-liquid strand passes and is sprayed with water or water and air to further solidify the strand.
4. Unbending and Straightening section.
5. A severing unit (cutting torch or mechanical shears) to cut the solidified strand into pieces for removal and further processing.

As our goal is to approximate the temperature distribution of the slab, we will need to model the primary cooling region (mold), secondary cooling region (water cooling and roll contact), and the simulation area should extend to the region where the slab is fully solidified, typically $15 - 20$ meters. Next, we introduce these regions in more detail.

Mold. The main function of the mold is to establish a solid shell sufficiently strong to contain its liquid core upon entry into the secondary spray cooling zone. Key product properties are shape, shell thickness, uniform shell temperature distribution, defect-free internal and surface quality with minimal porosity, and few non-metallic inclusions.

The mold is basically an open-ended box structure, containing a water-cooled inner lining fabricated from a high purity copper alloy. Mold water transfers heat from the solidifying shell. The working surface of the copper face is

often plated with chromium or nickel to provide a harder working surface, and to avoid copper pickup on the surface of the cast strand, which can facilitate surface cracks on the product.

Mold heat transfer is both critical and complex. Mathematical and computer modeling are typically utilized in developing a better understanding of mold thermal conditions, and to aid in proper design and operating practices. Heat transfer is generally considered a series of thermal resistances as follows:

1. Heat transfer through the solidifying shell. This is taken into account in the enthalpy formulation itself in which the phase change is taking into account.
2. Heat transfer from the steel shell surface to the copper mold outer surface. One may use several types of boundary conditions for this purpose. To simulate the temperature distribution of the slab, it suffices that the total heat flux can be measured.
3. Heat transfer through the copper mold. One may define a coupled model for this purpose, e.g., [43], but typically the main focus is on the secondary cooling region in which the cast can be controlled via water sprays.
4. Heat transfer from the copper mold inner surface to the mold cooling water. The total cooling energy can be measured from the difference of the ingoing and outcoming water. This information is sufficient to approximate the temperature distribution of the slab.

Secondary Cooling. Typically, the secondary cooling system is comprised of a series of zones, each responsible for a segment of controlled cooling of the solidifying strand as it progresses through the machine. The sprayed medium is either water or a combination of air and water.
Roll Contact. Depends on the type of roll and contact area. Rolls can be internal cooled or not, and a different value of the heat transfer coefficient has to be used depending on the roll type.
Radiation. Dominates heat transfer whenever seondary cooling or roll contacts are not active until sufficiently low temperature is achieved, and then natural convection (air convection) dominates. This means that the boundary condition in these area is combination of the linear part (natural convection) added with the Stefan Boltzmann radiation term.

2.2 Boundary conditions

In the industrial simulations one can find numerous ways of modeling both mold and secondary cooling. There is no mutual agreement on which type of boundary conditions are the best. The heat transfer coefficient on the boundary plays a major role and is typically calibrated to measurements with the used steel grade in the actual machine to be modeled. Our task is not to compare the different types of boundary conditions rather than compare different kind of approximations with various grid sizes. Nevertheless, the boundary conditions we will use

have been used to describe the continuous casting machine at the industrial level, and this suffices for our purposes. We will briefly discuss different types of approaches.

We first take a look at how the boundary conditions are combined from some basic cooling sequences on the secondary cooling region. To summarize, after the mold region the cooling happens repeatedly as a sequence of the water cooling, radiation, roll contact, radiation, water cooling... More precising, let Ω denote the slab in R^3 with the boundary Γ and Γ_{in} denote the part of the boundary Γ through which the material is spilled to the casting process. The part $\Gamma \setminus \Gamma_{\text{in}}$ is further divided into six groups of non overlapping subsets: $\Gamma \setminus \Gamma_{\text{in}} = \Gamma_{\text{mold}} \cup \Gamma_{\text{cool}} \cup \Gamma_{\text{rad}} \cup \Gamma_{\text{roll}} \cup \Gamma_{\text{out}} \cup \Gamma_{\text{sym}}$. Furthermore let n_{cool} denote the number of the water contact areas between rolls, n_{roll}, is the number of the rolls, and n_{rad} is the number of the radiation areas. Thus

$$\Gamma_{\text{cool}} = \underset{n_{\text{cool}}}{\cup} \Gamma^i_{\text{cool}},$$

$$\Gamma_{\text{roll}} = \underset{n_{\text{roll}}}{\cup} \Gamma^i_{\text{roll}},$$

$$\Gamma_{\text{rad}} = \underset{n_{\text{rad}}}{\cup} \Gamma^i_{\text{rad}}.$$

The basic cooling sequence in the casting direction after the mold region is then

$$\Gamma^i_{\text{cool}} \cup \Gamma^i_{\text{rad}} \cup \Gamma^i_{\text{roll}} \cup \Gamma^{i+1}_{\text{rad}}, \quad i = 1, \cdots, n_{\text{cool}},$$

and on the roll support area

$$\Gamma^{2n_{\text{cool}}+i}_{\text{rad}} \cup \Gamma^{n_{\text{cool}}+i}_{\text{roll}} \cup \Gamma^{2n_{\text{cool}}+i+1}_{\text{rad}}, \quad i = n_{\text{cool}}, \cdots, n_{\text{roll}},$$

and on the rest of the slab there is just natural convection and radiation. In the zone cooling model, these basic sequences are combined. In the FIGURE (**??**) we see how the heat transfer coefficient typically behaves in the detailed model.

Mold. Based on the temperature difference of the incoming and outgoing water in the mold, we can compute the total heat flow from the slab in the mold region

$$q = (\vartheta_{\text{in}} - \vartheta_{\text{out}})\rho_{\text{w}} c_{\text{w}} Q_{\text{w}},$$

where ϑ_{in} is the incoming water temperature, ϑ_{out} the outgoing water temperature, density of the water is ρ_{w}, and c_{w} its heat capacity. The quantity Q_{w} is the water flow rate.

However, the spatial distribution of heat flow is not known, at least not without detailed modeling of the mold. Naturally heat flow from liquid is greater than in the shell region. Thus the total heat flow is distributed so that it decreases towards to the mold end and corners. Thus the boundary condition

$$-\frac{\partial \theta}{\partial n} = q(x,t), \text{ on } \Gamma_{\text{mold}},$$

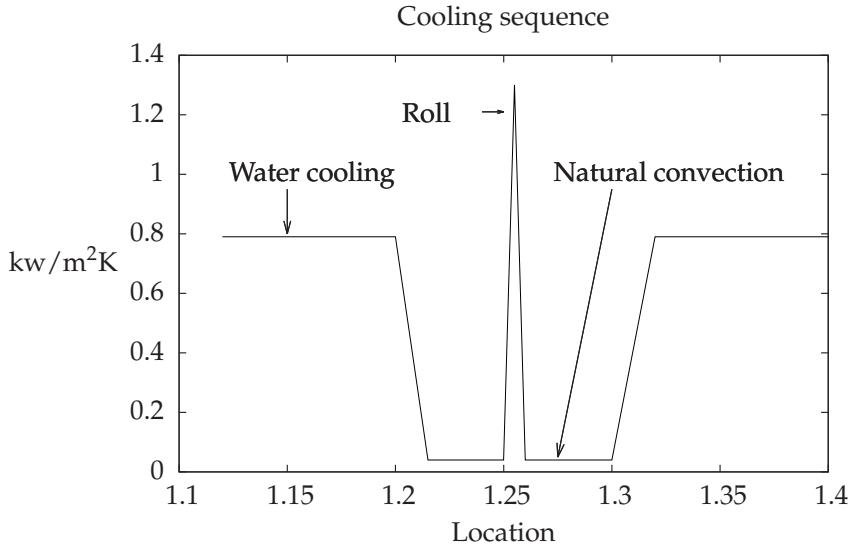

FIGURE 4 Variation of the heat transfer coefficient on the boundary

is one possible choice. Even thought the heat flux can be distributed, the starting point of the shell formation is hard to track.

Another possibility is to apply temperature-dependent heat transfer coefficient in such a manner that heat transfer decreases as the strand surface cools. So the boundary condition could be of the form (recall that $K^{-1}(\theta) = \vartheta$)

$$-\frac{\partial \theta}{\partial n} = v(\vartheta)(\vartheta - \vartheta_{\mathrm{m}}), \text{ on } \Gamma_{\mathrm{mold}},$$

where ϑ_{m} is the temperature of the mold surface and v is the heat transfer coefficient. As we know the total heat flow, we then can construct simple heat equation for approximating the temperature distribution in the mold by defining boundary conditions for the mold domain in such a manner that measured heat flow is satisfied. This leads to a coupled system of partial differential equation [43].

It has been observed that these different kinds of boundary conditions give rather different surface temperature profiles in the mold region, but as soon as the cast is pulled to the secondary cooling area the temperature profiles coincide if the total fluxes are equal, due the reheating effect of the liquid core [25].

Secondary cooling. On the secondary cooling region Γ_{cool}, the influence of the water cooling, together with the Stefan Boltzmann radiation law will be used, thus

$$-\frac{\partial \theta}{\partial n} = \bar{v}(\vartheta, x, t)(\vartheta - \vartheta_{\mathrm{ex}}) + \sigma\epsilon(\vartheta^4 - \vartheta_{\mathrm{amb}}^4), \text{ on } \Gamma_{\mathrm{cool}}, \tag{18}$$

where $\bar{v} > 0$ is the heat transfer coefficient, σ is the emissivity and ϵ is the Stefan Boltzmann constant. Term ϑ_{amb} is given ambient temperature, which is hard to define in practice and one could also drop the radiation since water cooling dominates.

The function $\bar{v}$ may have various forms, e.g., [24]

$$\bar{v} = L(\vartheta)(aW^c),$$

where L represents the Leidenfrost effect. It is known that with decreasing surface temperature a critical value, the Leidenfrost temperature typically about $900^\circ C$ in steel, is reached whereupon the mechanism of heat transfer changes from film boiling to transition boiling. At higher temperatures the heat transfer coefficient is relatively insensitive to surface temperature (under conditions of film boiling), but increases sharply below the Leidenfrost temperature. Above this temperature, the surface temperature is sufficiently hot to create a steam layer through which the water droplets do not fully penetrate. As the temperature decreases, a change in the heat transfer mechanism occurs with boiling on the surface. This temperature depends on the surface quality, amount of water, and steel grade.

The choice of secondary cooling model effects to the available theoretical results dramatically. If one uses Leidenfrost effect in the water cooling region, one looses the most important property that will be frequently used in the theoretical and numerical studies: boundary condition is not necessary monotone non decreasing as a function of temperature.

As we will introduce some new approximations, we limit our studies to the models to which we can show the convergence and some qualitative results. In this way, the validation of the software can be done on both theoretical and industrial levels so that the results are valid at least in the region where the heat transfer coefficient is independent of the surface temperature.

It has also been reported from the practical measurements that, for example in the case of the continuous casting of steel the heat transfer coefficient is independent of the surface temperature in the temperature region $900 - 1200^\circ C$, which is the proper water cooling surface temperature [50].

In this work, we will limit the studies to the boundary condition

$$-\frac{\partial \theta}{\partial n} = \bar{v}(x,t)(\vartheta - \vartheta_{\text{ex}}) + \sigma\epsilon(\vartheta^4 - \vartheta_{\text{amb}}^4), \text{ on } \Gamma_{\text{cool}}.$$

Roll Contact. In the roll contact area there is no radiation. Heat transfer varies depending on the type of roll, but it is kept independent on temperature, thus

$$-\frac{\partial \theta}{\partial n} = v(x,t)(\vartheta - \vartheta_{\text{ex}}) \text{ on } \Gamma_{\text{roll}}.$$

Natural convection and radiation. After the secondary cooling area, air convection together with radiation is assumed. The heat flux on the boundary is described by

$$-\frac{\partial \theta}{\partial n} = v(x,t)(\vartheta - \vartheta_{\text{ex}}) + \sigma\epsilon(\vartheta^4 - \vartheta_{\text{amb}}^4) \text{ on } \Gamma_{\text{rad}}.$$

This air convection is also active in the secondary cooling area where the water sprays are not needed or cannot reach the surface.

Outflow. On the outflow boundary, we assume heat balance.

$$\frac{\partial \theta}{\partial n} = 0 \text{ on } \Gamma_{\text{out}}.$$

This means that temperature is insulated toward casting direction at the lower part of the machine. This is, however, natural if the length of the simulation is long enough, meaning that the strand is cooled smoothly and the upper surface is cooling via natural convection and radiation only. Another type of condition is to used in [25].

Symmetry. Typically cooling is assumed to be symmetric to the width and thickness direction. So we can exploit symmetries in the geometry of the slab and set on symmetry axes the condition

$$\frac{\partial \theta}{\partial n} = 0 \text{ on } \Gamma_{\text{sym}}.$$

Now we gather the boundary condition under one function

$$g(\theta) = \begin{cases} v(K^{-1}(\theta) - \vartheta_m) \text{ or } (q(x,t), & x \in \Gamma_{\text{mold}}, \\ \bar{v}(K^{-1}(\theta) - \vartheta_{\text{wat}}) + \sigma\varepsilon(K^{-1}(\theta)^4 - \vartheta_{\text{amb}}^4), & x \in \Gamma_{\text{cool}}, \\ v(x,t)(K^{-1}(\theta) - \vartheta_{\text{ex}}), & x \in \Gamma_{\text{roll}}, \\ v(x,t)(K^{-1}(\theta) - \vartheta_{\text{air}}) + \sigma\varepsilon(K^{-1}(\theta)^4 - \vartheta_{\text{amb}}^4), & x \in \Gamma_{\text{rad}}, \\ 0, & x \in \Gamma_{\text{out}} \cup \Gamma_{\text{sym}}. \end{cases}$$

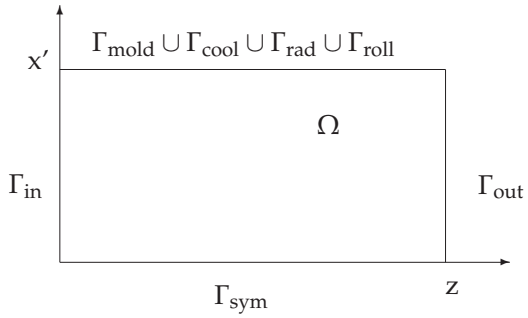

FIGURE 5 A domain Ω and the boundary notations.

2.3 Uniqueness, comparison, and continuous dependence

In this section, we present a formal model of the continuous casting processes. In FIGURE (5), we see the domain Ω and the boundary notations ($x' \in \mathbb{R}^2$)

which form assumption (H_Ω). Recalling that $\theta = \beta(u)$ and assuming the normalized temperature, we get assumption H_β. We denote d_{in} the casting temperature, which is extended to the whole domain in the assumption (H_d). Assumption (H_g) consists of the monotonicity requirement of the temperature dependent data and (H_b) states the variable casting speed. We use standard notations for the function spaces. We make the following assumptions:

$$
\begin{array}{ll}
(H_\Omega) & \Omega = X' \times]0, L[,\ X' \subset \mathbb{R}^2 \text{ is a polyhedral convex domain,} \\
(H_\beta) & \beta : \mathbb{R} \to \mathbb{R}, \text{ is monotone and Lipschitz continuous,} \\
 & 0 \le l_\beta < \beta'(s) \le L_\beta < +\infty, \text{ for a.e. } s \in \mathbb{R}, \\
 & \beta(0) = 0, \beta(u(0)) \in H^1(\Omega), \\
(H_d) & \exists\, d \in H^1(Q) \cap C^0(\bar{\Omega})\,,\ d = d_{\text{in}} \text{ on } \Sigma_{\text{in}} \text{ and } \|d\|_{L^\infty(Q)} \le M, \\
 & d \neq 0 \text{ a.e. on } \Sigma_{\text{in}}, \\
(H_g) & -\dfrac{\partial \theta}{\partial n} = g(x,t,\theta) \text{ on } \Sigma_{\text{n}}, g(x,t,\cdot), \text{ is local monotone non decreasing a.e} \\
 & (x,t) \in \Sigma_{\text{n}}, g \in L^2(\Sigma_{\text{n}}), \\
(H_b) & b(t) \ge 0, b \in L^\infty(0,T).
\end{array}
$$

Let $V(d) = \{\psi \in H^1(\Omega) | \quad \psi_{|\Gamma_{\text{in}}} = d\}$. We investigate the problem:
PROBLEM (P): Under the assumptions (H_Ω), (H_β), (H_d), (H_g), and (H_b), find $\{u, \theta\}$, $u \in \Upsilon(\theta)$ such that

$$u \in L^2(0,T;L^2(\Omega)), \text{ and } \theta \in L^2(0,T;V(d)),$$

and for all $\psi \in V := L^2(0,T;V(0)) \cap H^1(0,T;L^2(\Omega)) \cap L^\infty(Q)$ with $\psi(T) = 0$ the following equation holds

$$-\int_Q u(\partial_t \psi + b\partial_z \psi) + \int_{\Sigma_{out}} bu\psi + \int_Q \nabla\theta \cdot \nabla\psi + \int_{\Sigma_{\text{n}}} g(\theta)\psi = \int_\Omega u(0)\psi(0). \quad (19)$$

Before studying our problem further, we show how the boundary conditions play a crucial role in the well posedness of problem (P).

Example. Let $\Omega =]0,1[$ and $b = 1$ in (19) and $\beta(s) = min\{s, max\{s-1, 0\}\}$. Let us consider the problem

$$
\begin{aligned}
\frac{\partial u}{\partial t} + u_x - \beta(u)_{xx} &= 0 \text{ in }]0,1[\times[0,T], \\
\beta(u) &= 0 \text{ at } x = 0 \text{ and } x = 1, \\
u(0) &= u_0,
\end{aligned}
$$

where $0 \le u_0 \le 1$ in $]0,1[$. Then the problem (20) has a solution $u(x,t) = f(x-t)$, when f is any extension of u_0 to $]-\infty, 1]$ with $0 \le f \le 1$. Thus clearly it is not enough to impose $\beta(u)$ on the boundary to get uniqueness. On the other hand, if we consider the boundary conditions

$$u(0,t) = u^0(t), u(1,t) = u^1(t),$$

with $0 \leq u^0, u^1 \leq 1$, we observe immediately that the existence of a solution is not guaranteed.

These counterexamples mean that we have to set the boundary conditions in terms of temperature, with extra assumption to the Dirichlet data.

In the previous studies, various kind of assumptions are used. The only common assumption is that $d > 0$ on Σ_{in}, which is not needed in our case. However, this kind of assumption is natural in the case of continuous casting processes. In [45] the casting speed was assumed as a positive constant and the Dirichlet boundary condition were assumed on Σ_{in} with $d > 0$ and on Σ_{out} with $d < 0$. However, at the industrial level this kind of boundary condition is impractical as the temperature on Σ_{out} can not be measured. Naturally the casting speed cannot be assumed constant in the industrial cases.

In [62] the existence of a solution to the (P), with the boundary condition

$$u\psi\mathbf{b}\cdot\mathbf{n} - \frac{\partial\theta}{\partial n} = g(\theta) \text{ on } \Gamma_{\text{n}},$$

was shown.

The uniqueness of the solution was further obtained using assumption $\Gamma_n = \emptyset$, which is obviously even more restrictive from the practical point of view.

As our model differs from the previous ones, it is appropriate to show the existence and uniqueness of the solution. The existence of the solution can also be obtained from the convergence of our numerical approximations under some additional assumptions.

Typically the qualitative properties of the continuous casting processes have been shown using techniques introduced by Kamenomostskaya [19]. We proceed differently applying the L^1 techniques from [58].

We show that for fixed ε, (P^ε) has a unique solution (this shows the uniqueness in the alloys). Then we take a limit and prove that this property is preserved for (P) as well. In both cases, we show that the solution is bounded by initial data, which results in the uniqueness after simple contradiction argument. Furthermore, these results show the continuous dependence on initial data.

The regularized problem (P^ε) is: Find $u^\varepsilon = \text{Y}_\varepsilon(\theta^\varepsilon) \in H^1(0,T;L^2(\Omega))$,$\theta^\varepsilon \in L^2(0,T;V(d))$, such that

$$\int_Q (\partial_t u^\varepsilon \psi + b\partial_z u^\varepsilon \psi + \nabla\theta^\varepsilon \cdot \nabla\psi) + \int_{\Sigma_{\text{n}}} g(\theta^\varepsilon)\psi = 0 \tag{20}$$

for all $\psi \in V$.

Remark. Relation $\partial_z u^\varepsilon = \text{Y}'_\varepsilon(\theta^\varepsilon)\partial_z\theta^\varepsilon$ justifies the convection term.

Lemma 2.3.1 *Assume that assumptions for (P) are satisfied. Let $\{u_1^\varepsilon, \theta_1^\varepsilon\}$ and $\{u_2^\varepsilon, \theta_2^\varepsilon\}$ be any solutions to (P^ε), associated to the initial values $u_1^\varepsilon(0), u_2^\varepsilon(0)$ (otherwise assume same data), then*

$$\int_\Omega |u_1^\varepsilon(t) - u_2^\varepsilon(t)| \leq \int_\Omega |u_1^\varepsilon(0) - u_2^\varepsilon(0)|.$$

Proof. Let us set $\tilde{u} = u_1^\varepsilon - u_2^\varepsilon$,$\tilde{\theta} = \theta_1^\varepsilon - \theta_2^\varepsilon$, $\tilde{g}(\theta) = g(\theta_1^\varepsilon) - g(\theta_2^\varepsilon)$ and

$$H(\xi) := \begin{cases} \{0\} & \text{if } \xi < 0, \\ [0,1] & \text{if } \xi = 0, \\ \{1\} & \text{if } \xi > 0, \end{cases} \qquad H_j(\xi) := \begin{cases} 0 & \text{if } \xi \leq 0, \\ j\xi & \text{if } 0 \leq \xi \leq \frac{1}{j}, \\ 1 & \text{if } \xi \geq \frac{1}{j}, \end{cases}$$

for any $j \in \mathbb{N}$.
We use $H_j(\tilde{\theta}) \in V$ as a test function and take the difference between solutions. Then we have to estimate

$$\int_Q (\partial_t \tilde{u} H_j(\tilde{\theta}) + b\partial_z \tilde{u} H_j(\tilde{\theta})) + \int_Q \nabla\tilde{\theta} \cdot \nabla H_j(\tilde{\theta}) + \int_{\Sigma_n} \tilde{g}(\theta) H_j(\tilde{\theta}) = 0 \tag{21}$$
$$=: I + II + III + IV.$$

Now

$$III = \int_Q \nabla\tilde{\theta} \cdot \nabla H_j(\tilde{\theta}) = \int_Q H_j'(\tilde{\theta}) |\nabla\tilde{\theta}|^2 \geq 0.$$

Let us now pass to the limit as $j \to \infty$. Note that

$$H(\tilde{\theta})_j \to \phi = \begin{cases} 0 & \text{where } \tilde{\theta} \leq 0, \\ 1 & \text{where } \tilde{\theta} > 0, \end{cases}$$

a.e in Q. From the monotonicity of g it follows that

$$\lim_{j\to\infty} IV = \int_{\Sigma_n} \tilde{g}(\theta)\phi = \int_{\Sigma_n} \tilde{g}(\theta)^+.$$

Furthermore, we have $H(\tilde{u}) = H(\tilde{\theta})$ a.e in Q. Hence $\phi \in H(\tilde{u})$. After integrating and using monotonicity of u we get

$$\lim_{j\to\infty} II = \int_Q b\partial_z \tilde{u}\phi = b\int_{\Sigma_{\text{out}}} \tilde{u}^+ - b\int_{\Sigma_{in}} \tilde{u}^+ \geq 0.$$

For the term I we get after integrating in time

$$\lim_{j\to\infty} I = \int_\Omega \tilde{u}^+(t) - \int_\Omega \tilde{u}^+(0). \tag{22}$$

Gathering $I + II + III + IV$ as $j \to \infty$ we obtain

$$\int_\Omega (u_1^\varepsilon(t) - u_2^\varepsilon(t))^+ \leq \int_\Omega (u_1^\varepsilon(0) - u_2^\varepsilon(0))^+. \tag{23}$$

Now exchanging u_1^ε and u_2^ε in $\tilde{u}$ and adding resulting the inequalities we conclude (2.3.1).

Remark. We did not use the assumption $d \neq 0$ a.e on Σ_{in}. However, it will be needed to show the following theorem.

Theorem 2.3.2 *Assume that assumptions for (P) are satisfied. Let $\{u_1, \theta_1\}$ and $\{u_2, \theta_2\}$ be any solutions to the (P), then*

$$\int_\Omega |u_1(t) - u_2(t)| \leq \int_\Omega |u_1(0) - u_2(0)|.$$

Proof. We first show that (P) has a solution. We integrate (20) by parts and take a limit $\varepsilon \to 0$. As $u^\varepsilon \to u^*$ weakly in $L^2(Q)$ and $\theta^\varepsilon \to \theta^*$ strongly in $L^2(Q)$ we get, possible extracting subsequences

$$-\int_Q u^*(\partial_t \psi + b\partial_z \psi) + \int_{\Sigma_{out}} bu^*\psi + \int_Q \nabla\theta^* \cdot \nabla\psi + \int_{\Sigma_n} g(\theta^*)\psi = \int_\Omega u^*(0)\psi(0).$$

Furthermore, using the monotonicity argument it holds that $u^* \in \Upsilon(\theta^*)$, so $\{u^*, \theta^*\}$ solves (P) [15, 44, 45].
We may repeat the steps I, II, III, and IV in the previous theorem as $\varepsilon \to 0$ as well. The only difference comes from the term II, where we need extra assumption $d \neq 0$ on Σ_{in} in order to get enthalpy uniquely defined on Γ_{in}. Thus to any limits u_1^* and u_2^* of subsequences of u^ε associated to the same data it holds that

$$\int_\Omega |u_2^*(t) - u_1^*(t)| = 0.$$

As u^ε is bounded and any convergent subsequences have the same limit, we conclude that the whole sequence converges. The final conclusion follows from the fact that

$$\int_\Omega |u_2(t) - u_1(t)| \leq \liminf_{\varepsilon \to 0} \int_\Omega |u_2^\varepsilon(t) - u_1^\varepsilon(t)| \leq \int_\Omega |u_2(0) - u_1(0)|.$$

3 NUMERICAL APPROXIMATIONS

In this chapter we define four fully discrete approximations to problem (P) in the finite element form. We first describe some notations and frequently used results that are used to show estimates needed to prove the convergence of each approximation.

The basic strategy in all proofs is the same, we compute a priori estimates and limit. Thus in the proofs some of the steps are identical, and they will not be repeated. We start by showing the convergence of the characteristic approximation in detail and then for other approximations the proofs are modified for the approximation of convection term, time derivative, and the approximations to the boundary condition in a priori estimates. In the case of Chernoff type of approximations the limit process is also different.

3.1 Preliminaries

We first introduce notations used in the finite element approximations. Then we recall basic estimation tools necessary to show boundedness of the discrete solution in the suitable function spaces. Then we introduce mesh functions, the notation to the convection term, and the construction of the initial data necessary to show the convergence and make some additional assumptions.

3.1.1 Notations and basic property of finite element approximation

We first define some notations in order to define the discrete problem. We denote $V = H^1(\Omega), V(d) = \{\psi \in V : \psi_{\Gamma_{\text{in}}} = d\}$. Let $\{E_h\}_h$ be a family of regular partitions of Ω into cuboid finite elements. We define the discrete space we shall work with on each time level:

$$V_h := \{\psi \in C^0(\bar{\Omega}) : \psi_{|E} \in P^1(E) \quad \forall\, E \in E_h, \},$$
$$V_h(d) := \{\psi \in V_h : \psi = I_h d \text{ on } \Gamma_{in}\},$$

where $P^1(E)$ indicates the space of trilinear finite elements and I_h is the piecewise linear interpolant of d. Let Π_h be the local Lagrange interpolation operator $\Pi_h|_E : C^0(\Omega) \to P^1(E)$ for all $E \in E_h$. We associate with $\langle \cdot, \cdot \rangle$ a discrete inner product in V_h defined, for any piecewise uniformly continuous functions u and ψ, by

$$\langle u, \psi \rangle_h = \sum_{E \in E_h} \int_E \Pi_h|_E(u\psi) dx,$$

(typically called as mass lumping) to which it holds

$$\|u\|^2_{L^2(\Omega)} \leq \langle u, u \rangle_h \leq C\|u\|^2_{L^2(\Omega)} \quad \forall u \in V_h. \tag{24}$$

The following error bounds hold [35], [6]

$$|\langle u, \psi \rangle - \langle u, \psi \rangle_h| \leq Ch\|u\|_{L^2(\Omega)}\|\nabla\psi\|_{L^2(\Omega)}, \quad \forall u, \psi \in V_h, \tag{25}$$

$$|\langle u, \psi \rangle - \langle u, \psi \rangle_{\Gamma_{n,h}}| \leq Ch^{\frac{1}{2}}\|u\|_{L^2(\Gamma_n)}\|\nabla\psi\|_{L^2(\Omega)}, \quad \forall u, \psi \in V_h, \tag{26}$$

for some constant C independent of h.

The discrete L^2-projection operator P_h for any $u \in L^2(\Omega)$, where $P_h u \in V_h$, is defined by

$$\langle P_h u, \psi \rangle_h = \langle u, \psi \rangle, \forall \psi \in V_h(0). \tag{27}$$

For discrete time, we denote

$$\tau := T/N, \quad t^n =: n\tau, \quad I^n := [t^{n-1}, t^n), \quad 1 \leq n \leq N,$$

and

$$u^n := u(\cdot, t^n), \quad \partial u^n := \frac{u^n - u^{n-1}}{\tau}.$$

3.1.2 Basic estimation tools

We will frequently use the Cauchy-Schwarz inequality

$$\langle u, \psi \rangle \leq \|u\|_{L^2(\Omega)}\|\psi\|_{L^2(\Omega)} \quad u, \psi \in V_h, \tag{28}$$

relation

$$2ab \leq \varepsilon a^2 + \frac{b^2}{\varepsilon} \; a, b \in \mathbb{R} \quad \varepsilon > 0, \tag{29}$$

the summation by parts formula

$$\sum_{i=1}^{m} a_i[b_i - b_{i-1}] = a_m b_m - a_0 b_0 - \sum_{i=1}^{m} b_{i-1}[a_i - a_{i-1}], \tag{30}$$

and elementary relation

$$2a(a-b) = a^2 - b^2 + (a-b)^2, \text{ for } a, b \in \mathbb{R}. \tag{31}$$

We also recall a basic tool necessary for estimates. Let $\lambda : R \to R$ be an absolutely continuous function such that $\lambda(0) = 0$ and $0 \leq \lambda' \leq \Lambda < \infty$ and let Φ_λ be convex function defined by

$$\Phi_\lambda(s) := \int_0^s \lambda(z)dz \quad \text{for } s \in R.$$

Then Φ_λ has the properties

$$\frac{1}{2\Lambda}\lambda^2(s) \leq \Phi_\lambda(s) \leq \frac{\Lambda}{2}s^2 \quad \text{for } s \in R. \tag{32}$$

3.1.3 Mesh functions, additional assumptions, and notations

In the convergence proofs, we will use the following notations: Let $\psi \in F$, where

$$F = \{\psi \in C^2(\bar{Q}) \,:\, \psi(x,T) = 0, x \in \bar{\Omega},\, \psi(x,t) = 0, \quad (x,t) \in \Sigma_{in},\, t \in (0,T]\}.$$

We will use the notation $\rightharpoonup$ to denote the weak convergence in Hilbert space and $\to$ to denote the strong convergence. The mesh functions $\psi_{h,\tau}(t)$ and $\psi'_{h,\tau}(t)$ are defined by

$$\begin{aligned} \psi_{h,\tau}(t) &= I_h\left(\psi((n-1)\tau)\right) =: \psi^{n-1}, \quad t \in I_n, \\ \psi'_{h,\tau}(t) &:= \partial\psi^n, \quad t \in I_n, \end{aligned} \tag{33}$$

and have following approximation properties [15]

$$I_h\left(\psi(t)\right) \to \psi(t), \quad \text{in } V(0), \tag{34}$$

$$\psi_{h,\tau} \to \psi, \quad \text{in } L^2(0,T;V(0)), \tag{35}$$

$$\psi'_{h,\tau} \to \frac{\partial\psi}{\partial t}, \quad \text{in } L^2(0,T;H^1(\Omega)). \tag{36}$$

Let M_h denote the number of the unknowns in Ω_h. For trilinear basis $\psi_i(x), i = 1,\ldots,M_h$,we denote $u_h = u_h(x_i,t) = \sum_{i=1}^{M_h} u_i(t)\psi_i(x)$.

We identify functions $u_h, \theta_h \in V_h$ with the vectors $U^n, \Theta^n \in \mathbb{R}^{M_h}$ at $t = t^n$, containing their nodal values. We will also need the following mesh functions for the approximations, $\Theta^n \in V_h(d), U^n \in V_h(\Upsilon(d))$ at time level n. We define

$$\theta_{h,\tau} = \Theta^n(x) \text{ and } u_{h,\tau} = U^n(x)\ \forall t \in I_n.$$

We require that for the initial data, it holds

$$P_h u(0) \rightharpoonup u(0) \text{ in } L^2(\Omega), \tag{37}$$

$$\theta_h \rightharpoonup \theta(0) \text{ in } V(0). \tag{38}$$

The approximation and treatment of the convection term in problem (P) is essential, showing a priori estimates and convergence. We define for $u \in L^2(\Omega)$, $\psi \in V(0)$

$$b(u,\psi) := -\int_\Omega u\mathbf{b}\cdot\nabla\psi + \int_{\Gamma_{out}} bu\psi, \tag{39}$$

and we will show how characteristic and upwinding approximations converge to this term.

We make the following assumptions in the approximations in addition to the assumptions (H_Ω), (H_d), (H_β), and (H_g):

$$
\begin{aligned}
&(H_{\Omega_h}) \quad \text{Triangulation of the domain } \Omega \text{ is acute,}\\
&(H_{g_h}) \quad C \le \theta \text{ and } g(x,t,\theta) > 0 \,\forall (x,t) \in \Sigma_n, \mathbf{C} \in \mathbb{R},\\
&(H_{b_h}) \quad b(t) = b^n \in \mathbb{R}, t \in I_n, b^n \ge 0.
\end{aligned}
$$

Remarks. Assumption (H_{g_h}) is natural in the continuous casting context, since it states that the slab is cooled all the time with a reasonable lower bound to the temperature. It would be possible to show the convergence without assumptions (H_{Ω_h}) and (H_{g_h}) [6], but this will lead to the use of discrete Gronwall inequality in which the stability depends on the final time and the applicability to simulation of long time periods would be somewhat problematic.

3.2 The characteristic method

In this section, we introduce characteristic approximation of the problem (P). We now introduce the basic idea of this method. Recall the continuous equation

$$\partial_t u + b\partial_z u = \Delta\theta. \tag{40}$$

Denote $\tilde{u}(t) = u(x(t),t)$, such that $\frac{dx}{dt} = b(t)e_z$, where $e_z = (0,0,1)^T$, then

$$\frac{d\tilde{u}(t)}{dt} = \partial_t u + b\partial_z u.$$

The characteristic finite difference method is defined by writing

$$\bar{x}^{n-1} = x - \tau b^{n-1} e_z, \quad \bar{u}^{n-1} = u(\bar{x}^{n-1}, t^{n-1}),$$

for $n \ge 1$. Then

$$\frac{d\tilde{u}}{dt} \approx \frac{\tilde{u}^n - \tilde{u}^{n-1}}{\tau} \Rightarrow \partial u^n + b^n \partial_z u \approx \frac{u^n - \bar{u}^{n-1}}{\tau}.$$

Now (40) can be approximated as

$$\frac{u^n - \bar{u}^{n-1}}{\tau} = \Delta\theta^n.$$

Thus, the discrete problem with the characteristic approximation reads as:

Problem (PC). *Find* $\{U^n, \Theta^n\}_{n=1}^N$, $U^n \in \Upsilon(\Theta^n)$ *such that*

$$
\begin{aligned}
U^0 &:= P_h u(0),\\
\Theta^n &:= \Pi_h \beta(U^n),
\end{aligned}
$$

and for all $\psi \in V_h(0)$, we have

$$\begin{cases} \langle U^n, \psi\rangle_h + \tau\langle\nabla\Theta^n, \nabla\psi\rangle + \tau\langle g(\Theta^n), \psi\rangle_{h,\Gamma_n} = \langle\bar{U}^{n-1}, \psi\rangle_h, \\ \bar{U}^{n-1} = I_h U^{n-1}(\bar{x}^{n-1}, t^{n-1}). \end{cases} \tag{41}$$

In the a priori estimates and convergence proof, we need a discrete counterpart leading to the convergence to the convection term $b(u, \psi)$.

For this purpose, we define

$$b_h(U^{n-1}, \psi) := \langle \mathbf{b}^{n-1} \cdot \nabla I_\tau U^{n-1}, \psi\rangle, \forall\psi \in V_h(0), \tag{42}$$

where

$$\mathbf{b}^{n-1} \cdot \nabla I_\tau U^{n-1} := b^{n-1}\frac{U^{n-1}(x) - U^{n-1}(\bar{x})}{\tau b^{n-1}}.$$

Then to the right hand side of (41), it holds that

$$\langle\bar{U}^{n-1}, \psi_h\rangle_h = \langle U^{n-1}, \psi_h\rangle_h + \tau b_h(U^{n-1}, \psi), \forall\psi_h \in V_h(0). \tag{43}$$

As we are working in the free boundary form, it is necessary to use the discrete version of partial integration (30) in order to get the convergence. We are not able to do this without extra assumption $b\tau \le h$.

The following lemma shows the weak convergence of b_h to b and sufficient property to get a priori estimates for the solution of (PC).

Lemma 3.2.1 *Assume that $b\tau \le h$. Mapping $b_h : V_h \times V_h(0) \to R$ has the following properties:*

$$\begin{array}{ll} i) & b_h(u_h, \psi_{h,\tau}) \to b(u, \psi), \quad \forall u_h \rightharpoonup u \text{ in } L^2(\Omega), \psi_{h,\tau} \to \psi \text{ in } V(0), \\ ii) & |b_h(u_h, \psi_h)| \le C\|u_h\|_{L^2(\Omega)}\|\psi_h\|_{V(0)} \quad \forall u_h \in V_h, \psi_h \in V_h(0). \end{array}$$

Proof of i). Let $\psi \in F$. As $b\tau \le h$ we have

$$b^{n-1}\frac{U^{n-1}(x) - U^{n-1}(x - \tau b^{n-1}e_z)}{\tau b^{n-1}} = b^{n-1}\frac{U^{n-1}(x) - U^{n-1}(x - he_z)}{h}. \tag{44}$$

Thus using (30) we get

$$\begin{aligned} &\left|\lim_{h,\tau\to 0} b_h(U^{n-1}, \psi_{h,\tau}) - b(u, \psi) + b_h(u, \psi) - b_h(u, \psi)\right| = \\ &\left|\lim_{h,\tau\to 0}[-\langle U^{n-1}, \mathbf{b}^{n-1} \cdot \nabla I_\tau\psi_{h,\tau}\rangle_h] + \right. \\ &\qquad \left. b^{n-1}\langle U^{n-1}, \psi_{h,\tau}\rangle_{h,\Gamma_{\text{out}}} - b_h(u, \psi) + b_h(u, \psi) - b(u, \psi)]\right| \le \\ &|\lim_{h,\tau\to 0}[-\langle U^{n-1}, \mathbf{b}^{n-1} \cdot \nabla I_\tau(\psi_{h,\tau} - \psi)\rangle_h]| + |\lim_{h,\tau\to 0}[\langle U^{n-1} - u, \mathbf{b}^{n-1} \cdot \nabla I_\tau\psi\rangle_h]| + \\ &|\lim_{h,\tau\to 0}[b^{n-1}\langle U^{n-1}, \psi_{h,\tau} - \psi\rangle_{h,\Gamma_{\text{out}}}]| + |\lim_{h,\tau\to 0}[b^{n-1}\langle U^{n-1} - u, \psi\rangle_{\Gamma_{h,\text{out}}}]| + \\ &|\lim_{h,\tau\to 0}[b_h(u, \psi) - b(u, \psi)]| := I + II + III + IV + V. \end{aligned}$$

We estimate each term separately. From the definition of the derivative and (35), it holds that

$$|\lim_{h,\tau\to 0} I| = |\lim_{h\to 0}[-\langle u_h, \mathbf{b}\cdot\nabla I_\tau(\psi_h-\psi)\rangle_h]| \le C|\lim_{h\to 0}[-\langle u_h, \mathbf{b}\cdot\nabla I_\tau(\psi_h-\psi)\rangle]| \to 0.$$

As $u_h \rightharpoonup u \in L^2(\Omega)$, we get

$$|\lim_{h,\tau\to 0} II| = |\lim_{h\to 0}\langle u_h - u, \mathbf{b}\cdot\nabla I_\tau\psi\rangle_h| \le \lim_{h\to 0} C|\langle u_h - u, \mathbf{b}\cdot\nabla I_\tau\psi\rangle| \to 0.$$

Using (28) and from the fact that $\|\psi_{h,\tau}\|_{L^2(\Gamma_n)} \le \|\psi_{h,\tau}\|_{H^1(\Omega)}$, we obtain

$$|\lim_{h,\tau\to 0} III| = |\lim_{h\to 0} b\langle u_h, \psi_{h,\tau}-\psi\rangle_{h,\Gamma_{\text{out}}}| \le \lim_{h\to 0} C\|u_h\|_{L^2(\Gamma_{\text{out}})}\|\psi_{h,\tau}-\psi\|_{H^1(\Omega)} \to 0$$

and by weak convergence of u_h it follows that

$$|\lim_{h,\tau\to 0} IV| = |\lim_{h\to 0} b\langle u_h - u, \psi\rangle_{\Gamma_{h,\text{out}}}| \le \lim_{h\to 0} C|b\langle u_h - u, \psi\rangle_{\Gamma_{\text{out}}}| \to 0.$$

To the last term, we apply numerical integration estimate (26), the fact that $\langle u_h, \nabla I_\tau\psi_{h,\tau}\rangle_h - \langle u_h, \nabla I_\tau\psi_{h,\tau}\rangle = 0$ and convergence properties of u_h and (35) to obtain

$$|\lim_{h,\tau\to 0}[b_h(u,\psi) - b(u,\psi)]| \le \lim_{h\to 0}[Ch^{\frac{1}{2}}\|u\|_{L^2(\Gamma_{\text{out}})}\|\nabla\psi\|_{L^2(\Omega)} + |b(u_h - u, \nabla I_\tau\psi_{h,\tau})| + |b(u, \nabla I_\tau(\psi_{h,\tau}-\psi)|] \to 0.$$

Now *i)* holds, first for all $\psi \in F$ and then by density for all $\psi \in V(0)$.
Proof of ii). Let $\psi_h \in V_h(0)$, then

$$|b_h(U^{n-1},\psi_h)| \le C|\langle\nabla U^{n-1},\psi_h\rangle| \le C\|U^{n-1}\|_{L^2(\Omega)}\|\nabla\psi_h\|_{L^2(\Omega)} + C \le C\|U^{n-1}\|_{L^2(\Omega)}\|\psi_h\|_{V(0)},$$

thus *ii*) holds.
Remark. In the case of alloys we have no restriction $b\tau \le h$. This is because the problem can be stated as (P^ε) and the approximation

$$b_h(U^{n-1},\psi) = \langle \mathbf{b}^{n-1}\cdot\nabla I_\tau U^{n-1},\psi\rangle \rightharpoonup \langle \mathbf{b}\cdot\nabla u^\varepsilon,\psi\rangle, \forall\psi\in V(0), \tag{45}$$

for any fixed $\varepsilon > 0$.

Theorem 3.2.2 *Let $\{U^n,\Theta^n\}$ be the solutions of (PC) then under the assumptions (H_Ω), (H_{Ω_h}), (H_β) (H_d), (H_g), (H_{g_h}), and $b\tau \le h$.*

$$a)\quad \max_{1\le n\le N}\|U^n\|_{L^\infty(\Omega)} + \max_{1\le n\le N}\|\Theta^n\|_{L^\infty(\Omega)} \le C,$$

$$b)\quad \sum_{n=1}^{N}\tau\|\nabla\Theta^n\|^2_{L^2(\Omega)} \le C,$$

$$c)\quad \sum_{n=1}^{N}\tau\|\partial\Theta^n\|^2_{L^2(\Omega)} \le C.$$

Proof of a). We argue by induction. Assume that $\|U^{n-1}\|_{L^\infty(\Omega)} \leq C$. Then it follows that also $\bar{U}^{n-1}$ is bounded. Since the mesh is of acute type, the discrete maximum principle holds, so together with the assumption (H_{g_h})

$$\langle \nabla \Theta^n, \nabla \psi_j \rangle + \tau \langle g(\Theta^n), \psi_j \rangle_{h,\Gamma_n} \geq 0$$

at the node j, where Θ^n attains its maximum and thus

$$\langle U^n, \psi_j \rangle_h \leq \langle \bar{U}^{n-1}, \psi_j \rangle_h.$$

The lower bound is given by assumption (H_{g_h}) as $U^n = \Upsilon(\Theta^n)$ node wise. Note that the estimate $a)$ (with the different constants) holds for Θ^n.
Proof of b). Let $\Theta^n - d_h^n$ be a test function in (41) and sum it over n from 1 to m, $m \leq N$. Then the assertion follows by estimating each term separately. After using (43) and rearranging, we have to estimate

$$\begin{aligned}
&(I_\theta + I_d) + (II_\theta + II_d) + (III_\theta + III_d) + (IV_\theta + IV_d) := \\
&\sum_{n=1}^{m} [\langle U^n - U^{i-1}, \Theta^n - d_h^n \rangle_h + \tau b_h(U^{n-1}, \Theta^n - d_h^n) + \\
&\tau \langle \nabla \Theta^n, \nabla [\Theta^n - d_h^n] \rangle + \tau \langle g(\Theta^n), \Theta^n - d_h^n \rangle_{h,\Gamma_n}] = 0.
\end{aligned}$$

The idea is to use frequently L^∞ estimate and some positive terms will be neglected. From the term III_θ we get the desired norm and then by using Cauchy-Schwarz inequality (28) for the terms II_θ and IV_θ, some terms will be absorbed to the desired norm. The rest of the terms will be shown to be either bounded or positive, which leads to the estimate $b)$.

Since $\Theta^n = \beta(U^n)$ node wise, the convexity of Φ_β together with (32) I_θ leads to

$$\begin{aligned}
&\textstyle\sum_{n=1}^{m} (U_j^n - U_j^{n-1}) \Theta_j^n \geq \sum_{n=1}^{m} (\Phi_\beta(U_j^n) - \Phi_\beta(U_j^{n-1}) \\
&\geq \Phi_\beta(U_j^m) - \Phi_\beta(U^0) \geq \tfrac{1}{2L_\beta} (\Theta^m)^2 - \tfrac{L_\beta}{2} (U_j^0)^2.
\end{aligned}$$

Then using (24), (28), and $a)$

$$I_\theta = \sum_{n=1}^{m} \langle U^n - U^{n-1}, \Theta^n \rangle_h \geq C \|\Theta^m\|_{L^2(\Omega)}^2 - C \geq -C.$$

For I_d by (30), (29), and $a)$ we have

$$\begin{aligned}
|I_d| = &| \sum_{n=1}^{m} \tau \langle \partial U^n, d_h^n \rangle_h | = | \|U^m\|_{L^2(\Omega)} \|d_h^m\|_{L^2(\Omega)} - \|U^0\|_{L^2(\Omega)} \|d_h^0\|_{L^2(\Omega)} + \\
&\sum_{n=1}^{m} \tau \|\partial d_h^n\|_{L^2(\Omega)} \|U^{n-1}\|_{L^2(\Omega)} | \leq C + C' \sum_{n=1}^{m} \tau \|U^{n-1}\|_{L^2(\Omega)}^2 \leq C.
\end{aligned}$$

For the convection term, it holds by using (3.3.1) *ii)*, (28), and (29) that

$$\begin{aligned}|II_\theta| =& |\sum_{n=1}^{m} \tau b_h(U^{n-1}, \Theta^n)| \leq C \sum_{n=1}^{m} \tau \|U^{n-1}\|_{L^2(\Omega)} \|\nabla \Theta^n\|_{L^2(\Omega)} \\ &\leq C \sum_{n=1}^{m} \tau [\frac{1}{2\varepsilon} \|U^{n-1}\|^2_{L^2(\Omega)} + \frac{\varepsilon}{2} \|\nabla \Theta^n\|^2_{L^2(\Omega)}] \\ &\leq C + \sum_{n=1}^{m} \frac{\tau\varepsilon}{2} \|\nabla \Theta^n\|^2_{L^2(\Omega)}, \end{aligned} \tag{46}$$

and similarly

$$\begin{aligned}|II_d| =& |\sum_{n=1}^{m} \tau b_h(U^{n-1}, d_h^n)| \leq C \sum_{n=1}^{m} \tau \|U^{n-1}\|_{L^2(\Omega)} \|\nabla d_h^n\|_{L^2(\Omega)} \\ &\leq C \sum_{n=1}^{m} \tau [\frac{1}{2} \|U^{n-1}\|^2_{L^2(\Omega)} + \frac{1}{2} \|\nabla d_h^n\|^2_{L^2(\Omega)}] \leq C. \end{aligned}$$

From the diffusion term, we get the desired norm $b)$ as

$$III_\theta = \sum_{n=1}^{m} \tau \langle \nabla \Theta^n, \nabla \Theta^n \rangle = \sum_{n=1}^{m} \tau \|\nabla \Theta^n\|^2_{L^2(\Omega)},$$

and the Dirichlet data is estimated by (H_d), (28), and (29) as follows

$$\begin{aligned}III_d =& \sum_{n=1}^{m} \tau \langle \nabla \Theta^n, \nabla d_h^n \rangle \leq \sum_{n=1}^{m} \tau [\frac{\varepsilon}{2} \|\nabla \Theta^n\|^2_{L^2(\Omega)} + \frac{1}{2\varepsilon} \|\nabla d_h^n\|^2_{L^2(\Omega)}] \\ &\leq C + \frac{\varepsilon}{2} \sum_{n=1}^{m} \tau \|\nabla \Theta^n\|^2_{L^2(\Omega)}. \end{aligned} \tag{47}$$

For the boundary term, by using $a)$, (H_d), and (H_{g_h}) it holds that

$$|IV_\theta + IV_d| = |\sum_{n=1}^{m} \tau \langle g(\Theta^n), \Theta^n - d^n \rangle_{h,\Gamma_n}| \leq C.$$

Thus, choosing ε small enough in (46) and (47), these terms can be absorbed to III_θ and so $b)$ holds.

Proof of c). We use $\psi = \tau(\partial(\Theta^n - d_h^n))$ as a test function. After rearranging them, we have to estimate

$$\begin{aligned}&(I_\theta + I_d) + (II_\theta + II_d) + (III_\theta + III_d) + (IV_\theta + IV_d) := \\ &\sum_{n=1}^{m} [\tau \langle \partial U^n, \partial \Theta^n - \partial d_h^n \rangle_h - \tau b_h(U^{n-1}, \partial \Theta^n - \partial d_h^n) \\ &+ \tau \langle \nabla \Theta^n, \partial \nabla [\Theta^n - d_h^n] \rangle + \tau \langle g(\Theta^n), \partial \Theta^n - \partial d_h^n \rangle_{\Gamma_n}] = 0. \end{aligned}$$

As we only need an estimate for the time derivative, we will finally drop the positive terms from the estimate. The desired lefthand side of the estimate comes

from the term I_θ, then by using estimate for the term III_θ to absorb some parts of II_θ and IV_θ and using $a)$ and $b)$ the assertion follows.

From the monotonicity of Θ^n, it follows that

$$I_\theta = \sum_{n=1}^{m} \tau \langle \partial U^n, \partial \Theta^n \rangle \geq C \sum_{n=1}^{m} \tau \|\partial \Theta^n\|^2_{L^2(\Omega)}.$$

Then the Dirichlet data are handled by using (H_d), (28), and (29),

$$\begin{aligned} |I_d| &= \sum_{n=1}^{m} \tau |\langle \partial U^n, \partial d_h^n \rangle| \leq \sum_{n=1}^{m} \frac{\varepsilon}{2} \tau \|\partial \Theta^n\|^2_{L^2(\Omega)} + \sum_{n=1}^{m} \frac{1}{2\varepsilon} \|d_h^n - d_h^{n-1}\|^2_{L^2(\Omega)} \\ &\leq \frac{\varepsilon}{2} \sum_{n=1}^{m} \tau \|\partial \Theta^n\|^2_{L^2(\Omega)} + C. \end{aligned} \tag{48}$$

We make use of $b)$, (H_d), (3.3.1), and (29) to obtain

$$\begin{aligned} |II_\theta| &\leq \frac{1}{2} \sum_{n=1}^{m} \left[\frac{\tau}{\varepsilon} \|U^{n-1}\|^2_{L^2(\Omega)} + \varepsilon \|\nabla [\Theta^n - \Theta^{n-1}]\|^2_{L^2(\Omega)} \right] \\ &\leq C + \frac{\varepsilon}{2} \sum_{n=1}^{m} \|\nabla [\Theta^n - \Theta^{n-1}]\|^2_{L^2(\Omega)}, \end{aligned} \tag{49}$$

and

$$|II_d| \leq \sum_{n=1}^{m} \tau \frac{1}{2} \|U^{n-1}\|^2_{L^2(\Omega)} + \frac{1}{2} \sum_{n=1}^{m} \tau \|\nabla [d_h^n - d_h^{n-1}]\|^2_{L^2(\Omega)} \leq C.$$

For the diffusion part, we use (31) to conclude that

$$\begin{aligned} 2III_\theta &= \sum_{n=1}^{m} \tau \langle \nabla \Theta^n, \partial \nabla \Theta^n \rangle = \|\nabla \Theta^m\|^2_{L^2(\Omega)} - \|\nabla \Theta^0\|^2_{L^2(\Omega)} \\ &+ \sum_{n=1}^{m} \|\nabla [\Theta^n - \Theta^{n-1}]\|^2_{L^2(\Omega)} \geq \|\nabla \Theta^m\|^2_{L^2(\Omega)} + \sum_{n=1}^{m} \|\nabla [\Theta^n - \Theta^{n-1}]\|^2_{L^2(\Omega)} - C. \end{aligned}$$

Using (29) with $\varepsilon = 1$ we get

$$\begin{aligned} 2III_d &= 2 \sum_{n=1}^{m} \tau \langle \nabla \Theta^n, \partial \nabla d_h^n \rangle = \sum_{n=1}^{m} \tau \|\nabla \Theta^n\|^2_{L^2(\Omega)} \\ &+ \sum_{n=1}^{m} \|\nabla [d^n - d^{n-1}]\|^2_{L^2(\Omega)} \leq C. \end{aligned}$$

For the boundary term, we define $G(\Theta^n) = \int_0^T g(s) ds$, now

$$G(\Theta^n) - G(\Theta^{n-1}) = g(\hat{\Theta})(\Theta^n - \Theta^{n-1}),$$

where $\hat{\Theta} = \Theta^n + \tau^n(\Theta^{n-1} - \Theta^n)$. Thus

$$g(\Theta^n) - g(\hat{\Theta}) = g'(\xi) \tau^n (\Theta^n - \Theta^{n-1}),$$

and taking into account the monotonicity of g and mass lumping, we get

$$\begin{aligned} IV_\theta &= \sum_{n=1}^{m} \langle g(\Theta^n), \Theta^n - \Theta^{n-1} \rangle_{h,\Gamma_n} \\ &= \sum_{n=1}^{m} [\langle G(\Theta^n) - G(\Theta^{n-1}), 1 \rangle_{h,\Gamma_n} + \langle g(\Theta^n) - g(\hat{\Theta}), \Theta^n - \Theta^{n-1} \rangle_{h,\Gamma_n}] \\ &\geq \langle G(\Theta^m), 1 \rangle_{h,\Gamma_n} - C. \end{aligned}$$

For the Dirichlet data by $a)$ and (H_d)

$$|IV_d| = |\sum_{n=1}^{m} \tau \langle g(\Theta^n), \partial d_h^n \rangle_{h,\Gamma_n}| \leq C.$$

Now choosing ε small enough, terms involving ε in (48), (49), and (50) can be absorbed to the lefthand side, terms with Θ^n in III_θ remain positive and thus can be neglected, so $c)$ holds.

The stability results show that in the problem (PC)

$$\begin{array}{ll} \theta_{h,\tau} & \text{is bounded in } L^2(0,T;V(0)) \cap H^{\frac{1}{2}}(0,T;L^2(\Omega)), \\ u_{h,\tau} & \text{is bounded in } L^2(0,T;L^2(\Omega)). \end{array} \tag{50}$$

Theorem 3.2.3 *Of the sequences $\theta_{h,\tau}$, $u_{h,\tau}$ in the problem (PC) we can extract subsequences still denoted by the same symbol such that*

$$\begin{array}{ll} \theta_{h,\tau} & \to \theta \text{ in } L^2(0,T;L^2(\Omega)), \\ u_{h,\tau} & \rightharpoonup u \text{ in } L^2(0,T;L^2(\Omega)). \end{array}$$

Moreover, $\{u, \theta\}$ solves the problem (P).

Proof. As $\theta_{h,\tau} \in L^2(0,T;V(0)) \cap H^{\frac{1}{2}}(0,T;L^2(\Omega))$ we have strong convergence for $\theta_{h,\tau} \in L^2(Q)$. Moreover, this holds also on the boundary [6].
We show now that possible extracting subsequences in (PC) these limits solve (P). We write (19) as

$$\begin{aligned} 0 = &- \int_\Omega u(0)\psi(0) - \int_Q u \frac{\partial \psi}{\partial t} + \left[- \int_Q \mathbf{b} \cdot \nabla \psi + \int_{\Sigma_{out}} \mathbf{b} \cdot \mathbf{n} u \psi \right] + \int_Q \nabla \theta \cdot \nabla \psi \\ &+ \int_{\Sigma_n} g^* \psi := II + III + IV + V + VI. \end{aligned}$$

We integrate (41) with respect to time using ψ^{n-1} as the test function. A direct

calculation shows that

$$
\begin{aligned}
0 = &\sum_{n=1}^{N} \tau \left(\langle \partial U^n, \psi^{n-1} \rangle_h + b_h(U^{n-1}, \psi^{n-1}) + \langle \nabla \Theta^n, \nabla \psi^{n-1} \rangle + \langle g(\Theta^n), \psi^{n-1} \rangle_{h,\Gamma_n} \right) \\
= &\langle U^N, \psi^{N-1} \rangle_h - \langle U^0, \psi^0 \rangle_h - \sum_{n=2}^{N} \tau \langle U^n, \partial \psi^n \rangle + \sum_{n=1}^{N} (b_h(U^{n-1}, \psi^{n-1}) + \\
&\langle \nabla \Theta^n, \nabla \psi^{n-1} \rangle + \langle g(\Theta^n), \psi^{n-1} \rangle_{h,\Gamma_n}) \\
= &\langle u_{h,\tau}(T), \psi_{h,\tau}(T-\tau) \rangle_h - \langle P_h u(0), \psi_{h,\tau}(0) \rangle - \int_{\tau}^{T} \langle u_{h,\tau}, \psi'_{h,\tau}(t-\tau) \rangle_h \\
&+ \int_{\tau}^{T} b_h(u_{h,\tau}(t-\tau), \psi_{h,\tau}) + \int_0^T \langle \nabla \theta_{h,\tau}(t), \nabla \psi_{h,\tau}(t) \rangle + \int_0^T \langle g(\theta_{h,\tau}(t)), \psi_{h,\tau} \rangle_{h,\Gamma_n} \\
&:= I_{h,\tau} + II_{h,\tau} + III_{h,\tau} + IV_{h,\tau} + V_{h,\tau} + VI_{h,\tau}.
\end{aligned}
$$

For the term $I_{h,\tau}$, it holds by (25) and (35)

$$
\begin{aligned}
\lim_{h,\tau \to 0} I_{h,\tau} = &\lim_{h,\tau \to 0} \Big[|\langle u_{h,\tau}(T), \psi_{h,\tau}(T-\tau) \rangle_h + \langle u_{h,\tau}(T), \psi_{h,\tau}(T-\tau) \rangle - \\
&\langle u_{h,\tau}(T), \psi_{h,\tau}(T-\tau) \rangle| \Big] \leq \lim_{h,\tau \to 0} \Big[|\langle u_{h,\tau}(T), \psi_{h,\tau}(T-\tau) \rangle_h - \\
&\langle u_{h,\tau}(T), \psi_{h,\tau}(T-\tau) \rangle| + |\langle u_{h,\tau}(T), \psi_{h,\tau}(T-\tau) \rangle| \Big] \\
&\leq \lim_{h,\tau \to 0} \Big[Ch \|u_{h,\tau}\|_{L^2(\Omega)} \|\nabla \psi_{h,\tau}\|_{L^2(\Omega)} + \langle u_{h,\tau}(T), \psi_{h,\tau}(T-\tau) \rangle \Big] \to 0.
\end{aligned}
$$

Now $|\lim_{h,\tau \to 0} II_{h,\tau} - II| \to 0$, as by (25) and (27) we get

$$
\begin{aligned}
&\left| \lim_{h,\tau \to 0} II_{h,\tau} - \langle u(0), \psi(0) \rangle \right| \leq \lim_{h,\tau \to 0} \Big[Ch \|Pu_h(0)\|_{L^2(\Omega)} \|\nabla \psi_{h,\tau}\|_{L^2(\Omega)} + \\
&|\langle P_h u(0) - u(0), \psi_{h,\tau}(0) \rangle| + |\langle u(0), \psi_{h,\tau}(0) - \psi(0) \rangle| \Big] \to 0.
\end{aligned}
$$

Furthermore, $|\lim_{h,\tau \to 0} III_{h,\tau} - III| \to 0$ as

$$
\begin{aligned}
&|\lim_{h,\tau \to 0} III_{h,\tau} - \int_0^T \langle u, \frac{\partial \psi}{\partial t} \rangle| \leq \lim_{h,\tau \to 0} \Big[Ch \|u_{h,\tau}\|_{L^2(\Omega)} \|\nabla \psi'_{h,\tau}\|_{L^2(\Omega)} + \\
&|\int_{\tau}^{T} \langle u_{h,\tau} - u(t), \psi'_{h,\tau}(t-\tau) \rangle| + |\int_{\tau}^{T} \langle u_{h,\tau}, \psi'_{h,\tau}(t-\tau) - \frac{\partial \psi}{\partial t} \rangle| \Big] \to 0.
\end{aligned}
$$

The term IV converges by Lemma (3.2.1). By using convergence property (35), we get

$$
\begin{aligned}
&|\lim_{h,\tau \to 0} V_{h,\tau} - \int_Q \nabla \theta \cdot \nabla \psi| = \lim_{h,\tau \to 0} \left[\int_0^T \langle \nabla \theta_{h,\tau}, \nabla \psi_{h,\tau} \rangle - \int_0^T \langle \nabla \theta, \nabla \psi \rangle \right] \leq \\
&\lim_{h,\tau \to 0} \left[|\int_0^T \langle \nabla (\theta_{h,\tau} - \theta), \nabla \psi_{h,\tau} \rangle| + |\int_0^T \langle \nabla \theta_{h,\tau}, \nabla (\psi_{h,\tau} - \psi) \rangle| \right] \to 0
\end{aligned}
$$

On the boundary, it holds that $|\lim_{h,\tau} VI_{h,\tau} - VI| \to 0$, as by (26)

$$|\lim_{h,\tau\to 0} VI_{h,\tau} - \int_0^T \langle g^*, \psi\rangle_{\Gamma_n}| \le \lim_{h,\tau\to 0} \Big[Ch^{\frac{1}{2}}\|g(\theta_{h,\tau})\|_{L^2(\Gamma_n)}\|\nabla\psi_{h,\tau}\|_{L^2(\Omega)} + \int_0^T \langle g(\theta_{h,\tau}) - g^*), \psi_{h,\tau}\rangle_{\Gamma_n} + \int_0^T \langle g^*, \psi - \psi_{h,\tau}\rangle_{\Gamma_n}\Big] \to 0.$$

Now we have shown that to the limits u, θ, and g^* it holds

$$-\int_Q u\left(\frac{\partial\psi}{\partial t} + \mathbf{b}\cdot\nabla\psi\right) + \int_{\Sigma_{out}} \mathbf{b}\cdot\mathbf{n}u\psi + \int_Q \nabla\theta\cdot\nabla\psi + \int_{\Sigma_n} g^*\psi = \int_\Omega u(0)\psi(0), \tag{51}$$

for all $\psi \in F$. By the density argument together with (35), we find that (51) also holds for all $\psi \in L^2(0,T;V(0)) \cap H^1(0,T;L^2(\Omega))$, with $\psi(x,T) = 0$.

In order to prove $u \in \Upsilon(\theta)$, we use the relation $u \in \Upsilon(\theta) \iff \theta = \beta(u)$. Thus it suffices to prove $\theta = \beta(u)$.

We use the monotonicity argument. Recall that $\Theta_i^n = \Pi_h\beta(U_i^n)$, thus

$$\sum_{n=1}^N \tau\langle\Theta^n - \Pi_h\beta(\psi_{h,\tau}), U^{n-1} - \psi_{h,\tau}\rangle_h \ge 0.$$

As $\theta_{h,\tau}$ converges strongly in $L^2(0,T;L^2(\Omega))$, we have

$$\int_0^T \langle\theta - \beta(\psi), u - \psi\rangle \ge 0,$$

which implies that $\theta = \beta(u)$ (see [15]). The same argument can be used for the nonlinear boundary term to show that $g(\theta) = g^*$. Thus $\{u,\theta\}$ solves (P). Since the solution of (P) is unique, the convergence holds for the whole sequence $\{u_{h,\tau}, \theta_{h,\tau}\}$.

3.3 Upwinding

In this section, we use for the convection term the upwinding technique, which can be formulated introducing artificial diffusion in the streamline direction: The approximation to the convection term on the basis ψ_h is defined by

$$b_h(u_h,\psi_h) = \langle\mathbf{b}\cdot\nabla u_h, \psi_h\rangle_h + \frac{h}{2}\|\mathbf{b}\|^{-1}\langle\mathbf{b}\cdot\nabla u_h, \mathbf{b}\cdot\nabla\psi_h\rangle.$$

Lemma 3.3.1 *Mapping $b_h : V_h \times V_h(0) \to R$ has the following properties:*

$$\begin{array}{ll} i) & b_h(u_h,\psi_h) \to b(u,\psi), \quad \forall u_h \rightharpoonup u \text{ in } L^2(\Omega), \psi_h \to \psi \text{ in } V, \\ ii) & |b_h(u_h,\psi_h)| \le C\|u_h\|_{L^2(\Omega)}\|\psi_h\|_{V(0)} \quad \forall u_h \in V_h, \psi_h \in V_h(0). \end{array} \tag{52}$$

Proof. By integrating $b_h(u_h, \psi_{h,\tau})$, we get

$$b_h(u_h,\psi_{h,\tau}) = \int_\Omega \mathbf{b}\cdot\nabla u_h\psi_{h,\tau} + \frac{h}{2}\|\mathbf{b}\|^{-1}\int_\Omega \mathbf{b}\cdot\nabla u_h\mathbf{b}\cdot\nabla\psi_{h,\tau} = \\ -\int_\Omega u_h\mathbf{b}\cdot\nabla\psi_{h,\tau} + \int_{\partial\Omega}\mathbf{b}\cdot\mathbf{n}u_h\psi_{h,\tau} + \frac{h}{2}\|\mathbf{b}\|^{-1}\int_\Omega \mathbf{b}\cdot\nabla u_h\mathbf{b}\cdot\nabla\psi_h. \quad (53)$$

Let $\psi \in F$; then by using the Greens formula and inverse inequality $\|\nabla u_h\|_{L^2(\Omega)} \leq \frac{1}{h}C\|u_h\|_{L^2(\Omega)}$ we obtain

$$\frac{h}{2}\|\mathbf{b}\|^{-1}\int_\Omega \mathbf{b}\cdot\nabla u_h\mathbf{b}\cdot\nabla\psi_{h,\tau} = \\ \frac{h}{2}[\|\mathbf{b}\|^{-1}\int_\Omega \mathbf{b}\cdot\nabla u_h\mathbf{b}\cdot\nabla\psi + \|\mathbf{b}\|^{-1}\int_\Omega \mathbf{b}\cdot\nabla u_h\mathbf{b}\cdot\nabla(\psi_{h,\tau}-\psi)] \\ \leq \frac{h}{2}C_1\|u_h\|_{L^2(\Omega)}\|\psi\|_{H^2(\Omega)} + C_2\|u_h\|_{L^2(\Omega)}\|\psi_{h,\tau}-\psi\|_{H^1(\Omega)}.$$

Letting $h \to 0$ in (53) and using the convergence properties (35), we conclude

$$\lim_{h\to 0} b_h(u_h,\psi_{h,\tau}) = -\int_\Omega u\mathbf{b}\cdot\nabla\psi + \int_{\Gamma_{out}} bu\psi \quad \forall\psi\in C^2(\bar{\Omega}), \psi(x) = 0 \text{ on } x\in\Gamma_{\text{in}}.$$

By density this remains true for $\psi \in V(0)$, thus $ii)$ holds.

We now state the following approximation of the (P).

Problem (PU). *Find* $\{U^n, \Theta^n\}_{n=1}^N$ *such that* $U^n \in \Upsilon(\Theta^n)$

$$U^0 := P_h u_0,$$
$$\Theta^n := \Pi_h\beta(U^n),$$

and for all $\psi \in V_h(0)$, *it holds that*

$$\langle U^n,\psi\rangle_h + \tau b_h(U^n,\psi) + \tau\langle\nabla\Theta^n,\nabla\psi\rangle + \tau\langle g(\Theta^n),\psi\rangle_{h,\Gamma_n} = \langle U^{n-1},\psi\rangle_h. \quad (54)$$

Theorem 3.3.2 *Let* $\{U^n, \Theta^n\}$ *be the solutions of* (PU); *then under the assumptions* (H_Ω), (H_{Ω_h}), (H_β) (H_d), (H_g), *and* (H_{g_h}) .

$$a)\quad \max_{1\leq n\leq N}\|U^n\|_{L^\infty(\Omega)} + \max_{1\leq n\leq N}\|\Theta^n\|_{L^\infty(\Omega)} \leq C,$$
$$b)\quad \sum_{n=1}^N \tau\|\nabla\Theta^n\|_{L^2(\Omega)} \leq C,$$
$$c)\quad \sum_{n=1}^N \tau\|\partial\Theta^n\|^2_{L^2(\Omega)} \leq C.$$

Proof of a). We argue by induction. Assume that $\|U^{n-1}\|_{L^\infty(\Omega)} \leq C$. From the monotonicity of β, we obtain that Θ^n and U^n have the maximum at the same node, say j. Thus by assumptions (H_{Ω_h}) and (H_{g_h}), we have

$$\langle\nabla\theta^n,\nabla\psi_j\rangle + b_h(U^n,\psi_j) + \langle g(\Theta^n),\psi_j\rangle_{h,\Gamma_n} \geq 0,$$

and thus

$$\langle U^n, \psi_j \rangle_h \leq \langle U^{n-1}, \psi_j \rangle_h.$$

The lower bound is again obtained by (H_{g_h}) and the bounds hold also for Θ^n.

Proof of $b)$. We make use of $a)$ in order to obtain the bounds for the functions U^n and Θ^n. Let $\psi = \Theta^n - d_h^n$ be a test function in (54) and sum it over n from 1 to m, $m \leq N$. Then the assertion follows by estimating each term separately. We have to estimate

$$\begin{aligned}
&(I_\theta + I_d) + (II_\theta + II_d) + (III_\theta + III_d) + (IV_\theta + IV_d) := \\
&\sum_{n=1}^{m} [\langle U^n - U^{n-1}, \Theta^n - d_h^n \rangle_h + \tau b_h(U^n, \Theta^n - d_h^n) + \\
&\tau \langle \nabla \Theta^n, \nabla [\Theta^n - d_h^n] \rangle + \tau \langle g(\Theta^n), \Theta^n - d_h^n \rangle_{h,\Gamma_n}] = 0.
\end{aligned}$$

Thus the proof can be carried out as in (3.2.2), except for the convection term, which is now implicit; however, the same arguments still hold. Thus $b)$ holds.

Proof of $c)$. We can use the same test function as in (3.2.2) with the obvious changes to the convection term; thus (3.3.2) holds.

Theorem 3.3.3 *Of the sequences $\theta_{h,\tau}$, $u_{h,\tau}$ in the problem (PU), we can extract subsequences still denoted by the same symbol such that*

$$\begin{aligned}
\theta_{h,\tau} &\to \theta \text{ in } L^2(0,T;L^2(\Omega)), \\
u_{h,\tau} &\rightharpoonup u \text{ in } L^2(0,T;L^2(\Omega)).
\end{aligned}$$

Moreover, $\{u, \theta\}$ solves the problem (P).

Proof. Direct consequence of (3.2.3).

3.4 Combining the characteristic method and Chernoff formulas

We can also combine the characteristic method with nonlinear Chernoff formula. We introduce the following approximation:
PROBLEM (PCo): Find $\{U^n, \Theta^n\}_{n=1}^N$, $U^n \in Y(\Theta^n)$, such that

$$U^0 := P_h u_0, \tag{55}$$

$$\Theta^n := \Pi_h \beta(U^n), \tag{56}$$

and for all $\psi \in V_h(0)$, it holds that

$$\begin{aligned}
\langle \mathbf{A}(\Theta^n), \psi \rangle &= \langle F(U^{n-1}, \Theta^{n-1}), \psi \rangle, \\
U^n &= \bar{U}^{n-1} + \mu[\Theta^n - \beta(\bar{U}^{n-1})],
\end{aligned} \tag{57}$$

where

$$\begin{aligned}
\langle \mathbf{A}(\Theta^n), \psi \rangle &:= \langle \Theta^n, \psi \rangle_h + \frac{\tau}{\mu} \langle \nabla \Theta^n, \nabla \psi \rangle, \\
\langle F(U^{n-1}, \Theta^{n-1}), \psi \rangle &:= \langle \beta(\bar{U}^{n-1}), \psi \rangle_h - \tau \langle g(\Theta^{n-1}), \psi \rangle_{h,\Gamma_n}
\end{aligned}$$

for all $\psi \in V_h, 0 < \mu \leq L_\beta^{-1}$.

A priori estimates for this problem can be derived by combining the techniques of the previous chapters. Namely, in the estimates one can first write the Chernoff formula back to the equation, which leads to the characteristic formulation.

Theorem 3.4.1 *Let $\{U^n, \Theta^n\}$ be the solutions of (PCo), then under the assumptions $(H_\Omega), (H_{\Omega_h}), (H_\beta), (H_d), (H_g)$, (H_{g_h}), and $b\tau \leq h$.*

$$
\begin{aligned}
&a) \quad \max_{1\leq n\leq N} \|U^n\|_{L^\infty(\Omega)} + \max_{1\leq n\leq N} \|\Theta^n\|_{L^\infty(\Omega)} \leq C,\\
&b) \quad \sum_{n=1}^{N} \|U^n - U^{n-1}\|^2_{L^2(\Omega)} + \sum_{n=1}^{N} \tau \|\nabla\Theta^n\|^2_{L^2(\Omega)} \leq C,\\
&c) \quad \sum_{n=1}^{N} \|\Theta^n - \Theta^{n-1}\|^2_{L^2(\Omega)} \leq C.
\end{aligned}
$$

Proof. We proceed as follows. Assumptions (H_{Ω_h}) and (H_{g_h}) provide $L^\infty(Q)$ estimates. Then we need to show $b)$ in order to get the desired $L^2(0,T;H^1(\Omega))$ estimate for the temperature. The first norm of $b)$ can be viewed as discrete $H^{\frac{1}{2}}(0,T : L^2(\Omega))$ norm and it is needed to show same estimate for the temperature.

Proof of $a)$. Let $\|U^0\|_{L^\infty(\Omega)} = C$. We argue by induction. So assume that $\|U^{n-1}\|_{L^\infty(\Omega)} \leq C$. We rewrite the equation to the form

$$\langle \Theta^n, \psi\rangle_h + \frac{\tau}{\mu}\langle \nabla\Theta^n, \nabla\psi\rangle = \langle \beta(\bar{U}^{n-1}), \psi\rangle - \tau\langle g(\Theta^{n-1}), \psi\rangle_{h,\Gamma_n}.$$

From the maximum principle, it follows that at maximum point j, the diffusion term is positive and so due to (H_{g_h}),

$$\langle \Theta^n, \psi_j\rangle_h \leq \langle \beta(\bar{U}^{n-1}), \psi_j\rangle_h.$$

Thus we have the upper bound for Θ^n. Then from the update formula we have

$$\langle U^n, \psi_j\rangle_h = \langle U^{n-1} + \mu[\Theta^n - \beta(\bar{U}^{n-1})], \psi_j\rangle_h \leq \langle C, \psi_j\rangle_h.$$

So we have upper bound for U^n as well. Again, assumption (Hg_h) provides the lower bound.

Proof of $b)$. We use $\psi = \tau(\Theta^n - d_h^n)$ as a test function and sum (57) over n from 1 to $m \leq N$. After reordering, we have to estimate

$$
\begin{aligned}
&(I_\theta + I_d) + (II_\theta + II_{\theta_\Gamma}) + (II_d + II_{d_\Gamma}) + (III_\theta + III_d) + (IV_\theta + IV_d) :=\\
&\sum_{n=1}^{m} [\langle U^n - U^{n-1}, \Theta^n - d_h^n\rangle_h + \tau b_h(U^{n-1}, \Theta^n - d_h^n)\\
&+\tau\langle \nabla\Theta^n, \nabla[\Theta^n - d_h^n]\rangle + \tau\langle g(\Theta^{n-1}), \Theta^n - d_h^n\rangle_{h,\Gamma_n}] = 0. \qquad (58)
\end{aligned}
$$

Thus, by using same test functions as in (3.2.2), we notice that the difference of showing (3.4.1) $b)$ comes from the time derivative, as we do not have

$\Theta^n = \beta(U^n)$ node wise and from the explicit boundary condition. As we have the $L^\infty(Q)$ estimate, the boundary term is bounded, so it remains to show I_θ and I_d. Term I_d can also be handled as in (3.2.2). Thus we have to show that the time derivative remains bounded, and this can be done as in [39]. We define $\alpha(s) = s - \mu\beta(s)$. From the nonlinear Chernoff formula, it follows that

$$\begin{aligned}\Theta^n &= \frac{1}{\mu}[U^n - U^{n-1}] + \beta(U^{n-1}) \\ &= \frac{1}{2}\beta(U^n) - \frac{1}{2\mu}\alpha(U^{n-1}) + \frac{1}{2\mu}U^n + \frac{1}{2\mu}[\alpha(U^n) - \alpha(U^{n-1})].\end{aligned}$$

Hence we can split $(I_\theta) = (I_\theta)_1 + (I_\theta)_2 + (I_\theta)_3 + (I_\theta)_4$. Using the convexity of Φ_β and (32) we have

$$\begin{aligned}2(I_\theta)_1 = \int_\Omega \sum_{n=1}^{m}[\Phi_\beta(U^n) - \Phi_\beta(U^{n-1})] &= \int_\Omega [\Phi_\beta(U^m) - \Phi_{\beta_h}(U^0)] \\ \geq \frac{1}{2L_\beta}\|\beta(U^m)\|^2_{L^2(\Omega)} &- \frac{L_\beta}{2}\|U^0\|^2_{L^2(\Omega)},\end{aligned}$$

and similarly

$$\begin{aligned}2(I_\theta)_2 &\geq \frac{1}{\mu}\int_\Omega \sum_{n=1}^{m}[\Phi_\alpha(U^{n-1}) - \Phi_\alpha(U^n)] = \frac{1}{\mu}\int_\Omega [\Phi_\alpha(U^0) - \Phi_\alpha(U^m)] \\ &\geq \frac{1}{2\mu}\|\alpha(U^0)\|^2_{L^2(\Omega)} - \frac{1}{2\mu}\|U^m\|^2_{L^2(\Omega)}.\end{aligned}$$

Then we get the desired norm by (31)

$$(I_\theta)_3 = \frac{1}{4\mu}\left[\|U^m\|^2_{L^2(\Omega)} - \|U^0\|^2_{L^2(\Omega)} + \sum_{n=1}^{m}\|U^n - U^{n-1}\|^2_{L^2(\Omega)}\right].$$

Term $I(\theta)_4$ is now positive, since α is monotone. Combining terms and using (32), we can conclude

$$\sum_{n=1}^{m}\langle U^n - U^{n-1}, \Theta^n\rangle_h \geq -C + \frac{1}{4\mu}\sum_{n=1}^{m}\|U^n - U^{n-1}\|^2_{L^2(\Omega)},$$

Thus b) holds.

Proof of c). Note that $\Theta^n = U^n - \alpha(U^{n-1})$. As the relaxation parameter is chosen such that $0 < \mu \leq L_\beta^{-1}$, we have $0 \leq \alpha'(s) \leq 1$ a.e. $s \in \mathbb{R}$, then direct calculation shows that

$$\begin{aligned}&\sum_{n=2}^{N}\|\Theta^n - \Theta^{n-1}\|^2_{L^2(\Omega)} = \sum_{n=2}^{N}[\|U^n - U^{n-1} - (\alpha(U^{n-1}) + \alpha(U^{n-2}))]\|^2_{L^2(\Omega)} \\ &\leq C + \sum\|U^{n-1} - U^{n-2}\|^2_{L^2_{(\Omega)}} \leq C,\end{aligned}$$

and thus c) holds.

We have now shown the desired regularity in order to get a limit. It remains to show that this limit solves, the original problem.

Theorem 3.4.2 *Of the sequences $\theta_{h,\tau}$, $u_{h,\tau}$ in the problem (PCo), we can extract subsequences still denoted by the same symbol such that*

$$\begin{aligned} \theta_{h,\tau} &\to \theta \text{ in } L^2(0,T;L^2(\Omega)), \\ u_{h,\tau} &\rightharpoonup u \text{ in } L^2(0,T;L^2(\Omega)). \end{aligned}$$

Moreover, $\{u,\theta\}$ solves the problem (P).

We show now that $\theta = \beta(u)$ a.e. in Q. As $\beta_h(u_{h,\tau})$ is bounded in $L^2(0,T;L^2(\Omega))$, we can find a sub sequence that converges weakly to some $\beta^* \in L^2(0,T;L^2(\Omega))$. We use ψ^{n-1} as the test function, integrate the nonlinear Chernoff formula, and sum over time steps

$$\sum_{n=1}^{N} \tau \int_\Omega \frac{1}{\mu}(U^n - \bar{U}^{n-1})\psi^{n-1} = \sum_{n=1}^{N} \tau \int_\Omega (\Theta^n - \beta(\bar{U}^{n-1}))\psi^{n-1}. \tag{59}$$

The lefthand side of the equation is approximated with the Cauchy-Schwartz inequality

$$\begin{aligned} \sum_{n=1}^{N} \tau \int_\Omega \frac{1}{\mu}(U^n - \bar{U}^{n-1})\psi^{n-1} &\leq \tau^{\frac{1}{2}} \Big(\sum_{n=1}^{N} \|U^n - \bar{U}^{n-1}\|^2_{L^2(\Omega)}\Big)^{\frac{1}{2}} \Big(\sum_{n=1}^{N} \tau \|\psi^{n-1}\|^2_{L^2(\Omega)}\Big)^{\frac{1}{2}} \\ &\leq C\tau^{\frac{1}{2}} \|\psi_{h,\tau}\|_{L^2(Q)}, \forall\, \psi_{h,\tau} \in L^2(Q). \end{aligned}$$

This implies that $\theta_{h,\tau} - \beta(\bar{u}_{h,\tau}) \rightharpoonup 0$ in $L^2(0,T;L^2(\Omega))$. Hence $\beta^* = \theta$.

It remains to show that $\beta^* = \beta(u)$. Note that

$$\|\beta(\bar{u}_{h,\tau}) - \beta^*\|_{L^2(Q)} \leq \|\beta(\bar{u}_{h,\tau}) - \theta_{h,\tau}\|_{L^2(Q)} + \|\theta_{h,\tau} - \beta^*\|_{L^2(Q)}.$$

As $\theta_{h,\tau}$ converges strongly in $L^2(0,T;L^2(\Omega))$ and

$$\|\beta(\bar{u}_{h,\tau}) - \theta_{h,\tau}\|_{L^2(Q)} \leq C\tau \sum_{n=1}^{m} \|U^n - U^{n-1}\|_{L^2(\Omega)} \leq C\tau,$$

we have strong convergence for $\beta(\bar{u}_{h,\tau})$ in $L^2(Q)$. We can now use the monotonicity of β,

$$\sum_{n=1}^{N} \tau \langle \beta(\bar{U}^{n-1}) - \beta(\psi^{n-1}), \bar{U}^{n-1} - \psi^{n-1} \rangle_h \geq 0,$$

letting $\tau, h \to 0$ we have

$$\int_0^T \langle \beta(u) - \beta(\psi), u - \psi \rangle \geq 0,$$

which implies that $\beta^* = \beta(u)$ (see [15]). Thus $\{\theta, u\}$ solves (P). As the solution of (P) is unique, the convergence holds for the whole sequence $\{\theta_{h,\tau}, u_{h,\tau}\}$.

Remark. The same argument as in the problem (PC) shows that there is no restriction $\tau b \leq h$ in the alloys.

3.5 Combining upwinding and Chernoff formulas

The approximation is defined by:
PROBLEM (PCh): Find $\{U^n, \Theta^n\}_{n=1}^N$, $U^n \in \mathrm{Y}(\Theta^n)$, such that for given

$$U^0 = P_h u^0,$$
$$\Theta^0 = \beta(U^0),$$

it holds that

$$\begin{aligned} \langle \mathbf{A}(\Theta^n), \psi \rangle &= \langle F(U^{n-1}, \Theta^{n-1}), \psi \rangle, \\ U^n &= U^{n-1} + \mu[\Theta^n - \beta(U^{n-1})], \end{aligned} \tag{60}$$

where

$$\begin{aligned} \langle \mathbf{A}(\Theta^n), \psi \rangle &:= \langle \Theta^n, \psi \rangle_h + \tau b_h(\Theta^n, \psi) + \frac{\tau}{\mu} \langle \nabla \Theta^n, \nabla \psi \rangle, \\ \langle F(U^{n-1}, \Theta^{n-1}), \psi \rangle &:= \langle \beta(U^{n-1}), \psi \rangle_h + \tau b_h(\beta(U^{n-1}) - \tfrac{1}{\mu} U^{n-1}, \psi) \\ &- \tau \langle g(\Theta^{n-1}), \psi \rangle_{h, \Gamma_n}, \end{aligned}$$

for all $\psi \in V_h(0), 0 < \mu \leq L_\beta^{-1}$.

Remark. We have used the relation

$$\langle \mathbf{b} \cdot \nabla U^n, \psi \rangle = \langle \mathbf{b} \cdot \nabla \left(U^{n-1} + \mu[\Theta^n - \beta(U^{n-1})] \right), \psi \rangle,$$

in the definition of (PCh), as this allows us to eliminate the implicit enthalpy dependent convection term from the lefthand side of the equation (60).

Theorem 3.5.1 *Let $\{U^n, \Theta^n\}$ be the solutions of (PCo); then under the assumptions (H_Ω), (H_{Ω_h}), (H_β) (H_d), (H_g) and (H_{g_h}), and $b\tau < Ch$.*

$$a) \quad \max_{1 \leq n \leq N} \|U^n\|_{L^\infty(\Omega)} + \max_{1 \leq n \leq N} \|\Theta^n\|_{L^\infty(\Omega)} \leq C,$$
$$b) \quad \sum_{n=1}^N \|U^n - U^{n-1}\|_{L^2(\Omega)}^2 + \sum_{n=1}^N \tau \|\nabla \Theta^n\|_{L^2(\Omega)}^2 \leq C,$$
$$c) \quad \sum_{n=1}^N \|\Theta^n - \Theta^{n-1}\|_{L^2(\Omega)}^2 \leq C.$$

Proof of a). Again we make use of the maximum principle and argue by induction. Thus we have at node j using assumptions (H_{Ω_h}) and (H_{g_h})

$$\langle \Theta^n, \psi_j \rangle \leq \langle \beta(U^{n-1}), \psi_j \rangle_h + \tau b_h(\beta(U^{n-1}) - \frac{1}{\mu} U^{n-1}, \psi_j).$$

By extra assumption $\tau b < Ch$, we get

$$\langle \Theta^n, \psi_j \rangle \leq C \langle \beta(U^{n-1}), \psi_j \rangle_h.$$

The rest of the arguments of showing (3.5.1) can be obtained from (3.3.2).
Thus the same regularity as in the problem (PU) holds and the limit is obvious. On the other hand, the original problem is also solved simply by replacing $\beta(\bar{U}^n)$ with $\beta(U^n)$ in the proof (3.4.2). Thus we have shown the following theorem.

Theorem 3.5.2 *Of the sequences $\theta_{h,\tau}$, $u_{h,\tau}$ in the problem (PCh), we can extract subsequences still denoted by the same symbol such that*

$$\begin{aligned} \theta_{h,\tau} &\to \theta \text{ in } L^2(0,T;L^2(\Omega)), \\ u_{h,\tau} &\rightharpoonup u \text{ in } L^2(0,T;L^2(\Omega)). \end{aligned}$$

Moreover, $\{u,\theta\}$ solves the problem (P).

4 IMPLEMENTATION

In this chapter, we define the approximations in the matrix form using elimination of the Dirichlet nodes. We form the global matrices using tensor products. Then we present the basic algorithms and describe how the nonlinear algebraic system can be solved using the linear boundary condition. Finally, we give numerical examples and discuss numerical efficiency of the approximations with the used solvers.

We separate the Dirichlet nodes and denote by Dir the set of indexes associated with the Dirichlet boundary and by Ind, the set of indexes associated with the other nodes of the mesh. Then

$$\theta_h = \sum_{i \in \mathrm{Ind}} \theta_i \psi_i + \sum_{i \in \mathrm{Dir}} d_i \psi_i, \tag{61}$$

where ψ_i denotes the trilinear basis.

4.1 Tensor product matrices

We show now, how the global matrices can be computed via tensor products.

Definition 4.1.1 *Let* $\mathbf{A}$ *be* $n_1 \times n_1$ *matrix with components* a_{ij} *and let* $\mathbf{B}$ *be* $n_2 \times n_2$ *matrix. The* $n_1 n_2 \times n_1 n_2$ *matrix*

$$\mathbf{A} \otimes \mathbf{B} = \begin{pmatrix} a_{11}\mathbf{B} & a_{12}\mathbf{B} & \dots & a_{1n_1}\mathbf{B} \\ a_{21}\mathbf{B} & a_{22}\mathbf{B} & & \\ \vdots & \vdots & \ddots & \vdots \\ a_{n_1 1}\mathbf{B} & a_{n_1 2}\mathbf{B} & \dots & a_{n_1 n_1}\mathbf{B} \end{pmatrix} \in \mathbb{R}^{n_1 n_2 \times n_1 n_2}$$

is called tensor product of the matrices $\mathbf{A}$ *and* $\mathbf{B}$.

Let us consider rectangular slab $\Omega = (a_1, b_1) \times (a_2, b_2) \times (a_3, b_3)$. We construct a rectangular mesh to Ω, denoted by Ω_h using mesh points

$$(x_i^1, x_j^2, x_k^3), \quad i = 1, \dots, n_1,\ j = 1, \dots, n_2,\ k = 0, \dots\ n_3,$$

where in the x^1 and x^2 direction, we have

$$a_l = x_1^l < x_2^l < \cdots < x_{n_l}^l = b_l, \quad l = 1, 2,$$

and in the casting direction we have

$$a_3 = x_0^3 < x_1^3 < \cdots < x_{n_3}^3 = b_3, \quad h_i^3 = x_i^3 - x_{i-1}^3, \quad i = 1, \ldots, n_3.$$

In what follows, we denote

$$h_i^l = x_i^l - x_{i-1}^l, \quad i = 2, \ldots, n_l.$$

Then the standard central finite difference stiffness matrices $\mathbf{A}_l$ and mass matrices $\mathbf{M}_l$, taking into account the boundary conditions of (P) and the elimination of the Dirichlet boundary nodes, are

$$\mathbf{A}_l = \begin{pmatrix} \frac{1}{h_1^l} & -\frac{1}{h_2^l} & & & 0 \\ -\frac{1}{h_2^l} & \frac{h_1^l + h_2^l}{h_1^l h_2^l} & & & \\ & \ddots & \ddots & \ddots & \\ & & & \frac{h_{n_l-1}^l + h_{n_l-1}^l}{h_{n_l-1}^l h_{n_l}^l} & -\frac{1}{h_{n_l}^l} \\ 0 & & & -\frac{1}{h_{n_l}^l} & \frac{1}{h_{n_l}^l} \end{pmatrix} \in \mathbb{R}^{n_l \times n_l},$$

and

$$\mathbf{M}_l = \operatorname{diag}\left(\frac{h_1^l}{2}, \frac{h_1^l + h_2^l}{2}, \ldots, \frac{h_{n_l-1}^l + h_{n_l}^l}{2}, \frac{h_{n_l}^l}{2}\right) \in \mathbb{R}^{n_l \times n_l}, \quad l = 1, 2.$$

Furthermore,

$$\mathbf{A}_3 = \begin{pmatrix} \frac{h_1^3 + h_2^3}{h_1^3 h_2^3} & -\frac{1}{h_2^l} & & & 0 \\ -\frac{1}{h_2^l} & \frac{h_2^3 + h_3^3}{h_2^3 h_3^3} & & & \\ & \ddots & \ddots & \ddots & \\ & & & \frac{h_{n_3-1}^3 + h_{n_3}^l}{h_{n_3-1}^3 h_{n_3}^3} & -\frac{1}{h_{n_3}^3} \\ 0 & & & -\frac{1}{h_{n_3}^3} & \frac{1}{h_{n_3}^3} \end{pmatrix} \in \mathbb{R}^{n_3 \times n_3},$$

and for the mass matrix, by using mass lumping

$$\mathbf{M}_3 = \operatorname{diag}\left(\frac{h_1^3 + h_2^3}{2}, \ldots, \frac{h_{n_3-1}^3 + h_{n_3}^3}{2}, \frac{h_{n_3}^l}{2}\right) \in \mathbb{R}^{n_3 \times n_3}.$$

Let $N_d := n_1 n_2 n_3$. Then Ind has N_d nodes. The global stiffness matrix $\mathbf{A} \in \mathbb{R}^{N_d \times N_d}$ can be presented as

$$\mathbf{A} = \sum_{i \in \text{Ind}} \langle \nabla \psi_i, \nabla \psi_j \rangle = \mathbf{A}_1 \otimes \mathbf{M}_2 \otimes \mathbf{M}_3 + \mathbf{M}_1 \otimes \mathbf{A}_2 \otimes \mathbf{M}_3 + \mathbf{M}_1 \otimes \mathbf{M}_2 \otimes \mathbf{A}_3, \quad j \in \text{Ind}.$$

In a similar manner, the global mass matrix has the presentation

$$\mathbf{M} = \sum_{i \in \text{Ind}} \langle \psi_i, \psi_j \rangle_h = \mathbf{M}_1 \otimes \mathbf{M}_2 \otimes \mathbf{M}_3 \in \mathbb{R}^{N_d \times N_d}, j \in \text{Ind}. \tag{62}$$

For the convection term, we define

$$\bar{\mathbf{C}} = \mathbf{I}_1 \otimes \mathbf{I}_2 \otimes \mathbf{C}_3 \in \mathbb{R}^{N_d \times N_d}, j = 1, \ldots, N_d, \tag{63}$$

where $\mathbf{C}_3$ is calculated with the upwinding formula

$$\mathbf{C}_3 = \begin{pmatrix} \frac{1}{h_1^3} & 0 & & & 0 \\ -\frac{1}{h_2^3} & \frac{1}{h_2^3} & & & \\ & \ddots & \ddots & \ddots & \\ & & & & 0 \\ 0 & & & -\frac{1}{h_{n_3}^3} & \frac{1}{h_{n_3}^3} \end{pmatrix} \in \mathbb{R}^{n_3 \times n_3},$$

$\mathbf{I}_1 \in \mathbb{R}^{n_1 \times n_1}$ and $\mathbf{I}_2 \in \mathbb{R}^{n_2 \times n_2}$ are identity matrices; then

$$\mathbf{C} = \sum_{i \in \text{Ind}} [\langle e_z \cdot \nabla \psi_i, \psi_j \rangle + \frac{h_i^3}{2} \langle e_z \cdot \nabla \psi_i, e_z \cdot \nabla \psi_j \rangle] = \mathbf{M}\bar{\mathbf{C}}, \quad j \in \text{Ind}.$$

The boundary blocks are computed as

$$\mathbf{B}_1 = \mathbf{M}_1 \otimes \mathbf{M}_3, \quad j = 1, \ldots, n_1 n_3,$$
$$\mathbf{B}_2 = \mathbf{M}_2 \otimes \mathbf{M}_3, \quad j = 1, \ldots, n_2 n_3,$$

and the sum of their zero extension to $\mathbb{R}^{N_d \times N_d}$ is then $\mathbf{B}$ such that

$$\mathbf{B} = \sum_{i \in \text{Ind}} \langle \psi_i, \psi_j \rangle_{\Gamma_{n,h}}, \quad j \in \text{Ind}.$$

Let $\mathbf{A}_\Gamma = \text{diag}(\frac{1}{h_1^3}, 0, \ldots, 0) \in \mathbb{R}^{n_3 \times n_3}$ and $\mathbf{C}_\Gamma = \text{diag}(\frac{h_1^3 + h_2^3}{2h_1^3}, 0, \ldots, 0) \in \mathbb{R}^{n_3 \times n_3}$. Then

$$\mathbf{A}_{\Gamma_{\text{in}}} = \sum_{i \in \text{Dir}} \langle \nabla \psi_i, \nabla \psi_j \rangle = \mathbf{M}_1 \otimes \mathbf{M}_2 \otimes \mathbf{A}_\Gamma \in \mathbb{R}^{N_d \times N_d}, j \in \text{Ind},$$

and

$$\begin{aligned} \mathbf{C}_{\Gamma_{\text{in}}} &= \sum_{i \in \text{Dir}} [\langle e_z \cdot \nabla \psi_i, \psi_j \rangle + \frac{h_i^3}{2} \langle e_z \cdot \nabla \psi_i, e_z \cdot \nabla \psi_j \rangle] \\ &= \mathbf{M}_1 \otimes \mathbf{M}_2 \otimes \mathbf{C}_\Gamma \in \mathbb{R}^{N_d \times N_d}, \quad j \in \text{Ind}. \end{aligned}$$

Furthermore, let $\mathbf{u} = (u_1, \ldots, u_{N_d})^T$, $\boldsymbol{\theta} = (\theta_1, \ldots, \theta_{N_d})$ and $\boldsymbol{\Upsilon}(\boldsymbol{\theta}) = (\Upsilon(\theta_1), \ldots, \Upsilon(\theta_{N_d}))$ denote the nodal values of the U, Θ, and $\Upsilon(\Theta)$ at the points $x_m := (x_i^1, x_j^2, x_k^3)$, $i = 1, \ldots, n_1$, $j = 1, \ldots, n_2$, $k = 1, \ldots n_3, m = 1, \ldots N_d$.

The Dirichlet boundary value of the diffusion term is eliminated as $\mathbf{A}_{\Gamma_{\text{in}}}\mathbf{Y}(\mathbf{d})$, where $\mathbf{Y}(\mathbf{d})^T \in \mathbb{R}^{N_d}$ such that

$$\mathbf{Y}(d_m) = \begin{cases} \mathrm{Y}(d(x_i^1, x_j^2, 0)) & \text{for } i = 1, \ldots, n_1,\ j = 1, \ldots, n_2, \\ 0 & \text{for all } (x_i^1, x_j^2, x_k^3), \text{when } k > 1, \end{cases}$$

and the convection part of the Dirichlet value is eliminated by $\mathbf{C}_{\Gamma_{\text{in}}}\mathbf{Y}(\mathbf{d})$.

On the boundary we set $\Gamma_{n,h} = \Gamma_{\text{mold},h} \cup \Gamma_{\text{roll},h} \cup \Gamma_{\text{rad},h} \cup \Gamma_{\text{cool},h}$ and by $\mathbf{g}(\boldsymbol{\theta})^T \in \mathbb{R}^{N_d}$, we denote the boundary values such that

$$\mathbf{g}(\boldsymbol{\theta}_m) = \begin{cases} g(\theta_m) & \text{if } x_m \in \Gamma_{n,h}, \\ 0 & \text{if } x_m \notin \Gamma_{n,h}. \end{cases}$$

In the implementation, we make use of sparsity and the symmetry of the matrices. Thus the total storage requirement is proportional to $4N_d$ for the stiffness matrix $\mathbf{A}$. The mass matrix $\mathbf{M}$ is diagonal, and the convection matrix C is stored in two vectors.

Remark. As on the corner, the normal vector is not well defined in a classical sense, it is sometimes practical to separate the boundary mass matrices on each sides, rather than forming the global matrix. Then on the corner nodes, normal derivatives can be given for the both directions and our matrices can be considered as finite difference approximations. For notational convenience, we give the matrix formulations using global boundary mass matrix $\mathbf{B}$.

4.2 Matrix formulations and numerical solution methods of the approximations

Now we present our approximations, using the matrix notations defined in the previous section. In the nonlinear approximations (PU) and (PC) where the algebraic system must be solved iteratively, the choice of the actual solution algorithm depends on the form of the material data and the boundary condition. In the classical two-phase Stefan problem, one typically has constant material data in both phases, and we use this assumption in the solution algorithm of (PC) and (PCo). In this way, analytical solutions can be constructed and implemented to the model problem. In this type of situation, it is convenient to use the algorithm presented in [15] in the (PC). In the problem (PU), we have to use enthalpy as the solution variable.

When the resulting algebraic system is linear, the choice of solution methods is wider. One could use, e.g., conjugate gradient type, lower upper (LU) decomposition, or multigrid methods. Our choice is the partial solution variant of cyclic reduction by Rossi and Toivanen [47], and we refer to its implementation as (DC3D). They have also developed a version of this software, which can handle a convection term to the casting direction (DCC3D).

We now describe matrix forms of the approximations, including the algebraic system solved in each time step.

We set $\hat{\mathbf{M}} = \frac{1}{\tau}\mathbf{M}$.

Algorithm 4.2.1 *Matrix formulation for PC*

Set $\mathbf{u}^0 = P_h u_0$.
For $n = 1, \cdots, N$
  Set $\bar{\mathbf{u}}^{n-1} = (u^{n-1}(\bar{x}_1), \ldots, u^{n-1}(\bar{x}_{N_d}))$
  Solve $\boldsymbol{\theta}^n, \mathbf{u^n}$ from the equation
  $\hat{\mathbf{M}}\mathbf{u}^n + \mathbf{A}\boldsymbol{\theta}^n + \mathbf{B}\mathbf{g}(\boldsymbol{\theta}^n) = \hat{\mathbf{M}}\bar{\mathbf{u}}^{n-1} - \mathbf{A}_{\boldsymbol{\Gamma}_{in}}\mathbf{d}^n := \mathbf{f}$
End

Assuming that the enthalpy is given by

$$\Upsilon(\theta) = \begin{cases} d_1\theta, & \theta < 0, \\ [0, L], & \theta = 0, \\ d_2\theta + L, & \theta > 0, \end{cases} \tag{64}$$

and that the boundary condition is given as a flux, one can solve the problem (PC) as follows. Let $\theta_i^{n,0} = \theta_i^{n-1}$. At each node i at time level n, we first perform a Gauss Seidel iteration $k = 1, 2, \ldots$, by solving the inclusion

$$z_i^k := f_i - \sum_{j<i} a_{ij}\theta_j^{n,k+1} - \sum_{j>i} a_{ij}\theta_j^{n,k} \in a_{ii}w_i^{k+1} + \hat{m}_{ii}\Upsilon(w_i^{k+1})$$

for w_i^{k+1},

$$w_i^{k+1} = \begin{cases} (z_i^k - \hat{m}_{ii}L)/(a_{ii} + d_2\hat{m}_{ii}), & z_i^k > \hat{m}_{ii}L, \\ 0, & z_i^k \in [0, \hat{m}_{ii}L], \\ z_i^k/(a_{ii} + d_1\hat{m}_{ii}), & z_i^k < 0. \end{cases}$$

If we use Gauss Seidel, we set

$$\theta_i^{n,k+1} = w_i^{k+1}.$$

In the case we want to apply SOR with a relaxation parameter with a relaxation parameter $\omega \in]0, 2[$, we test if

$$\theta_i^{n,k}\{\theta_i^{n,k} + \omega(w_i^{k+1} - \theta_i^{n,k})\} > 0 \tag{65}$$

and set

$$\theta_i^{n,k+1} = \theta_i^{n,k} + \omega(w_i^{k+1} - \theta_i^{n,k}),$$

otherwise only the Gauss Seidel step is taken. In (65) it is tested whether the phase is changing. If the phase does not change, overrelaxation can be used. This test is necessary since the overrelaxation would change the phase, leading to a solution in which the false material parameters are used, and this can cause difficulties with convergence.

When the convergence criteria for $\boldsymbol{\theta}$ is reached, the enthalpy is updated as follows

$$u_i^n = \begin{cases} d_1\theta_i^n, & \theta_i^n < 0, \\ [f_i - \sum_{j<i} a_{ij}\theta_j^n - \sum_{j>i} a_{ij}\theta_j^n - a_{ii}\theta_i^n)]/\hat{m}_{ii}, & \theta_i^n = 0, \\ d_2\theta_i^n + L, & \theta_i^n > 0. \end{cases} \tag{66}$$

The matrix form of (PU) is as follows :

Algorithm 4.2.2 *Matrix form of PU*

Set $\mathbf{u}^0 = P_h u_0$
For $n = 1, \cdots, N$
  Solve $\mathbf{u}^n$from the equation
  $\hat{\mathbf{M}}\mathbf{u}^n + b^n\mathbf{C}\mathbf{u}^n + \mathbf{A}\boldsymbol{\beta}(\mathbf{u}^n) + \mathbf{B}\mathbf{g}(\boldsymbol{\beta}(\mathbf{u}^n)) = \hat{\mathbf{M}}\mathbf{u}^{n-1} - \mathbf{A}_{\Gamma_{in}}\mathbf{d}^{\mathbf{n}} - b^n\mathbf{C}_{\Gamma_{in}}\mathrm{Y}(\mathbf{d}^{\mathbf{n}})$
End

The solution to the matrix form (PU) is guaranteed noting that

$$G(\mathbf{u}) := \hat{\mathbf{M}}\mathbf{u} + b^n\mathbf{C}\mathbf{u} + \mathbf{A}\boldsymbol{\beta}(\mathbf{u}) + \mathbf{B}\mathbf{g}(\boldsymbol{\beta}(\mathbf{u})) \tag{67}$$

defines the M-function, i.e., G is continuous diagonally isotone and offdiagonally antitone. The solution can be obtained using the nonlinear Gauss Seidel method [42], with under relaxation parameter $\omega \in]0, 1]$.

The matrix form of (PCo) is as follows:

Algorithm 4.2.3 *Matrix form for PCo*

For given initial data $\Theta^0 = K(P_h\vartheta^0)$
For $n = 1, \cdots, N$
  Solve $\boldsymbol{\theta}^n$ from the equation
  $\hat{\mathbf{M}}\boldsymbol{\theta}^n + \frac{1}{\mu}\mathbf{A}\boldsymbol{\theta}^n = \mathbf{f}^{\mathbf{n-1}}$, where
  $\mathbf{f}^{n-1} = \hat{\mathbf{M}}\boldsymbol{\beta}(\bar{\mathbf{u}}^{n-1}) - \mathbf{B}\mathbf{g}(\boldsymbol{\theta}^{n-1}) - \mathbf{A}_{\Gamma_{\mathrm{in}}}\mathbf{d}^n$ and set
  $\mathbf{u}^n = \bar{\mathbf{u}}^{n-1} + \mu[\boldsymbol{\theta}^n - \boldsymbol{\beta}(\bar{\mathbf{u}}^{n-1})]$
End

As mentioned, we use *DCC3D* as the solver for the algebraic problem.

The matrix form of (PCh) is as follows:

Algorithm 4.2.4 *Matrix form for* (PCh)

For given initial data $\Theta^0 = K(P_h\vartheta^0)$

Set $\mathbf{u}^0 = \mathbf{Y}(\boldsymbol{\theta}^0)$

For $n = 1, \cdots, N$

Solve $\boldsymbol{\theta}^n$ from the equation

$$\hat{\mathbf{M}}\boldsymbol{\theta}^n + b^n\mathbf{C}\boldsymbol{\theta}^n + \frac{1}{\mu}\mathbf{A}\boldsymbol{\theta}^n = \mathbf{f}^{\mathbf{n-1}}, \text{ where}$$

$$\mathbf{f}^{n-1} = \hat{\mathbf{M}}\boldsymbol{\beta}(\mathbf{u}^{n-1}) + b^n\mathbf{C}[\boldsymbol{\beta}(\mathbf{u}^{n-1}) + \frac{1}{\mu}(\mathbf{u}^{n-1})] - \mathbf{Bg}(\boldsymbol{\theta}^{n-1})$$

$$- \mathbf{A}_{\Gamma_{\text{in}}}\Theta^n_{\text{in}} - b^n\mathbf{C}_{\Gamma_{\text{in}}}(\mathbf{d}^{\mathbf{n}})$$

Set $\mathbf{u}^n = \mathbf{u}^{n-1} + \mu[\boldsymbol{\theta}^n - \boldsymbol{\beta}(\mathbf{u}^{n-1})]$

End

Remark. On the boundary, depending on the actual type of boundary condition, one can easily develop some variations without effecting the convergence of the presented methods. One could also use explicit boundary conditions in the nonlinear methods. In the linear approximation, the implicit boundary term could also be defined. In particular, when the boundary term can be split to the linear and nonlinear parts, one could use mixed type of formulation (which will be the case in industrial applications). Since the boundary conditions will be defined via temperature in practical situations, the boundary conditions will, however, remain nonlinear in practice.

4.3 Numerical examples

In this section, we test our implementation. All numerical examples with the model problems and in the industrial applications will be computed on Lenovo T400 laptop, with Intel(R) Core(TM) Duo CPU T9800 @ 2.93 GHz, with 2.99 GB of RAM using Visual Fortran compiler and Windows XP operating system. We perform our computations using a single processor. In the implementations, various kinds of parallel algorithms can be used. For example, the direct solvers (DC3D) and (DCC3D) have almost optimal parallel scalability. As we have introduced some new approximations, a natural starting point for the research is to compare numerical efficiency in a single processor and then based on these results, one can conclude which type of parallel numerical solution algorithms can be considered.

We define a numerical example by using a linear boundary condition. We use the boundary condition of type

$$-\frac{\partial\theta}{\partial n} = f \text{ on } \Sigma_{\text{n}}, \tag{68}$$

where f is computed from the analytical solution. This way there is no difference between the approximations of the boundary condition and differences are related to the approximation of the convection term and to the use of the nonlinear

Chernoff formula. Let $\Omega =]0, \frac{1}{2}[\times]0, \frac{1}{2}[\times]0, \frac{1}{2}[$ and $T = \frac{1}{4}$. Let the free boundary be $\phi(x, y, z) = -x - y - z + 4t + 0.1 = 0$.

We choose

$$\beta(u) = \begin{cases} u, & u < 0, \\ 0, & u \in [0, L], \\ u - L, & u > L. \end{cases}$$

In terms of our approximation, we now have

$$\Upsilon(\theta) = \begin{cases} \theta, & \theta < 0, \\ [0, L], & \theta = 0, \\ \theta + L, & \theta > 0. \end{cases}$$

We define the exact enthalpy by

$$u = \begin{cases} a_1(\exp(\phi) - 1), & \phi < 0, \\ a_2(\exp(\phi) - 1) + L, & \phi > 0. \end{cases}$$

We choose $a_1 = 1, a_2 = 2$ and $L = 1$.

We investigate now the actual order of convergence for θ. We set

$$E_\theta^h := 10^2 \cdot \left\{ \frac{\sum_{n=1}^N \tau(\Theta^n - P_h\theta^n)^T \mathbf{M}(\Theta^n - P_h\theta^n)}{\sum_{n=1}^N \tau P_h\theta^{nT}\mathbf{M}P_h\theta^n} \right\}^{\frac{1}{2}}.$$

We also compute the rate of convergence. Assuming the relation $E_\theta^h = Ch^{p_\theta}$, it follows that

$$p_\theta = \frac{\log(E_\theta^{h_1}/E_\theta^{h_2})}{\log(h_1/h_2)}.$$

In the following examples, Dirichlet data are imposed when $z = 0$. In order to fulfill the uniqueness condition, we assume that the enthalpy can be measured also on Σ_{in} and initially such that $u = 0$, if $\theta = 0$.

In Table 1, we see the obvious benefit of the overrelaxation.

TABLE 1 Effect of overrelaxation $h = \tau = \frac{1}{64}$ (PC)

ω	1.0	1.8	1.85	1.86	1.87
Iterations	1995	269	193	177	193

With the SOR method, the number of iterations will, however, increase in terms of the size of the algebraic system. This is illustrated in Table 2.

In the problem (PU) one can consider the underrelaxation, with $\omega \in]0, 1]$. However, this will not decrease the number of the iterations. This is illustrated in Table 3.

When the optimal overrelaxation parameter is found, we can check the average CPU times, which are reported to the largest problem in Table 4. We can

TABLE 2 Maximum number of iterations in (PC), with optimal ω

$\frac{1}{h} = \frac{1}{\tau}$	4	8	16	32	64
Iterations	22	41	69	106	177
ω	1.44	1.62	1.74	1.81	1.86

TABLE 3 Maximum number of iterations in (PU), with underrelaxation, $\frac{1}{h} = \frac{1}{\tau} = 16$

Iterations	557	670	809	985	1215
ω	1.	0.9	0.8	0.7	0.6

can see that for a single time step, the direct solver is faster than the iterative one. This means that, for example, for a linear problem they are the preferred choice over to the SOR. We observe that the Gauss Seidel solver in (PU) is clearly the slowest solution algorithm. As the accuracy of the Stefan problem depends on the choice of approximation method, the total efficiency requires more studies.

TABLE 4 Average CPU times in seconds

$\frac{1}{h} = \frac{1}{\tau}$	(PC)	(PU)	(PCo)	(PCh)
64	3.26	75.7	0.17	0.20

In Table 5, we can see the errors in terms of temperature norms, and the rate of convergence for each approximation. For the standard linear problems, the characteristic approximation has a better rate of convergence in spatial discretisation $O(h^2)$ compared to the upwinding $O(h)$. The better approximation property seems to remain also in the free boundary problem.

We can see that in practice the nonlinear methods seem to have a better rate of convergence. When the same problem is solved, (PC) and (PU) give more accurate results.

The simplest way to improve the accuracy of the linear approximations is to solve the problem with smaller time steps. The effect of the convergence in this case is illustrated in Table 6, when $h = \frac{1}{64}$.

Thus one can achieve the same accuracy as the nonlinear methods using a Chernoff type of approximation as well by decreasing the time step in the computed example.

Numerical efficiency of the approximations. We assume that in the actual computations, sufficient size of the problem is $h = \frac{1}{64}$ and make our efficiency considerations based on this. In the case without convection for the linear boundary condition, it has been shown that the rate of convergence for the temperature is $O(h^{\frac{1}{2}})$, and this rate was obtained with all of the methods. Clearly (PC) is the most accurate in this example, when the same size of problem is solved. In order to find the most computationally efficient method, we first have to solve the (PC) and (PCo) with the same accuracy. This can be done by decreasing the time step.

TABLE 5 E_θ^h and rate of convergence in the Stefan problem

$\frac{1}{h}=\frac{1}{\tau}$	(PC)	(PU)	p_θ^C	p_θ^U	(PCo)	(PCh)	p_θ^{Co}	p_θ^{Ch}
4	6.19	10.44			22.19	31.51		
8	2.93	5.82	1.08	0.84	15.32	19.71	0.58	0.68
16	1.42	3.10	1.04	0.91	9.75	12.19	0.65	0.69
32	0.80	1.56	0.83	0.99	6.40	7.82	0.61	0.64
64	0.46	0.80	0.80	0.96	4.27	5.13	0.58	0.61

TABLE 6 Effect of time step for (PCo) , $\frac{1}{h}=64$

$\frac{1}{\tau}$	64	128	256	512	1024	2048	4096	8192
E_θ^h	4.27	2.93	2.03	1.42	1.01	0.72	0.53	0.40
CPU	15.0	30.1	59.89	120.12	241.23	495.15	1052.17	2122.6

It took 209 seconds of CPU time to solve problem (PC) in the largest problem, and for (PCo) it was 15 seconds using relation $h=\tau$. As the solution time with respect to the time step increases linearly in (PCo), it can be considered efficient if the same accuracy is reached using $\tau \approx \frac{1}{800}$. However, from Table 6, we observe that in this case (PCo) is still less accurate. Eventually, length of the required time step in the problems (PCo) and (PCh) cancel the benefit of fast solution methods for to the linear algebraic equation. Thus (PC) can be considered the most efficient technique in this example.

Remark. It would be possible to use monotone multigrid method in the problems (PC) and (PCo) and then the efficiency considerations might be different.

4.4 Conclusions

We introduced four approximations for the free boundary problem arising from the continuous casting processes and showed their convergence. We gave a numerical example and compared the numerical efficiency. The conclusions about the efficiency are restricted to the actual problem size, material data, type of boundary condition, approximations, and used numerical solution algorithms.

Characteristic methods. In order to prove convergence, we required $\tau b \leq h$. Compared to the nondegenerate case, this is stronger assumption and can be too restrictive in some cases. However, in the computed examples this was satisfied, and we found out that in this case (PC) is computationally the most efficient method in the largest computed problem. For a single time step, (PCo) was found almost 20 times faster, but the Chernoff formula required relation $\tau^2 \approx h$. In the larger problems the asymptotic computational work will eventually make the direct solvers more efficient, but we have not considered multigrid methods, in which the number of the iterations will not depend on the problem size.

Upwinding approximations. We have no stability restriction in (PU). But as we cannot use overrelaxation we found out that it is more than 20 times slower in the largest problem compared to (PC). The number of iterations is more than ten times greater compared to the overrelaxation. In (PU) one also has to evaluate the value of $\beta(u)$ in the diffusion part, which causes extra computational work. On the other hand the phase test is avoided. In practice we found out the the underrelaxation will not decrease the number of the iterations and as a result, the solver in (PU) is about 400 times slower for a single time step compared to $(DCC3D)$ in the largest problem.

The problem (PCh) requires stability condition $\tau b \leq Ch$ and a similar conclusion for the numerical efficiency holds as for (PCo) for a single time step.

In the computed example, we found that (PC) is the most numerically efficient way to approximate the problem. The approximations (PCo) and (PCh) can be considered more efficient that (PU).

5 APPLICABILITY FOR INDUSTRIAL DATA

In this chapter, we discuss the continuous casting processes in industrial settings. In the computed examples and thereby in the solution algorithms, the material parameters were assumed as constant in each phase. The temperature dependence is, however, more general in practice. As an industrial application, we consider steel casting. As steel is an alloy, this also effects the numerical efficiency considerations.

We take actual industrial data provided by IDS software [32] and transform it to a suitable form for our approximations. The material properties will require changes to the iterative solvers in (PC) and (PU). We make use of the fact that in the alloys enthalpy is continuous, and this suggests the use of Kirchhoff transformation θ as a solution variable in the upwinding approximation as well. The nonlinear boundary condition is added to the solution algorithm. We introduce a modification of the nonlinear Gauss Seidel method for this purpose to the nonlinear iterative solvers.

We present an algorithm that is used to solve nonlinear algebraic system at each time level. We introduce this for the problem (PU), but it can be easily modified for (PC) as well.

We will implement the modifications and validate of our implementation by using an existing model called Tempsimu [24], which can compute steady states with prescribed convection in 2D. The detailed model i.e., model including supporting rolls, water cooling etc. is used for this purpose and results are compared to the problem (PU), which is the most natural choice, as the approximations are expected to give very similar results. We also make use of the fact that the steady state can be computed directly using upwinding approximation.

After that we start to compare our approximations to each other in the transient situations. For the sake of simplicity, we will use the zone cooling type of modeling of the machine as the first example. Then we return back to the detailed model and perform some transient simulations.

Finally, we will be in a position to make some conclusions about the numerical efficiency of the presented approximations in the actual industrial processes.

5.1 Formulation of the material data

From metallurgical sources (like IDS software) we get the material properties as a tabulated function of temperature. Let N_l denote the number of the temperature points ϑ^l for which the values of the thermal conductivity $k(\vartheta^l)$ and the enthalpy $e(\vartheta^l)$ are provided. We interpolate these values with a piecewise linear function to obtain

$$e(\vartheta) = \frac{e(\vartheta^l) - e(\vartheta^{l-1})}{\vartheta^l - \vartheta^{l-1}}(\vartheta - \vartheta^{l-1}) + e(\vartheta^{l-1}), \vartheta \in [\vartheta^{l-1}, \vartheta^l[.$$

From the temperature dependent data of k, we compute the Kirchhoff transformation as

$$\Theta^l := K(\vartheta^l) = \int_0^{\vartheta^l} k(s)ds \approx \sum_{i=2}^{l} \frac{1}{2}(k(\vartheta^l) + k(\vartheta^{l-1}))(\vartheta^l - \vartheta^{l-1}) + K(\vartheta^{l-1}),$$

for each $l = 2, \cdots, N_l$ and $K(\vartheta^1) = \frac{1}{2}k(\vartheta^1)\vartheta^1$. The value of Kirchhoff transformation is then computed as

$$\theta = K(\vartheta) = \frac{\Theta^l - \Theta^{l-1}}{(\vartheta^l - \vartheta^{l-1})}(\vartheta - \vartheta^{l-1}) + \Theta^{l-1}, \vartheta \in [\vartheta^{l-1}, \vartheta^l[,$$

and the value of the enthalpy as a function of Kirchhoff transformation is

$$u = \Upsilon(\theta) = \frac{e(\vartheta^l) - e(\vartheta^{l-1})}{\Theta^l - \Theta^{l-1}}\left[\theta - \Theta^{l-1}\right] + e(\vartheta^{l-1}), \theta \in [\Theta^{l-1}, \Theta^l[,$$

where $l = 2, \ldots, N_l$. In the linear approximations we also need the value of $\beta(u)$, which is

$$\beta(u) = \frac{\theta^l - \theta^{l-1}}{\Upsilon(\theta^l) - \Upsilon(\theta^{l-1})}\left[u - \Upsilon(\theta^{l-1})\right] + \theta^{l-1}, \quad u \in [\Upsilon(\theta^{l-1}), \Upsilon(\theta^l)].$$

In the approximations (PCh) and (PCo), one has to calculate the relaxation parameter μ also, which is

$$\mu = \max\left(\frac{\Upsilon(\theta^l) - \Upsilon(\theta^{l-1})}{\theta^l - \theta^{l-1}}\right), \quad l = 2, \ldots, N_l. \tag{69}$$

We denote by K_s^l the slope of the Kirchhoff transformation on the temperature interval $[\vartheta^{l-1}, \vartheta^l[$ and K_c^l is the corresponding constant. That is

$$K_s^l = \frac{K(\vartheta^l) - K(\vartheta^{l-1})}{(\vartheta^l - \vartheta^{l-1})},$$
$$K_c^l = -K_s^l\vartheta^{l-1} + K(\vartheta^{l-1})$$

and similarly for the enthalpy

$$\mathrm{Y}_s^l = \frac{\mathrm{Y}(\theta^l) - \mathrm{Y}(\theta^{l-1})}{\theta^l - \theta^{l-1}},$$
$$\mathrm{Y}_c^l = -\mathrm{Y}_s^l \theta^{l-1} + \mathrm{Y}(\theta^{l-1}).$$

Now the temperatures can be calculated as

$$\vartheta_i = \frac{1}{K_s^l}(\theta_i - \Theta^{l-1}) + \vartheta^{l-1},\ \theta_i \in [\Theta^{l-1}, \Theta^l],$$

for each node $i = 1, \ldots, N_d$.

In the computations, we will use typical stainless steel data with the kind permission of Outokumpu Tornio Stainless Steel factory. The details of the data are presented in Appendix 1. In Figure 6, we see the temperature dependence of the enthalpy and the heat conductivity.

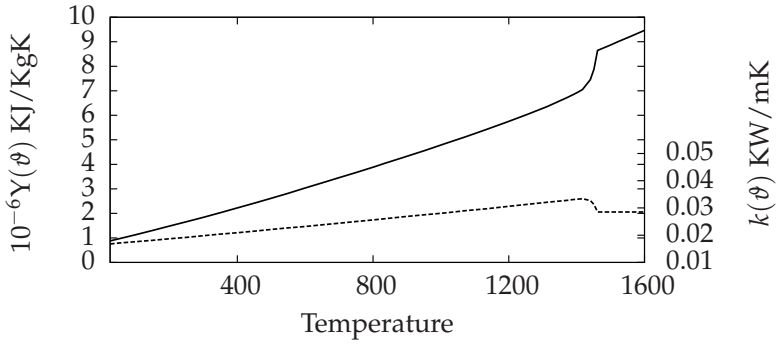

FIGURE 6 Material data

This material starts to solidify at $\vartheta = 1461.74°C$ and is completely solid at $\vartheta = 1417.21°C$.

5.1.1 Gauss Seidel-type solution algorithms

In the linear approximations (PCo) and (PCh), it is straightforward to apply the material data to the given algorithms; however, in the nonlinear Gauss Seidel-type of methods the solution algorithm has to be modified. The algorithm also depends on the approximation of the boundary condition. One can add the part of the boundary condition (water cooling, natural convection, and roll contact) as an implicit term in the solution algorithm. This causes the inverse of the Kirchhoff variable to be computed at each boundary node, making the algorithm nonlinear in all the cases, but the Gauss Seidel step can be solved directly.

If one prefers the fully implicit approximation of the boundary term, the solution of the each Gauss Seidel step cannot be computed directly. Instead of

solving the GS step exactly, one typically uses the Newton-Raphson step on the boundary [22, 26, 43]. However, as the data is only piecewise linear, the convergence of the Newton Raphson is not guaranteed.

In this work, we use the following approach. Let θ_i^1 be the solution to the first Gauss Seidel at iteration, with the initial guess θ_i^0 at node i, as the algorithm comes for the first time to the node, where $b_{ii} \neq 0$ and the boundary condition are of type $g(\theta_i) = v(K^{-1}(\theta_i) - \vartheta_{ex}) + \sigma\epsilon(K^{-1}(\theta_i)^4 - \vartheta_{\text{ex}}^4)$. Then one has to solve θ_i^1 from the equation

$$a_{11}\theta_i^1 + (\hat{m}_{ii} + bc_{ii})\Upsilon(\theta_i^1) + b_{ii}g(\theta_i^1) = f_i,$$

to which we use the following approximation

$$a_{ii}(\tilde{\theta}_i^1) + (\hat{m}_{ii} + bc_{ii})(\Upsilon(\tilde{\theta}_i^1)) = f_i - b_{ii}g(\theta_1^0).$$

By taking the difference between approximated and accurate solutions we get

$$|a_{ii}(\tilde{\theta}_i^1 - \theta_i^1) + (\hat{m}_{ii} + bc_{ii})(\Upsilon(\tilde{\theta}_i^1) - \Upsilon(\theta_i^1))| = b_{ii}|(g(\theta_i^1) - g(\theta_i^0))|.$$

Typically the value of the heat transfer coefficient is $v \leq 2\ \text{kw/Km}^2$. The effect of the radiation term in this type of situation can be estimated as $\sigma\epsilon(K^{-1}(\theta)^4 - \vartheta_{\text{ex}}^4) < 10^{-2}v(K^{-1}(\theta) - \vartheta_{\text{ex}})$. Now we can roughly estimate the error between solutions from the data. As the slope of the secant of $g < 5 \cdot 10^{-2}$, we have

$$|a_{ii}(\tilde{\theta}_i^1 - \theta_i^1) + (\hat{m}_{ii} + bc_{ii})(\Upsilon(\tilde{\theta}_i^1) - \Upsilon(\theta_i^1))| < 10^{-1}h^2|\theta_i^1 - \theta_i^0|.$$

As Υ dominates the system and slope of the secant of $\Upsilon > 10^5$, we can estimate with $\tau = 1, b \approx 10^{-1}, \hat{m}_{ii} = h^3, c_{ii} = h^2$

$$|a_{ii}(\tilde{\theta}_i^1 - \theta_i^1) + (\hat{m}_{ii} + bc_{ii})(\Upsilon(\tilde{\theta}_i^1) - \Upsilon(\theta_i^1))| > h|\tilde{\theta}_i^1 - \theta_i^1|.$$

Assuming $h \approx 10^{-2}$, this type of approximation can be viewed as a numerical solution to the Gauss Seidel step with the following level of accuracy

$$|\tilde{\theta}_i^1 - \theta_i^1| < 10^{-3}|\theta_i^1 - \theta_i^0|.$$

Remark. The use of this modification depends on the mesh size and data. We observed that this type of modification converges to the solution in the numerical examples we are going to study.

In each time step, the following algorithm is used to solve the nonlinear algebraic equations in the approximation (PU).

Algorithm 5.1.1 *Nonlinear Gauss-Seidel method*

1. Initialization
   Assign $\boldsymbol{\theta}^{n,0} = \boldsymbol{\theta}^{n-1}$.
   $\mathbf{f} = \hat{\mathbf{M}}\Upsilon(\boldsymbol{\theta}^{n-1}) - \mathbf{A}_{\Gamma_{in}}\mathbf{d}^n - \mathbf{C}_{\Gamma_{in}}\Upsilon(\mathbf{d}^n)$
2. Iterations, for $k = 1, \ldots, N, i = 1, \ldots, N_d$

$$f_s = f_i - \sum_{j<i} \left(a_{ij}\Theta_j^{n,k} + b^n c_{ij}\mathbf{Y}(\theta_j^{n,k}) \right)$$
$$\text{- } \sum_{i<j} \left(a_{ij}\theta_j^{n,k-1} + b^n c_{ij}\mathbf{Y}(\theta_j^{n,k-1}) \right) - b_{ii}g(\theta_i^{n,k-1})$$

Find l such that

$f_s \in [f^l, f^{l+1}]$, *where* $f^l = a_{ii}\Theta^l + (\hat{m}_{ii} + b^n c_{ii})\mathrm{Y}(\Theta^l)$

Set

$$\theta_i^{n,k} = \frac{f_s - (\hat{m}_{ii} + b^n c_{ii})\mathrm{Y}_c^l}{a_{ii} + (\hat{m}_{ii} + b^n c_{ii})\mathrm{Y}_s^l}$$

3. Test the convergence:

If $\|\Theta^{n,k+1} - \Theta^{n,k}\| > \varepsilon$ *goto 2*

It is straightforward to modify this algorithm to be suitable for the problem (PC) as well. In the problem (PU), one can compute the steady state directly by setting $\mathbf{M} = 0$.

5.2 Validation of the software

In this section, we show how the detailed model can be formed and validate our implementation in comparison to existing software. We use 2D model as a reference. We take boundary conditions as given and compare the results. This sample case comes with the setup package of the Tempsimu [24] software, which computes the steady state with the 2D model. The purpose of these sample data is to illustrate how the detailed model is done and how this 2D model and our approximations (PU) compare to each other. The model itself does not describe any real machine. This sample case, however, has all the features of the actual continuous casting machine.

We now describe the model that is used to approximate the steady state. Since the problem is convection dominated in the steady state model

$$\mathbf{b} \cdot \nabla u = \frac{\partial^2 \theta}{\partial x^2} + \frac{\partial^2 \theta}{\partial y^2} + \frac{\partial^2 \theta}{\partial z^2},$$

heat conductivity into the casting direction can be neglected (supposing that casting speed is high enough), thus one has

$$b\frac{\partial u}{\partial z} \approx \frac{\partial^2 \theta}{\partial x^2} + \frac{\partial^2 \theta}{\partial y^2}.$$

Now by semidiscretizing the previous with respect to z we arrive at the initial value problem.

$$\begin{cases} u_0 = u(0) \\ b\dfrac{u_k - u_{k-1}}{h_k^3} = \dfrac{\partial^2 \theta_k}{\partial x^2} + \dfrac{\partial^2 \theta_k}{\partial y^2}, \quad k = 1, \ldots, n_3, \end{cases} \tag{70}$$

where h^3 denotes the length of the approximation in the casting direction. This type of approach can be considered an implicit Euler approximation where h^3 defines a time step. In the 2D implementation triangular finite elements with mass lumping are used in the spatial approximation and the symmetry of the cooling is assumed, thus one fourth of the actual machine size is computed. The boundary conditions we use are

$$g(\theta) = \begin{cases} q(x,t), & x \in \Gamma_{\text{mold}}, \\ v(x,t)(K^{-1}(\theta) - \vartheta_{\text{wat}}) + \sigma\varepsilon(K^{-1}(\theta)^4 - \vartheta_{\text{amb}}^4), & x \in \Gamma_{\text{cool}}, \\ v(x,t)(K^{-1}(\theta) - \vartheta_{\text{ex}}), & x \in \Gamma_{\text{roll}}, \\ v(x,t)(K^{-1}(\theta) - \vartheta_{\text{air}}) + \sigma\varepsilon(K^{-1}(\theta)^4 - \vartheta_{\text{amb}}^4), & x \in \Gamma_{\text{rad}}, \\ 0, & x \in \Gamma_{\text{out}} \cup \Gamma_{\text{sym}}. \end{cases}$$

We perform computations using Kelvins as the temperature unit; thus the input data are also given in Kelvins. We present our results in degrees Celsius.

The description of the machine and the process details are as follows:

- Casting speed: 0.7 m/min
- Casting temperature: 1756.89 K
- Mold cooling: 700 kW/m^2
- $\vartheta_{\text{twat}} = \vartheta_{\text{amb}} = \vartheta_{\text{ex}} = 305.15$K
- Slab dimension: 0.28×0.28 m
- Mold length: 0.6 m
- Four secondary cooling zones. The lengths are $0.45, 0.65, 1.5$, and 3 m.
- Water flow rates for the zones are: $0.35, 0.25, 0.25$, and 0.10 liter/sec.
- There are 41 rolls in the x-side and 41 in the y-side. The first two rolls from the mold are solid rolls (no cooling), and the others are internally cooled. The roll diameters vary from 0.1 mm to 0.15 m.
- The locations (m) of the rolls are (from the mold end):

0.1/0.25/0.45/0.65/0.85/1.1/1.4/1.7/2.0/2.3/2.6/2.9/3.2/3.5/3.8/
4.1/4.4/4.7/5.0/5.3/5.6/5.9/6.2/6.5/6.8/7.1/7.4/7.7/8.0/8.3/8.6/
8.9/9.2/9.5/9.8/10.1/10.4/10.7/11.0/11.3/11.6/

There are two type of nozzles used in this case: air-mist nozzles and water-only nozzles. In the modeling, the difference between these nozzles come from the different heat transfer coefficients. The formula used to compute the effect of water cooling is

$$v = aW^c. \tag{71}$$

In the air-mist nozzles, the values $a = 0.336, c = 0.724$ are used and in the water-only spray $a = 0.25, c = 0.64$. Typically in the cooling zone the water flow goes through several nozzles. In this case as follows:

- There are 21 spray nozzles in the x-size and 21 in the y-size, respectively
  - Zone 1: three air-mist nozzles:
    - 1. nozzle: 40 % of the total zone water through this nozzle
    - 2. nozzle: 30 % of the total zone water through this nozzle
    - 3. nozzle: 30 % of the total zone water through this nozzle
  - Zone 2: three air-mist nozzles
    - The nozzles are similar: 1/3 of the total zone water through each nozzle.
  - Zone 3: five air-mist nozzles:
    - The nozzles are similar: 1/5 of the total zone water through each nozzle.
  - Zone 4: ten water-only spray nozzles:
    - The nozzles are similar: 1/10 of the total zone water through each nozzle.
- The location (m) of the nozzles are (from the mould end):

0.03/0.175/0.35/0.55/0.75/0.97/1.25/1.55/1.85/2.15/2.45/2.75/
3.05/3.35/3.65/3.95/4.25/4.55/4.85/5.15/5.45

The computed heat transfer coefficients given by Tempsimu vary between $0.3 - 1.13$ kw/m^{2}K on the boundary, so that the highest value is obtained at the beginning of the secondary cooling. On the corner nodes, only the natural convection and the radiation are assumed. The value of the emissivity is $\epsilon = 0.9$.

The size of the computed problem was $29 \times 29 \times 1534 = 1290094$ degrees of freedom. This means that in 2D one has to solve 29×29 degrees of freedom in the algebraic equation at each time step, and this is why the early models preferred this type of approach. We do not compare the numerical efficiency between 2D and 3D models. This is because we use the data as given in our computations and Tempsimu software compute the model of the machine (boundary conditions) as the cast proceeds and we cannot separate the computational cost between them. The basic observation is that 2D model performs simulation faster than the 3D models to the steady state.

In the transient situations, this type of 2D model is rather challenging. As the casting speed varies, the approximations between the real-time steps are problematic. Also in the case of low casting speed, conductivity to the casting direction affects to the solution of (70).

We compare only the temperature distributions between 2D and 3D approximations in the steady state situation.

Since the Tempsimu saves the boundary conditions to a file, the simulation can be performed in 3D independently with exactly the same data. In the problem (PU) one can solve the steady state directly, setting the time derivative as zero. As

a result, we found out that the solution in 3D could be obtained in 743 iterations with the stopping criteria

$$\|\theta_i^k - \theta_i^{k-1}\|_{L^\infty} < 10^{-6}\|\boldsymbol{\theta}\|_{L^\infty},$$

in this sample case. The CPU time used in the solution was about 50 seconds. In Figure 7, we can see the temperature distribution in the casting direction.

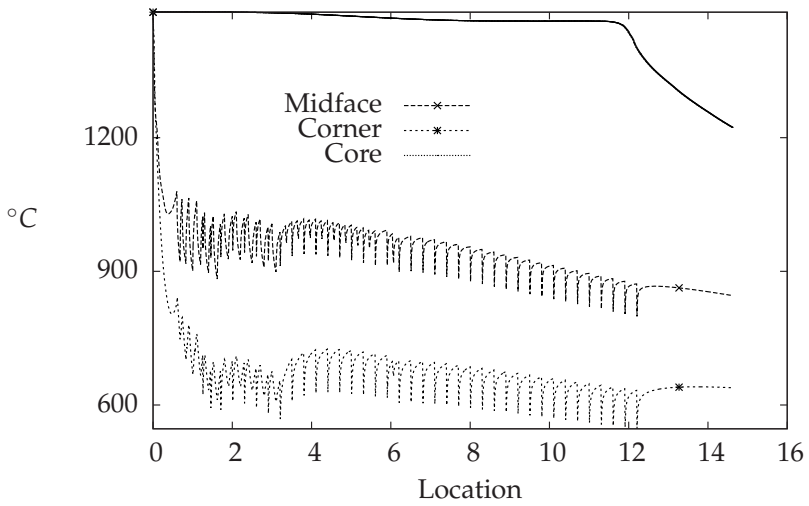

FIGURE 7 Surface temperature profiles

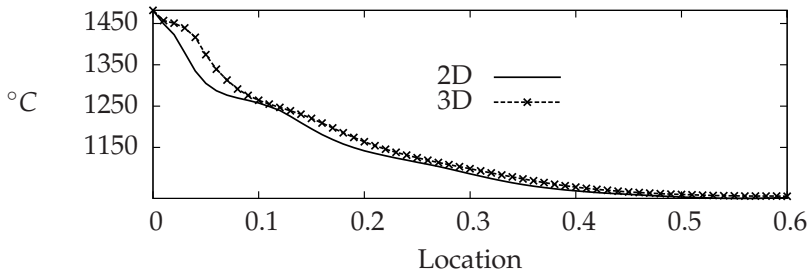

FIGURE 8 Surface temperatures in the mold region

We take a closer look to illustrate the difference between 2D and 3D models. In Figure 8, we see that in the liquid region, the 3D model gives higher temperatures, which is natural due to the conductivity in the casting direction. In the solid region, temperatures start to converge and at the end of the cast surface temperatures differs only few degrees Celsius. The metallurgical length obtained

in the 2D model was 12.14 meters and in the 3D model 12.22 meters; by metallurgical length we mean the length of the pole, where the material is fully or partly liquid, measured from the core.

The basic observation is that the 2D model reacts more rapidly to the changes in cooling. In the water cooling area, the 2D model cools faster. On the other hand when the natural convection is reached the increase of the temperature is bigger than in the 3D model; this is illustrated in Figure 9. At the end of the cast difference between surface temperatures was about 5°C on the midface and corner, and 20°C in the core such that the 3D model gave hotter temperatures, namely 850°C on the surface and 1248°C in the core. In conclusion, the differences between the methods are small and behave as expected.

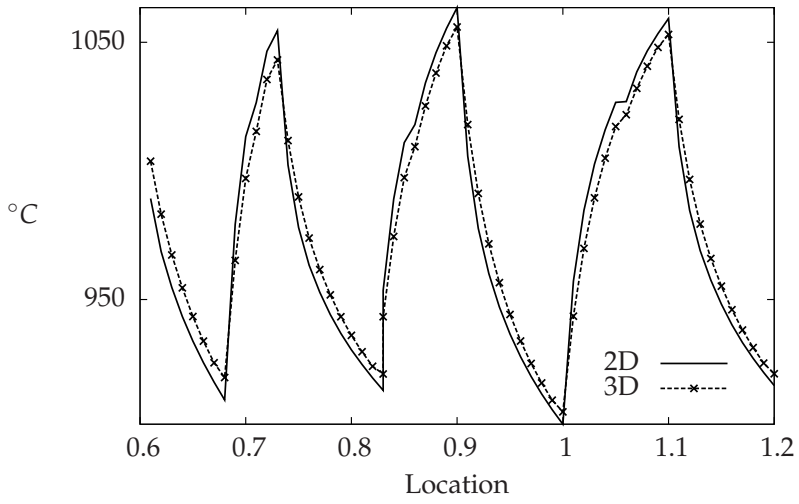

FIGURE 9 Surface temperatures on the midface

5.3 Transient zone cooling model

We define a small slab to which we can easily make some asymptotic studies. We start by comparing the steady states. From these studies we select a case to which we perform transient simulations.

5.3.1 Steady state simulations

We start by comparing our approximations to each other. For the linear approximations, we have shown that the phase change phenomena can be approximated by the diffusion equation with a constant coefficient, where the algebraic correction formula reflects the actual material parameters. The relaxation parameter

TABLE 7 Steady state 3x3x80, $\tau = 1.s$

	PC	*PU*	*PCo*	*PCh*
Zone1	1352.6	1352.5	1355.6	1352.5
Zone2	908.3	908.3	908.4	908.3
Zone3	839.9	839.9	839.9	839.9
Zone4	888.2	882.8	883.3	882.8
M_l	3.22	3.22	3.22	3.20

computed with the formula (69) with the material data presented in Appendix A is

$$\mu \approx 1.6 \cdot 10^5. \tag{72}$$

A priori we cannot analyze in details what is expected to happen between the approximations. Therefore, we conduct numerical tests, as due to the size of the actual casting machines, it is hard to study the asymptotic behavior of the solutions. For this purpose, we introduce a "slab" with the dimensions of 0.12m x 0.12m x 4m. We set the casting temperature as $1471^\circ C$ and speed 1 m/min in the steady state situation. We have four zones: Zone1 represents the mold, Zone2 and Zone3 are water cooling zones, and on Zone4 there is only radiation and air convection. The length of the each zone is 1m. In Tables 7, 8, 9, and 10, we see the steady state temperature at the control point, which is located at the midface in the center of each zone.

As before, we give the boundary data in Kelvins and present the results in terms of Celsius.

$$g(\theta) = \begin{cases} \vartheta - 575.15, & x \in \Gamma_{\text{Zone1}}, \\ 0.8(\vartheta - 305.15) + 0.9\epsilon(\vartheta^4 - (305.15)^4), & x \in \Gamma_{\text{Zone2}}, \\ 0.4(\vartheta - 305.15) + 0.9\epsilon(\vartheta^4 - (305.15)^4), & x \in \Gamma_{\text{Zone3}}, \\ 0.04(\vartheta - 305.15) + 0.9\epsilon(\vartheta^4 - (305.15)^4), & x \in \Gamma_{\text{Zone4}}, \\ 0, & x \in \Gamma_{\text{out}} \cup \Gamma_{\text{sym}}. \end{cases}$$

We investigate the behavior of the solution with the different grid sizes $n1 \times n2 \times n3$. As a stopping criteria, we use

$$\|\theta_i^k - \theta_i^{k-1}\|_{L^\infty} < 10^{-6}\|\boldsymbol{\theta}\|_{L^\infty}. \tag{73}$$

We observe that almost the same steady state was obtained with the same grid size with all the methods. When the grid step is 1cm (Table 8), sufficient accuracy on a macroscopic level is achieved with all the approximations.

5.3.2 Transient simulations.

As we have seen in the steady state situation, all the approximated temperatures were close each others with the same grid size. In addition, the grid step 1cm,

TABLE 8 Steady state 6x6x400, $\tau = 0.5s$

	PC	PU	PCo	PCh
Zone1	1170.4	1170.4	1169.5	1170.4
Zone2	900.5	900.5	900.1	900.5
Zone3	865.0	865.0	865.0	865.0
Zone4	920.4	920.4	920.6	920.4
M_l	3.41	3.41	3.41	3.41

TABLE 9 Steady state 12x12x800, $\tau = 0.25s$

	PC	PU	PCo	PCh
Zone1	1180.5	1180.5	1179.7	1179.7
Zone2	901.5	901.5	901.6	901.6
Zone3	867.7	867.7	867.8	867.8
Zone4	924.0	924.0	924.2	924.2
M_l	3.42	3.42	3.42	3.42

TABLE 10 Steady state 24x24x1600, $\tau = 0.125s$

	PC	PU	PCo	PCh
Zone1	1181.6	1181.6	1181.5	1181.6
Zone2	901.5	901.5	901.5	901.5
Zone3	868.0	868.0	868.1	868.0
Zone4	924.4	924.4	924.5	924.4
M_l	3.42	3.42	3.42	3.42

$\tau = 0.5$s gave reasonable accuracy, and we choose these parameters and conduct some transient simulations. We now study the transient situation as follows. We choose (PC) as a reference and compute the difference between the methods at control points. We set

$$\begin{aligned} e_1 &= \vartheta_i^{(PC)} - \vartheta_i^{(PU)}, \\ e_2 &= \vartheta_i^{(PC)} - \vartheta_i^{(PCh)}, \\ e_3 &= \vartheta_i^{(PC)} - \vartheta_i^{(PCo)}. \end{aligned}$$

In order to compare the methods, we choose the examples so that temperatures vary more rapidly with respect to time than in the actual machine in order see the difference between the methods.

We first discuss what is expected to happen in the transient case. In order to understand the physical nature of the Chernoff type of approximations one has to take a look back at the method called phase relaxation, which was introduced by Visintin [57]. The basic idea is to add a delay to the phase change with the so-called phase variable. In this method, Y is split as

$$\mathrm{Y} = \mu I + \tilde{H},$$

where I is the identity, $\tilde{H}$ is still a maximal monotone graph, and $0 < \mu$. Denoting $\chi := u - \mu\theta$ as phase variable, the classical constitutive relation reads

$$\chi \in \tilde{H}(\theta) \quad \text{or} \quad \theta \in \Lambda(\chi) := \tilde{H}^{-1}(\chi).$$

As a substitute for the stationary relation, Visintin introduced

$$\delta\chi_t^\delta + \Lambda(\chi^\delta) \ni \theta^\delta, \tag{74}$$

where $\delta > 0$ is a small relaxation parameter. Therefore, (74) incorporates a time delay in the constitutive relation. The original partial differential equation was replaced by

$$\begin{cases} \mu\theta_t^\delta + \chi_t^\delta - \Delta\theta^\delta & = 0, \\ \delta\chi_t^\delta + \Lambda(\chi^\delta) & \ni \theta^\delta. \end{cases}$$

The connection between phase relaxation and the nonlinear Chernoff formula is the following. Relaxed time discrete problem can be presented as

$$\begin{cases} \mu\partial\theta^n + \partial\chi^n - \Delta\theta^n & = 0, \\ \delta\partial\chi^n + \Lambda(\chi^n) & \ni \Theta^{n-1}. \end{cases} \tag{75}$$

Set now $\tau = \mu\delta$. Then the inclusion in (75) becomes

$$\chi^n + \mu\Lambda(\chi^n) \ni \mu\Theta^{n-1} + \chi^{n-1} =: u^{n-1},$$

or equivalently

$$\chi^n = (I + \mu\Lambda)^{-1}u^{n-1} = (I - \mu\beta)u^{n-1} = u^{n-1} - \mu\beta(u^{n-1}),$$

since

$$u^n = (I + \mu\Lambda)(u^n - \mu\beta(u^n)) = (1 + \mu\Lambda)(\chi^n) = \chi^n + \mu\theta^n.$$

As a consequence, we obtain

$$u^n = \mu\Theta^n + \chi^n = u^{n-1} + \mu[\Theta^n - \beta(u^{n-1})],$$

which is the algebraic correction in the nonlinear Chernoff formula. Thus the Chernoff formulas are expected to have some delay in the equilibrium condition. The amount of delay for a fixed time step, say $\tau = 1$s, can be computed using relation $\tau = \mu\delta$, i.e.,

$$\delta = \frac{\tau}{\mu} \approx 6 \cdot 10^{-6}.$$

This means that the delay itself is not supposed to have an effect on the results.

We simulate the start of casting in such a manner, that we first assume the mold with liquid and set $b = 0$ for one minute and activate the mold cooling. During this time the solid shell is formed and the casting can be started. The initial temperature of the whole slab is $\vartheta = 1471^\circ C$. The casting speed is linearly increased in one minute's time from zero to 1 m/min. We take a point $z = 0.5$ m on the midface surface as a control point and in Figure 10 we see the behavior of the methods, when the solidifying shell is formed on the mold before the casting starts. The maximum temperature difference during the first minute at the control point was about $10^\circ C$, and it occurs as the shell starts to grow. When the cast is started the difference on the control point is about $2^\circ C$. Naturally, the upwinding approximations give the same result as there is no convection during the first minute.

We activate the boundary conditions as the castinng proceeds such that cooling is activated 1m before the cast will reach the corresponding boundary point. In this way we can make observations in various transients situations, namely variable casting speed, cooling, and reheating. As the cast starts very slow and as the cooling is activated at $z = 0.5$m all the time the temperatures decrease until the cast passes the control point. Then due to the full casting speed we have reheating to the steady state.

The obtained temperature profile and differences are illustrated in Figure 11. The basic observation is that the major difference in the solutions come from the approximation of the convection term and the differences between linear and non linear methods are small. The temperatures settle to the same value in a 30 seconds time such that characteristic method achieves a steady state sooner. This type of reheating is rather radical if the actual machines is considered and in practice, differences between the approximations are smaller.

Then we turn our attention to the second zone. The cast passes the control point after 180 seconds. Figure 12 illustrate the differences between approximations.

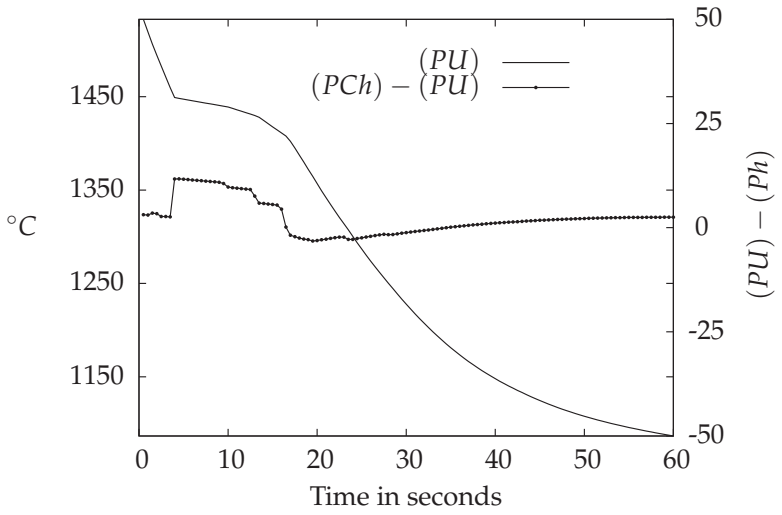

FIGURE 10 Temperatures on the midface during $b = 0$ at $z = 0.5$

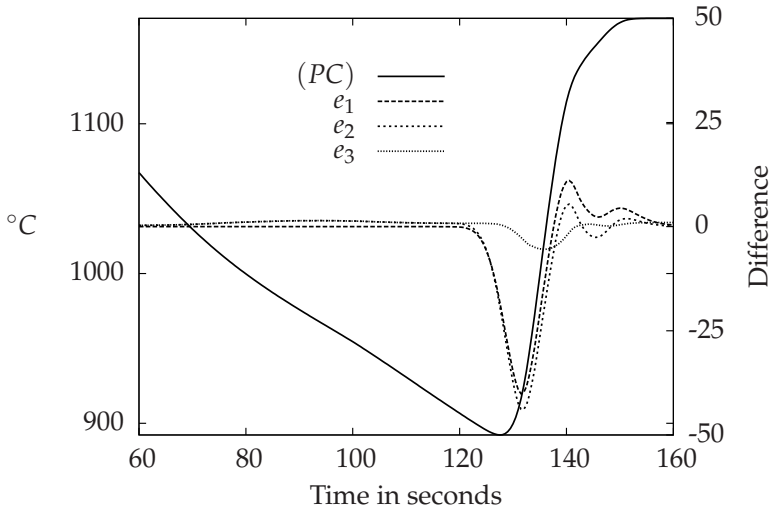

FIGURE 11 Development to the steady state (PC) and temperature differences at z=0.5

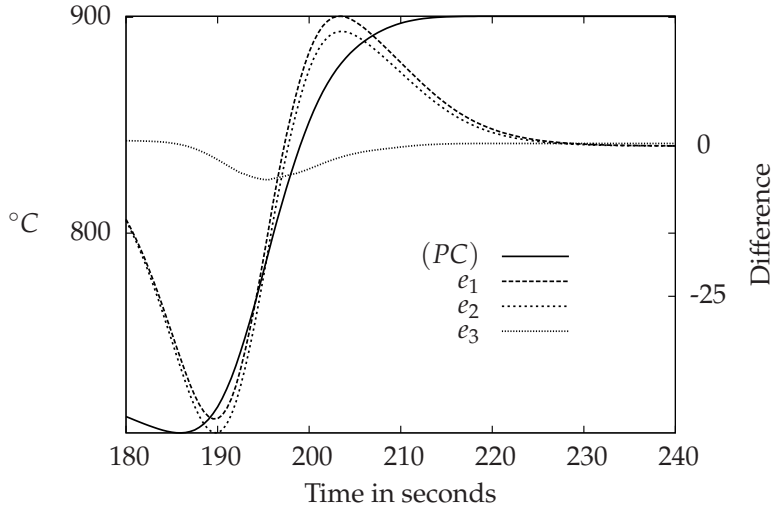

FIGURE 12 Development to the steady state (PC) and temperature differences at z=1.5

We take a closer look at major differences in temperatures. We plot both upwinding and characteristic approximation to the same picture. In Figure 13, we see that the upwinding approximation starts to reheat sooner and settle to the steady state later.

In the other zones, the same kind of behavior was observed. As a conclusion, the presented approximations are suitable for further studies.

5.4 Detailed model

We finish by performing experiments using a detailed model. We consider the same case as in the validation example. We do not consider asymptotic studies, as they would require more detailed presentation of the Tempsimu. We compute the steady state and present some simple transient situations. As we are working with a large-scale problem the CPU times are of interest.

Steady state considerations. We use the same stopping criteria (73) as in the zone cooling model. We take casting temperature as the initial value, and compute to the steady state.

As we are starting far from the solution, we assume that the number of the iterations in the transient situations stays below the maximum number of the iterations towards steady state.

As we have more than 10^6 degrees of freedom in the algebraic system, working in real time is a natural concern. By real-time solution we mean that the CPU times in each time step should less than τ. As it comes to CPU times $(DCC3D)$, take ≈ 0.53 seconds at each time step and $(DC3D) \approx 0.45$ seconds.

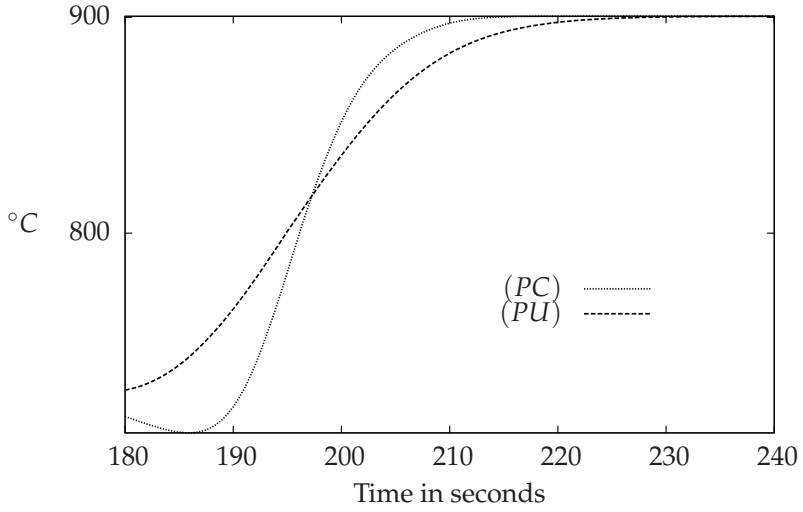

FIGURE 13 Temperature profiles (PC) and (PU) at $z = 1.5$ m

In the nonlinear iterative solvers, the solution time depends on the size of the time step. Roughly speaking, in the direct solvers we can have $\tau = 1$ still working in real time. In the (PC) and (PU) with this time step solvers take typically less than 15 iterations and as a result, average CPU times are 0.7 seconds in (PU) and 0.6 seconds in (PC).

As the number of iterations is small in the problems (PC) and (PU), this suggests the use of an iterative solver in the Chernoff type of approximations as well. We implemented the basic linear Gauss-Seidel method with overrelaxation for this purpose. We observed that about the same number of iterations is needed as in (PC) and (PU). By using overrelaxation parameter we can decrease the number of the iterations by one with mild overrelaxation when $\tau = 1$. With the smaller time steps we do not observed any improvement in the solution speed with the overrelaxation and we report our CPUs without it.

We refer to the linear Gauss-Seidel solver in (PCo) as (GS) and (GSU) in problem (PCh). We report CPU times in a single iteration. As in nonlinear problems these depend also on the number of the operations required to find the temperature interval; we report the average time when the maximum number of the iterations is obtained with $\tau = 0.5$s. The variation between CPU times in a single step in the nonlinear solvers is typically about 20%. With (GS) and (GSU) the solution time is directly related to the number of iterations.

In Table 11, we see the solution time in a single iteration.

TABLE 11 CPU times in a single iteration, $\tau = 0.5$ s

τ	(PC)	(PU)	(GS)	(GSU)
CPU	0.0390	0.0560	0.0241	0.0312

The number of the iterations required for the solution in the iterative methods depends on τ via stopping criteria, which is illustrated in Table 12.

TABLE 12 Maximum number of iterations, with the different time steps

τ	$1/8$	$1/4$	$1/2$	1
(PC)	8	8	10	13
(PU)	7	8	10	13
(GS)	7	9	11	15
(GSU)	7	8	10	13

The CPU time in (GS) is ≈ 0.25 seconds, with $\tau = 0.5$ s, which is almost twice as fast as in $(DC3D)$. This means that iterative solvers are preferred in all the approximations in this case.

When $\tau = 0.5$ the solutions are close to each other, which is illustrated in Table 13. In this case, the number of iterations decreased in the (PC) and (PU) such that they can work in real time as well as CPU time in about half a second.

Both upwinding approximations give exactly the same temperatures in the steady state. Between (PC) and (PCo), we observe only a slight difference. As there is no artificial diffusion in the characteristic approximation, the metallurgical length can be longer compared to the upwinding approximation. From Table 13 we see that this happens in the computed example.

Transient simulations. We perform some transient tests. We observed that the differences between approximations in the zone cooling model were related to the approximations of the convection term rather than other differences in the approximations. Thus we define

$$
\begin{aligned}
e_1 &= \vartheta_i^{(PC)} - \vartheta_i^{(PU)}, \\
e_2 &= \vartheta_i^{(PU)} - \vartheta_i^{(PCh)}, \\
e_3 &= \vartheta_i^{(PC)} - \vartheta_i^{(PCo)},
\end{aligned}
$$

and plot these differences at some control points together with the characteristic approximation.

We choose the control points from the mold and first secondary cooling region. We simulate start of the casting by activating cooling after the cast passes

TABLE 13 Steady state temperatures on the midface, $\tau = 0.5$

	(PC)	(PU)	(PCo)	(PCh)
$z = 0.3$	1059.12	1059.12	1058.92	1059.12
$z = 0.65$	960.78	960.78	960.47	960.78
$z = 10$	913.31	910.92	913.35	910.92
$z = 14.6$	847.86	846.05	847.92	846.05
M_l	12.28	12.22	12.29	12.22

the corresponding boundary node. We take initial temperature to be $1000°C$. In the computed examples the data are kept constant unless otherwise mentioned.

Cases 1 and 2. We check how the temperature profile and different approximations settle to the steady state at $z = 0.3$ in the mold region and at $z = 0.65$ in the water cooling region. We start by increasing the casting speed linearly to the value 0.7 m/s during the first minute.

Case 3. We increase the water cooling by 20% at $t = 180$ and compute then the steady state.

Case 4. We increase the casting speed to 0.8m/s in two minutes linearly from the steady state.

Case 5. We first compute with the casting speed 0.8m/s to the steady state and then in two minutes time drop the speed to the value 0.7 m/s linearly.

Cases 6 and 7. After 3 minutes, we start to increase the casting speed as in **Case 4** and increase the water cooling as in **Case 3**. Then the steady state is obtained at control point, at $t = 360$. After this we set back original water cooling and decrease the casting speed as in **Case 5**.

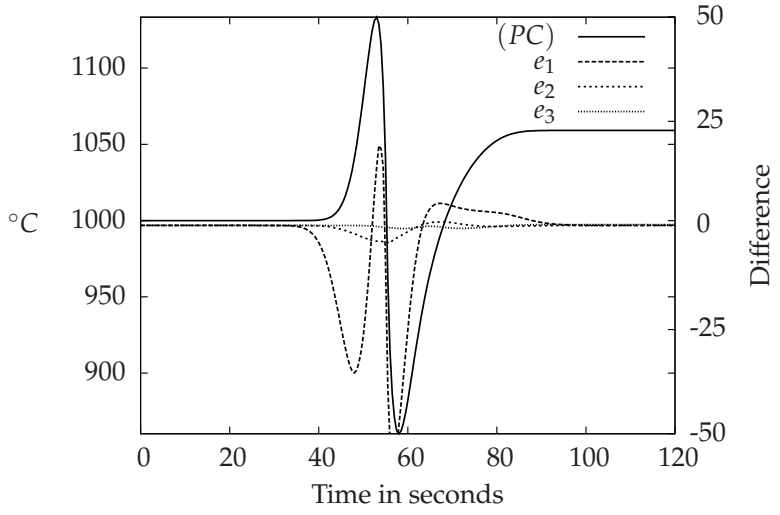

FIGURE 14 **Case 1**

Results from Cases 1 and 2. We observe reheating before the cooling is activated. This is because the liquid core, i.e., the still rather thin solid shell and the cooling is activated after the cast has already passed the corresponding boundary node. Then due to the slow casting speed and full mold cooling, temperatures decrease. When the steady state casting speed is reached, the temperatures converge.

Again we found out that the major differences are related to the approximation of the convection term. The difference between the Chernoff type of approximations and nonlinear ones are a few degrees Celsius, and this happens when

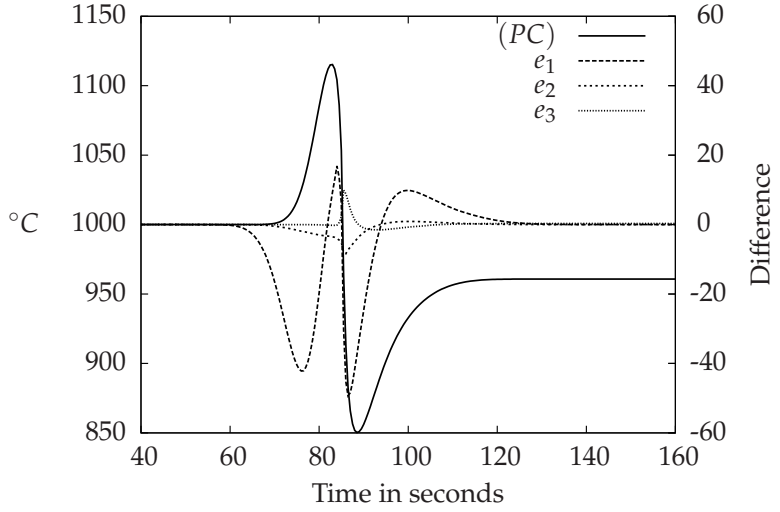

FIGURE 15 **Case 2**

the cooling is activated. Naturally these types of shocks in the cooling are unrealistic and are related to the simulation practices in the start. These shocks can be avoided; however, in this way we can see clear differences between approximations. To avoid unrealistic reheating in the start one could consider, e.g., smaller initial temperature of the slab or activate the cooling before the cast passes the boundary node.

Results from Case 3. We study how the change in water cooling influences the solutions. For this purpose, we simply modify the heat transfer coefficient in the water cooling region. For example, by increasing the amount of water cooling by 20% the new heat transfer coefficient can be computed as

$$v_{\text{new}} = v_{\text{ref}} \frac{a(1.2w_{\text{ref}})^c}{a(w_{\text{ref}})^c}.$$

In this sample case, this increases the heat transfer coefficient by 14%. This change in water cooling is activated at t = 180s. In the secondary cooling area, the differences are expected come also from the type of boundary condition, because there is a delay in cooling in relaxation methods. In the used time step, we noticed that this has very little impact on the results. The differences between approximations are small; between (PU) and (PCh) less than $0.1°C$ and between (PC) and (PCo) less than $1°C$. Again the maximum difference between approximations is related to the approximation of the convection term. Even though we suddenly increased the cooling by 20%, the error between nonlinear approximations with the implicit boundary condition compared to the explicit boundary condition with the nonlinear Chernoff formula is less that $1°C$. The results are illustrated in Figure 16.

Results of Cases 4 and 5. As the convection dominates, we perform transient simulations by changing the casting speed from the steady state. From the

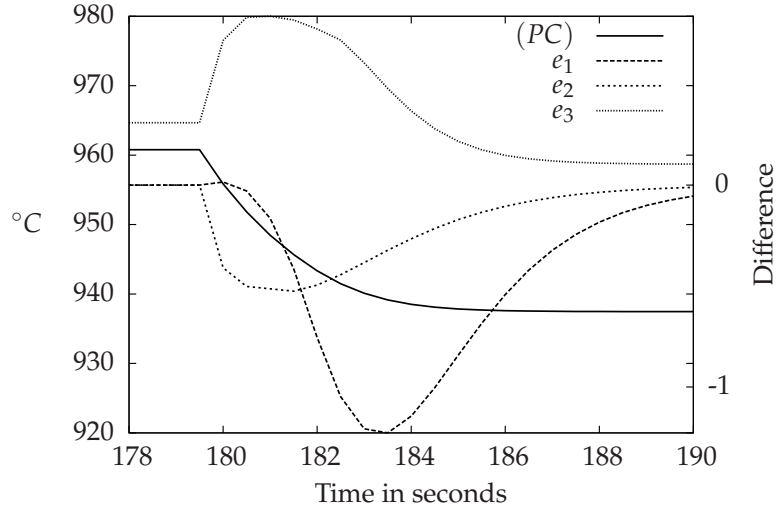

FIGURE 16 **Case 3**

steady state, during two minute's time we decrease the casting speed linearly to the value 0.8 m/min and then compute to a steady state. During this time, the temperatures at the control point $z = 0.65$ increase from 960 to 990°C (Figure 17). This type of change in the casting speed during the continuous casting processes can be considered sufficient for realistic simulation purposes. The difference between approximations with the variable casting speed from the steady state situation is only related to the approximation of the convection term and the Chernoff formula, and we observed that the difference between temperatures is less than 0.2°C. In Figure 18, we see that when the casting speed is similarly slowed down from the steady state, the same differences between approximations remain.

Results from Cases 6 and 7. Again we observe that the maximum differences are related to the approximation of the convection term, despite the fact that the water cooling changes suddenly. Overall the differences between methods are small: about one degree Celsius difference when the cooling is activated and temperatures converge in a few seconds.

Remark. We have not considered multigrid methods in this work, but we can discuss this choice based on our observations. We found out that Gauss-Seidel type of solution algorithms are fastest when the industrial kind of data is used, which corresponds to the pre and post smoothing steps in the multigrid, so we get the upper bound for a number of these steps.

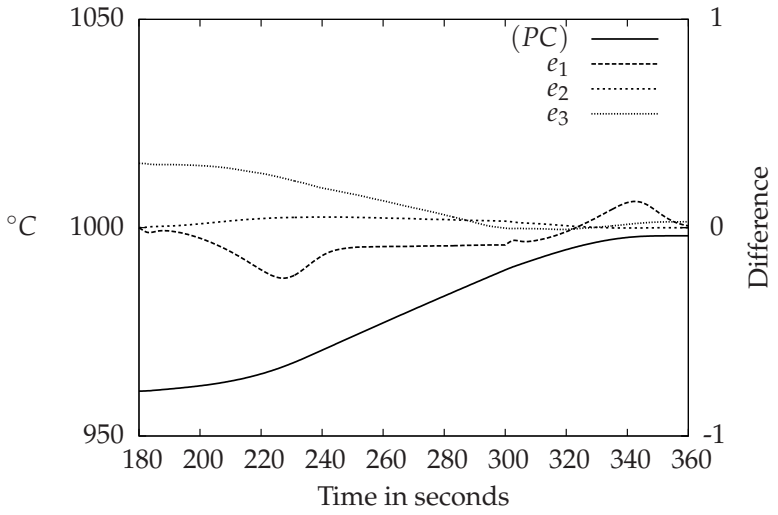

FIGURE 17 **Case 4**

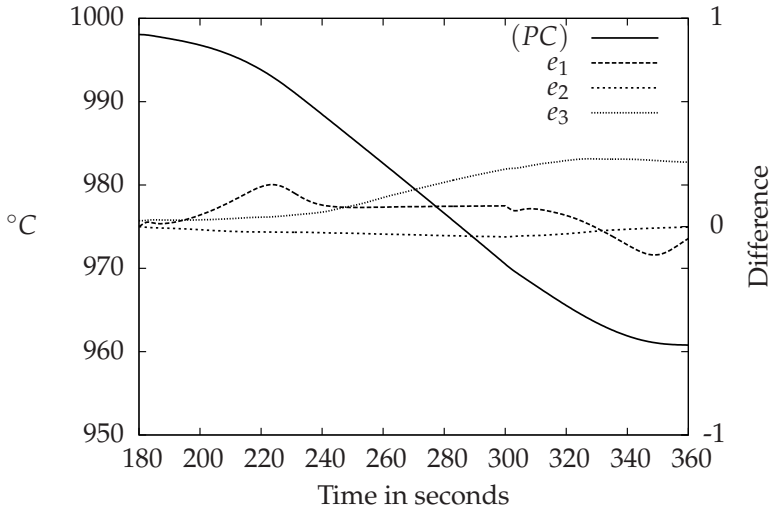

FIGURE 18 **Case 5**

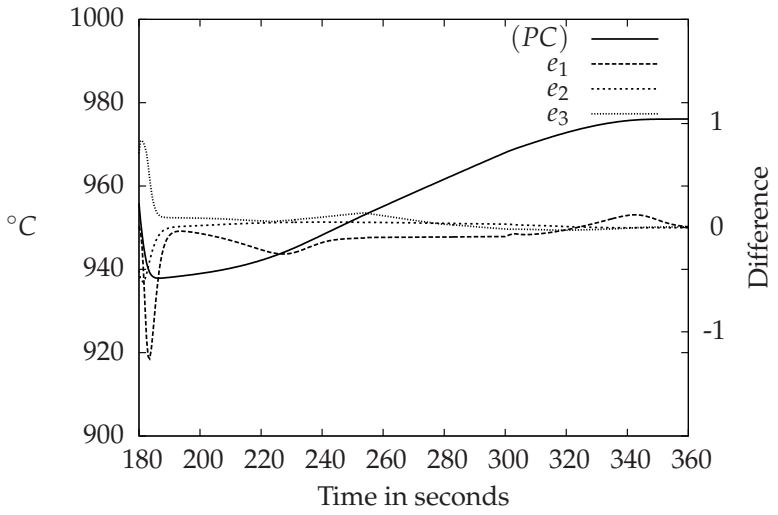

FIGURE 19 **Case 6**

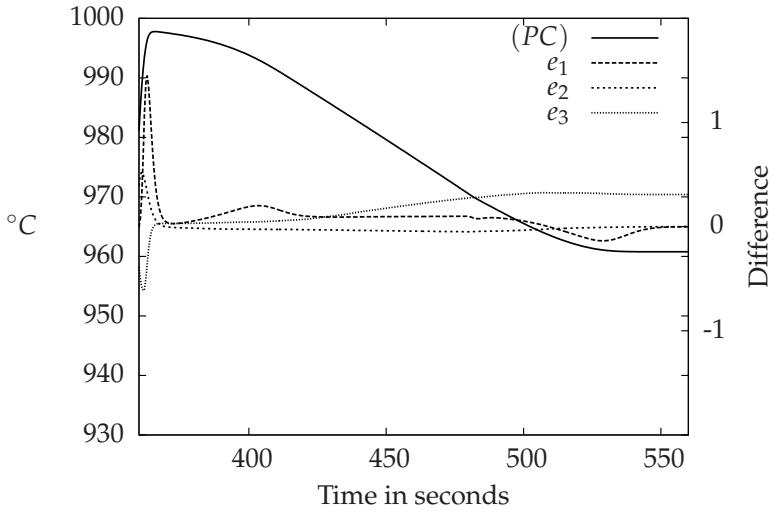

FIGURE 20 **Case 7**

5.5 Conclusions

We have now tested four different approximations with realistic industrial data. We determined that, in principle, all the approximations can be used in the industrial scale in real time with to 10^6 unknowns with a standard laptop. The difference between relaxation methods and nonlinear ones are small and the major differences are related to the approximation of the convection term.

The use of the explicit boundary condition together with the Chernoff approximations do not influence to the results vs. implicit nonlinear approximations with the time steps we are able to use. The iterative solvers were found to be faster in the industrial case compared to the direct solver in the Chernoff approximations. However, we cannot generalize this observation to larger problems, as the number of iterations will increase with the iterative solver as the mesh size is decreased.

By using the Kirchhoff transformation as the solution variable, we were able to implement very efficient iterative solution algorithms with the implicit boundary condition. The efficiency of the method is based on two factors. First, we have linear diffusion part in the nonlinear approximations, which decreases the work in each iteration. Secondly, we have a diagonally dominant system and thus the number of iterations is small.

We gather our observations:

Problem (PC). In the computed examples characteristic method gave a little higher temperatures than (PU) in the steady state, which is natural due to the artificial diffusion related to the upwinding approximation. As we have only one nonlinear term in each Gauss Seidel step, we reduce CPU times compared to (PU).

Problem (PU). The most important feature of (PU) is that one can directly compute the steady state, which has been a starting point of the simulations on the industrial scale.

Problem (PCo). We observed that the temperature differences between the nonlinear and linear characteristic approximations are small. The benefit of this type of approximation is the possibility to use any linear algebraic solution method, which decreases the solution speed. As the accuracy remains almost the same, we conclude that (PCo) is the most efficient numerical method for the continuous casting problem in the computed examples.

Problem (PCh). In practice this approximation gave the same result as (PU); however, the stability resctriction $\tau b < Ch$ exists and the constant C may depend on the data. The benefit of the possibility to use a linear algebraic solver is obvious in the computed example.

5.6 Further developments

Naturally all of the methods require far more testing on the industrial scale, but these preliminary tests give a good starting point. But there are more considerations that may improve to the numerical efficiency of the approximations and simulation practices.

Boundary condition. We have noticed that Chernoff approximations with the explicit boundary condition are very close to the fully implicit nonlinear approximation. This suggest that the explicit boundary condition can be used in the nonlinear approximations as well, improving the efficiency. As in the nonlinear methods, we have linear diffusion due to the Kirchhoff transformation and thus the differences in the CPU times reduce then to the nonlinear evaluation of the enthalpy on each Gauss-Seidel step. One could also consider approximating the boundary condition in such a way that the water cooling is kept implicit and radiation term explicit. This way the standard Gauss-Seidel method could be used without any approximation in each Gauss-Seidel step.

The detailed modeling of the machine causes the heat transfer coefficient to vary in a discontinuous manner. This suggests the use of bilinear finite elements on the boundary, which can be a improvement in practice. In the roll contact and especially at the corners, due to the discontinuities in the detailed model, one may obtain quite different approximations to the thermal stresses. In our approximations, this can be done as follows. The bilinear boundary mass matrices on the boundary can be computed as tensor products of the following mass matrices

$$\mathbf{M}_l = \begin{pmatrix} \frac{h_1^l}{6} & \frac{h_2^l}{6} & & & 0 \\ \frac{h_2^l}{6} & \frac{h_1^l+h_2^l}{3} & & & \\ & \ddots & \ddots & \ddots & \\ & & & \frac{h_{n_l-1}^l+h_{n_l l}}{3} & \frac{h_{n_l}^l}{6} \\ 0 & & & \frac{h_{n_l}^l}{6} & \frac{h_{n_l}^l}{6} \end{pmatrix} \in \mathbb{R}^{n_l \times n_l}, l = 1, 2,$$

and

$$\mathbf{M}_3 = \begin{pmatrix} \frac{h_1^3}{3} & \frac{h_3^l}{6} & & & 0 \\ \frac{h_2^3}{6} & \frac{h_1^3+h_2^3}{3} & & & \\ & \ddots & \ddots & \ddots & \\ & & & \frac{h_{n_l-1}^3+h_{n_l 3}}{3} & \frac{h_{n_l}^3}{6} \\ 0 & & & \frac{h_{n_l}^3}{6} & \frac{h_{n_l}^3}{6} \end{pmatrix} \in \mathbb{R}^{n_3 \times n_3}.$$

The resulting matrices can be compared to the nine-point stencil acting on the boundary by "averaging" the heat transfer coefficient, and thus smoother temperature profiles are expected.

If the explicit boundary condition can be used as well, as it seems to be the case, this would not cause a considerable increase in the CPU times. If the

implicit boundary condition is used, then on the boundary nodes we would have a nine-point stencil and this will have an impact on the solution time.

Parallel computing. As we have performed the computations in a single processor and the approximations are close to each others, parallel computing may also effect to the efficiency of the approximations. As the linear algebraic solvers can be used as well, which are regularly developed by experts, this means that these results can be directly applied.

Inverse approach. Another aspect is the calibration of the approximations to the industrial measurements. As we have fast solution methods, one could consider inverse problems for this purpose. As the effect of water cooling is typically fitted empirically, by using the presented approximations, this process can be automated by minimizing the difference between the solution of the approximations and the measurements, making the simulations more cost efficient and accurate.

6 FINAL CONCLUSIONS

We studied the continuous casting processes first on the continuous level using the free boundary formulation. We found out that existing models are too restrictive, as they require either unrealistic measurements of the temperature on the boundary, fixed casting speed, or linear boundary conditions.

We replaced extra requirements of the temperature measurements by modeling the heat flux on the outflow by the homogenous Neumann boundary condition. Furthermore, we stated the problem with the variable casting speed, using the nonlinear monotone nondecreasing boundary condition to describe a continuous casting process. We showed existence, uniqueness and continuous dependence on initial data to this problem.

We introduced four different fully discrete approximations to the model in the free boundary form. For physical data, fully discrete problems will eventually lead to the convection dominated problem. In order to avoid stability issues, we used upwinding and the characteristic method.

We first described the Galerkin approximations to the both of these. Furthermore, we were able to apply the nonlinear Chernoff formula to these approximations. Thus, we can approximate the problem by solving linear algebraic equations at each time step. We showed the convergence of each method and performed some numerical examples. In the characteristic approximations, however, we required assumption $\tau b \leq h$ in order to get the convergence in the free boundary form. With the upwinding approximations, using the Chernoff formula we required $\tau b < Ch$.

In an academic problem, the nonlinear characteristic approximation was computationally the most efficient approximation. This is because the Chernoff approximations required a smaller time step in order to have the same accuracy compared to the nonlinear methods. On the other hand, we observed that a linear algebraic solver can have superior performance in a single time step.

Then we described how the approximations can be applied on the industrial scale. As we can use the Kirchhoff transformation as the solution variable in the alloys, we have linear diffusion in the nonlinear approximations, resulting in the efficient numerical solution algorithm. Unlike in the academic problem we

noticed that we do not have to decrease the time step in order to get the same level of accuracy in the steady state.

In the transient simulations, we noticed that the CPU times in the presented nonlinear solvers are close to the direct methods used in the linear algebraic solvers. This suggested the use of iterative methods in the Chernoff type of approximations as well. It turned out that the linear Gauss-Seidel solver can be faster, depending on the size of the time step.

With $\tau = 0.5$s, the linear Gauss-Seidel methods were faster than the used direct solvers in the computed industrial example. This is why we chose iterative solvers in all the approximations and conducted some transient studies.

The simulation results show that Chernoff approximation with the characteristic method is the fastest method to approximate the continuous casting processes and the main differences are related the approximation of the convection term. In the practical transient situations, the differences between approximations were small, so the efficiency considerations could be made based on the CPU time.

We can conclude, due to the artificial diffusion related to the upwinding and based on CPU times, that the use of the method of characteristic is the most efficient numerical method for simulation continuous casting processes in the computed examples. On a general level we can not pick up clear winner from our approximations based on these few tests.

However, we have shown that at the present time it is possible to simulate the continuous casting processes in real time at the industrial scale up to 10^6 degrees of freedom using a standard laptop.

YHTEENVETO (FINNISH SUMMARY)

Tämä väitöskirja, suomenkieliseltä nimeltään Tehokkaita numeerisia menetelmiä jatkuvavaluprossessien simulointiin, käsittelee valunauhan lämpötilojen matemaattisia malleja sekä niiden approksimaatioita ja tehokasta tietokonetoteutusta.

Tällaisia malleja käytetään teollisuudessa simuloimaan tuotteen laatua, ennustamaan uusien materiaalien käyttäytymistä valussa ja jopa reaaliaikaisessa prosessin säädössä.

Tehtävän laskennallisesta vaativuudesta ja käytettävissä olleesta laskentakapasiteetista johtuen on perinteisesti käytetty yksinkertaistettuja, kaksi- ja yksiulotteisia malleja. Näin on jo 1970-luvulta alkaen voitu soveltaa mallinnusta valun laatuun ja prosessin kontrolloimiseen liittyvissä ongelmissa. Riippuen yksinkertaistuksesta, näitä malleja on voitu käyttää joko ajasta riippumattomaan tilanteeseen, eli mallilla on simuloitu valua tasapainotilassa tai dynaamiseen simulointiin, jolloin ei kuitenkaan voida arvioida lämpötilajakaumaa leveyssuunnassa, ja osa valuvirheistä jää ennustamatta.

Tutkimuksen lähtökohtana on klassinen entalpiaformulointi, joka on käytetyin menetelmä mallinnettaessa sulan ja kiinteän aineen vuorovaikutusta. Työssä valunauhalle esitetään kolmiulotteinen matemaattinen malli. Tehtävälle osoitettiin laadulliset ominaisuudet, jotka takaavat mallin matemaattisen mielekkyyden.

Työssä esiteltiin neljä eri menetelmää approksimoida valun lämpötiloja mallintavaa osittaisdifferentiaaliyhtälöä. Ensin esitellään ns. karakteristinen menetelmä ja ylävirta-approksimaatio. Kaksi muuta tapaa approksimoida valuun liittyvää epälineaarista osittaisdifferentiaaliyhtälöä ovat kokonaan uusia. Näiden avulla simulointi voidaan suorittaa ratkaisemalla epälineaarisen yhtälöryhmän sijasta lineaarinen yhtälöryhmä mikä pienentää tehtävän laskennallista vaativuutta. Toinen esitetyistä menetelmistä käyttää ylävirta- ja toinen karakteristista approksimaatiota.

Approksimaatioille osoitetaan konvergenssi käyttämällä entalpian mallina klassista Stefanin kaksifaasiongelmaa. Implementointi testattiin numeeristen esimerkkien avulla.

Esitettyjä menetelmiä testattiin teollisen mittakaavan ongelmissa käyttäen materiaalina ruostumatonta terästä. Valukoneen mallina käytetään teollisuudessa käytettävän ohjelmiston asennuspaketin mukana tulevaa esimerkkikonetta siten, että tehtävän laskennallinen vaativuus on realistinen.

Kaikki esitetyt menetelmät ovat soveltuvia valun simulointiin, mutta niiden tarkkuus ja laskennallinen vaativuus vaihtelevat simuloitavan tilanteen mukaan.

Periaatteessa ylävirta-approksimaatio aiheuttaa ylimääräistä diffuusiota valun suuntaan. Tämä aiheuttaa sen, että ylävirta-approksimaation antama sulakartio voi olla lyhyempi kuin karakteristisen menetelmän vastaava ns. steady state tilanteessa, niin kuin teollisen mittakaavan esimerkissä kävikin.

Parhaan menetelmän valinta laskettujen muutamien esimerkkien nojalla ei

ole yksiselitteisesti mahdollista, mutta yksi asia voidaan todeta: käyttämällä tehokkaita numeerisia ratkaisumenetelmiä, kolmiulotteinen reaaliaikainen jatkuvavalun simulointi on mahdollista nykyään tavallisessa PC:ssä.

REFERENCES

[1] D. R. Atthey. A finite difference scheme for melting problems. *IMA Journal of Applied Mathematics*, 13(3):353–366, 1974.

[2] A. E. Berger, H. Brezis, and J. C. W. Rogers. A numerical method for solving the problem $u_t - \Delta f(u) = 0$. *ESAIM: Mathematical Modelling and Numerical Analysis - Modélisation Mathématique et Analyse Numérique*, 13(4):297–312, 1979.

[3] H. Brezis and A. Pazy. Semigroups of nonlinear contractions on convex sets. *Journal of Functional Analysis*, 6(2):237–281, 1970.

[4] J.R. Cannon and E. DiBenedetto. On the existence of weak-solutions to an n-dimensional Stefan problem with nonlinear boundary conditions. *SIAM Journal on Mathematical Analysis*, 11(4):632–645, 1980.

[5] Z. Chen. Numerical solutions of two-phase continuous casting problem. In *Numerical methods for free boundary problems*. Birkhauser, 1991.

[6] Z. Chen, T. Shih, and X. Yue. Numerical methods for Stefan problems with prescribed convection and nonlinear flux. *IMA Journal of Numerical Analysis*, 20(1):81–98, 2000.

[7] J.F. Ciavaldini. Analyse numérique d'un problème de stefan à deux phases par une méthode d'éléments finis. *SIAM Journal on Numerical Analysis*, 12(3):464–487, 1975.

[8] M. G. Crandall and T. M. Liggett. Generation of semi-groups of nonlinear transformations on general Banach spaces. *American Journal of Mathematics*, pages 265–298, 1971.

[9] A. Damlamian. Some results on the multi-phase Stefan problem. *Communications in Partial Differential Equations*, 2(10):1017–1044, 1977.

[10] R. Dautov, R. Kadyrov, E. Laitinen, A. Lapin, J. Pieskä, and V. Toivonen. On 3d dynamic control of secondary cooling in continuous casting process. *Lobachevskii Journal of Mathematics*, 13(0):3–13, 2003.

[11] J. Douglas, Jr., T. Dupont, and R. E. Ewing. Incomplete iteration for time-stepping a Galerkin method for a quasilinear parabolic problem. *SIAM Journal on Numerical Analysis*, 16(3):503–522, 1979.

[12] J. Douglas, Jr. and T. Russell. Numerical methods for convection-dominated diffusion problems based on combining the method of characteristics with finite element or finite difference procedures. *SIAM Journal on Numerical Analysis*, 19(5):871–885, 1982.

[13] J. Douglas Jr. and T.M. Gallie Jr. On the numerical integration of a parabolic differential equation subject to a moving boundary condition. *Duke Mathematical Journal*, 22(4):557–571, 1955.

[14] C. M Elliott. On the finite element approximation of an elliptic variational inequality arising from an implicit time discretization of the Stefan problem. *IMA Journal of Numerical analysis*, 1(1):115–125, 1981.

[15] C. M. Elliott and J. R. Ockendon. *Weak and variational methods for moving boundary problems*, volume 59. Pitman London, 1982.

[16] C.M. Elliott. Error analysis of the enthalpy method for the Stefan problem. *IMA Journal of Numerical Analysis*, 7(1):61–71, 1987.

[17] A. Friedman. The Stefan problem in several variables. *Trans. Amer. Math. Soc.*, 133:51–87, 1968.

[18] J. W. Jerome and M. E. Rose. Error estimates for the multidimensional two-phase Stefan problem. *Mathematics of Computation*, 39(160):377–414, 1982.

[19] C. N. Kamenomostskaya. On a Stefan problem. *Mat. Sb.*, 53:489–514, 1961.

[20] O.A. Ladyzenskaya, V.A. Solonnikov, and N.N. Uralceva. Linear and quasi-linear equations of parabolic type, amer. math. *Soc. Transl., Providence, RI*, 1968.

[21] E. Laitinen, A. Lapin, and J. Pieskä. Asynchronous domain decomposition methods for continuous casting problem. *Journal of Computational and Applied Mathematics*, 154(2):393–413, 2003.

[22] Erkki Laitinen. *On the Simulation and Control of the Continuous Casting Processes*. PhD thesis, University of Jyväskylä, 1989.

[23] J. Lions. *Quelques méthodes de résolution des problemes aux limites non linéaires*, volume 76. Dunod Paris, 1969.

[24] S. Louhenkilpi. *Tempsimu, Heat transfer Model for Continuous Casting*.

[25] S. Louhenkilpi, E. Laitinen, and R. Nieminen. Real-time simulation of heat transfer in continuous casting. *Metallurgical Transactions B*, 24(4):685–693, 1993.

[26] S. Louhenkilpi, M. Mäkinen, S. Vapalahti, T. Räisänen, and J. Laine. 3d steady state and transient simulation tools for heat transfer and solidification in continuous casting. *Materials Science and Engineering: A*, 413:135–138, 2005.

[27] E. Magenes, R.H. Nochetto, and C. Verdi. Energy error estimates for a linear scheme to approximate nonlinear parabolic problems. *Modélisation Mathématique et Analyse Numérique*, 21(4):655–678, 1987.

[28] E. Magenes, C. Verdi, and A. Visintin. Theoretical and numerical results on the two-phase Stefan problem. *SIAM Journal on Numerical Analysis*, 26(6):pp. 1425–1438, 1989.

[29] Y. Meng and B. G. Thomas. Heat-transfer and solidification model of continuous slab casting: Con1d. *Metallurgical and Materials Transactions B*, 34(5):685–705, 2003.

[30] G. H. Meyer. A numerical method for two-phase Stefan problems. *SIAM Journal on Numerical Analysis*, 8(3):pp. 555–568, 1971.

[31] G. H. Meyer. Multidimensional Stefan problems. *SIAM Journal on Numerical Analysis*, 10(3):pp. 522–538, 1973.

[32] J. Miettinen, S. Louhenkilpi, H. Kytönen, and J. Laine. Ids: Thermodynamic kinetical empirical tool for modelling of solidification, microstructure and material properties. *Mathematics and Computers in Simulation*, 80(7):1536 – 1550, 2010.

[33] M. Niezgódka and I. Pawłow. A generalized Stefan problem in several space variables. *Applied Mathematics and Optimization*, 9(1):193–224, 1982.

[34] R. Nochetto, A. Schmidt, and C. Verdi. A posteriori error estimation and adaptivity for degenerate parabolic problems. *Mathematics of Computation of the American Mathematical Society*, 69(229):1–24, 2000.

[35] R. Nochetto and C. Verdi. Approximation of degenerate parabolic problems using numerical integration. *SIAM Journal on Numerical Analysis*, 25(4):784–814, 1988.

[36] R. H. Nochetto. Error estimates for two-phase Stefan problems in several space variables, i: Linear boundary conditions. *Calcolo*, 22(4):457–499, 1985.

[37] R. H. Nochetto. Error estimates for two-phase Stefan problems in several space variables, ii: Non-linear flux conditions. *Calcolo*, 22(4):501–534, 1985.

[38] R. H. Nochetto, M. Paolini, and C. Verdi. A fully discrete adaptive nonlinear chernoff formula. *SIAM Journal on Numerical Analysis*, 30(4):pp. 991–1014, 1993.

[39] R. H. Nochetto and C. Verdi. An efficient linear scheme to approximate parabolic free boundary problems: Error estimates and implementation. *Mathematics of Computing*, 51(183):27–53, 1988.

[40] R.H. Nochetto and C. Verdi. The combined use of a nonlinear chernoff formula with a regularization procedure for two-phase Stefan problems. *Numerical Functional Analysis and Optimization*, 9(11-12):1177–1192, 1988.

[41] O.A. Oleinik. A method of solution of the general Stefan problem. *Soviet-Math.Dokl.,*, 1:1350–1353, 1960.

[42] J.M. Ortega and W.C. Rheinboldt. *Iterative Solution of Nonlinear Equations in Several Variables*. Computer science and applied mathematics. Academic press, 1970.

[43] T. Räisänen, S. Louhenkilpi, T. Hätönen, J. Toivanen, J. Laine, and M. Kekäläinen. A coupled heat transfer model for simulation of continuous casting. In *European Congress on Computational Methods in Applied Sciences and Engineering, ECCOMAS*, pages 24–26. Citeseer, 2004.

[44] J. Rodrigues. The Stefan problem revisited. In *Mathematical models for phase change problems*, pages 129–190. Springer, 1989.

[45] J. F. Rodrigues and F. Yi. On a two-phase continuous casting Stefan problem with nonlinear flux. *European Journal of Applied Mathematics*, 1:259–278, 8 1990.

[46] M. E. Rose. A method for calculating solutions of parabolic equations with a free boundary. *Mathematics of Computation*, 14(71):249–256, 1960.

[47] T. Rossi and J. Toivanen. A parallel fast direct solver for block tridiagonal systems with separable matrices of arbitrary dimension. *SIAM Journal on Scientific Computing*, 20(5):1778–1793, 1999.

[48] L.I. Rubinstein. The Stefan problem translations of mathematical monographs, vol. 27. In *Am. Math. Soc*, 1971.

[49] J. Rulla. Weak solutions to Stefan problems with prescribed convection. *SIAM Journal on Mathematical Analysis*, 18(6):1784–1800, 1987.

[50] J. Sengupta, B.G. Thomas, and M.A. Wells. The use of water cooling during the continuous casting of steel and aluminum alloys. *Metallurgical and Materials Transactions A*, 36(1):187–204, 2005.

[51] A. Solomon. Some remarks on the Stefan problem. *Mathematics of Computation*, 20(95):347–360, 1966.

[52] B. G. Thomas. Modeling of the continuous casting of steel, past, present, and future. *Metallurgical and Materials Transactions B*, 33(6):795–812, 2002.

[53] C. Verdi. On the numerical approach to a two-phase Stefan problem with non-linear flux. *Calcolo*, 22(3):351–381, 1985.

[54] C. Verdi. Stefan problems and numerical analysis. In F. Brezzi, Colli F. P., U. Gianazza, and G. Gilardi, editors, *Analysis and Numerics of Partial Differential Equations*, volume 4 of *Springer INdAM Series*, pages 37–45. Springer Milan, 2013.

[55] C. Verdi and A. Visintin. Error estimates for a semi-explicit numerical scheme for Stefan-type problems. *Numerische Mathematik*, 52(2):165–185, 1988.

[56] A. Visintin. Sur le problème de Stefan avec flux non linéaire. *Boll. Un. Mat. Ital*, 18:63–86, 1981.

[57] A. Visintin. Stefan problem with phase relaxation. *IMA Journal of Applied Mathematics*, 34(3):225–245, 1985.

[58] A. Visintin. *Models of phase transitions*. Springer, 1996.

[59] V.R. Voller, C.R. Swaminathan, and B.G. Thomas. Fixed grid techniques for phase change problems: a review. *International Journal for Numerical Methods in Engineering*, 30(4):875–898, 1990.

[60] R. E. White. An enthalpy formulation of the Stefan problem. *SIAM Journal on Numerical Analysis*, 19(6):1129–1157, 1982.

[61] R. E. White. A numerical solution of the enthalpy formulation of the Stefan problem. *SIAM Journal on Numerical Analysis*, 19(6):1158–1172, 1982.

[62] F. Yi and T.M. Shih. Stefan problem with convection. *Applied Mathematics and Computation*, 95(2):139–154, 1998.

[63] M. Zlamal. A finite element solution of the monlinear heat equation. *ESAIM: Mathematical Modelling and Numerical Analysis*, 14(2):203–216, 1980.

APPENDIX 1 MATERIAL DATA

$\vartheta\,^{\circ}C$	$u \times 10^{-6}$	θ
25	0.877546	0.42
50	0.963862	0.84375
100	1.129301	1.71125
150	1.301933	2.60375
200	1.481758	3.52375
250	1.661583	4.47125
300	1.841408	5.44625
350	2.028426	6.45125
400	2.222637	7.48375
450	2.416848	8.54375
500	2.618252	9.63375
550	2.819656	10.75375
600	3.035446	11.90125
650	3.244043	13.07625
700	3.459833	14.28125
750	3.66843	15.51625
800	3.88422	16.78125
833.21	4.035273	17.638068
893.21	4.301414	19.222068
953.21	4.567555	20.851068
1013.21	4.848082	22.522068
1073.21	5.128609	24.238068
1133.21	5.416329	25.999068
1193.21	5.718435	27.805068
1253.21	6.027734	29.659068
1313.21	6.358612	31.561068
1373.21	6.732648	33.508068
1390.21	6.847736	34.068218
1403.21	6.941245	34.499168
1417.21	7.04914	34.965368
1440.16	7.451948	35.7238655
1450.95	7.876335	36.0691455
1461.74	8.645986	36.3917665
1500	8.868969	37.4821765
1520	8.99125	38.0521765
1540	9.106338	38.6221765
1560	9.221426	39.1921765
1580	9.343707	39.7621765
1600	9.465988	40.3321765